1-1-2005

Yield improvement in chemical mechanical planarization via material removal variation on a surface

Muthukkumar Kadavasal Sivaraman
Iowa State University

Yield improvement in chemical mechanical planarization via material removal variation on a surface

by

Muthukkumar Kadavasal Sivaraman

A thesis submitted to the graduate faculty

in partial fulfillment of the requirements for the degree of

MASTER OF SCIENCE

Major: Mechanical Engineering

Program of Study Committee:
Abhijit Chandra, Co-major Professor
Ashraf F. Bastawros, Co-major Professor
Thomas J. Rudolphi
Atul Kelkar

Iowa State University

Ames, Iowa

2005

Graduate College
Iowa State University

This is to certify that the master's thesis of

Muthukkumar Kadavasal Sivaraman

has met the thesis requirements of Iowa State University

Signatures have been redacted for privacy

Table of Contents

Acknowledgements

I would like to express my sincere thanks to both of my major professors, Prof. Abhijit Chandra and Prof. Ashraf Bastawros for their excellent guidance without which this work would have not been possible. I am very much indebted for the amount of support my advisors provided me.

I am very much thankful to my other committee members Prof. Thomas J. Rudolphi and Dr. Atul Kelkar of Aero Space and Mechanical engineering department respectively. My sincere and hearty thanks also go to Dr. Guanghui Fu who provided me ample guidance and knowledge on various basic aspects of CMP during the initial stages of my research.

This work is partly funded my National Science Foundation (NSF).

Abstract

Chemical Mechanical Planarization is one of the most required semiconductor processing module used in fabrication facilities world wide. Among various surface material removal processes, CMP process is primed for its ability to obtain both local and global planarity on a given surface. The model developed by Fu and Chandra et al, calculates the dishing height based on MRR equations. The model provides a way for step by step material removal based on proportionality parameters like interface pressure, table speed and pattern density.

The thesis provides a complete chart for developing a control mechanism for CMP process. The thesis bifurcate the approach into Die scale and Wafer Scale. In die scale, a comprehensive control algorithm is developed based on the MRR equations with pressure and velocity as the control parameter. The model establishes a control over the step height uniformity and upper surface uniformity in both uniform pattern density and varying pattern density surfaces. At wafer scale, an analytical model that relates wafer-pad interface pressure and carrier loading is explained and based on that a FEM analysis is carried out to study the impact of non uniform loading on wafer-pad interface.

Both the die scale and wafer models, paved way for developing a integrated control flow chart that can have an impact on the wafer surface at both die scale and wafer scales at the same time. Although, a chart or flow map with necessary models and simulations are in place, to put the entire control mechanism work in a realistic environment there are many other requirements. Like a full fledged pixel or zonal controller should be developed and large scale experimental analysis should be performed based on real time data from manufacturing units.

CHAPTER 1. Introduction to Chemical Mechanical Polishing (CMP)

1.1. Introduction

Planarization technology is one of the key process steps in the fabrication of ultra large-scale integrated (ULSI/VLSI) chips in integrated circuit manufacturing. One among the various technologies for involved in IC manufacturing is Chemical Mechanical Planarization (CMP). CMP has emerged to be the most promising process because of its demonstrated capability to provide better local and global planarization of wafer surfaces (Steigerwald, *et al.*, 1997). The planarization, achieved by the use of chemical mechanical means, has enabled the interconnection of ever increasing number of devices. The effectiveness of the CMP in both improving the yield and performance of the circuits has let to its application in the front-end processes and many other microelectronic applications.

Chemical Mechanical Planarization is a combination of chemical and mechanical processes, where wafers are held face down against a spinning polisher (see figure 1.1). The polisher's top surface consists of a flat polishing pad, which is made of roughened polyurethane. A slurry solution made of certain abrasives and chemicals is introduced between the pad and the wafer. Slurry selection process is one of the important steps in CMP. Many criteria depend on the chemical composition and pH of the slurry and also on the type of material being polished. For planarizing an oxide layer, a high pH alkali-based solution is used, whereas a low pH, oxidizer based solution is commonly used for metals. There are various methods for material removal using CMP. Removal rate stability, non-uniformity in wafer and die scale, control and cost ownership are some important issues in CMP.

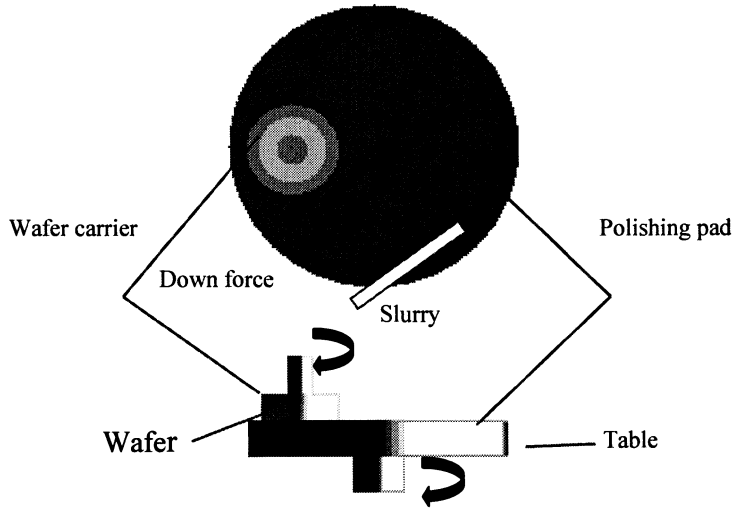

Figure 1.1 Illustration of the CMP process.

1.2. Chemical Mechanical Planarization (CMP)

The following page explains in detail, about the components and their functions as a part of CMP.

1.2.1. Slurry

Slurry is a type of abrasive chemical solution, where the abrasives involve themselves in the mechanical removal of material and the chemical base helps in chemical softening. The chemical base reacts with the wafer surface material to produce a softer surface layer, which is easier for removal by the abrasives.

Abrasives are generally inorganic oxides viz. silica, alumina, ceria etc. They are ultra-pure and have almost uniform size and shape in order to achieve consistent. The concept of material removal by abrasive is a vast research topic with lots of speculations. The most

common one is that, the surface material is removed by the abrasives through mechanical wear. The local heat generation and friction by the high contact pressure between abrasive and surface causes plastic flow. The particle parameters that are generally believed to influence material removal are particle shape, particle size and its distribution, concentration, polishing environment and abrasive hardness.

The solution used acts as a coolant and removes the abraded material out of the system. It also aid the distribution of chemicals and at the same time causes certain chemical reactions on the wafer and pad surfaces.

1.2.2. Pad

The polishing pads used in semiconductor applications can be grouped into four main classes based on their structural characteristics. These are

- Felts and polymer impregnated felts
- Micro-porous synthetic leathers
- Filled polymer films
- Unfilled textured polymer films

The pad is generally a polymeric structure and its manufacturing method determines its microstructure. Pad surfaces are perforated or grooved in order to aid slurry transport. In the material removal process, it is the necessity of the pad surface to hold the abrasives and transfer the load to the abrasives.

The mechanical properties that are generally believed to influence the pad performance are Young's modulus, Poisson's ratio, hardness and compressibility, visco-elasticity, surface roughness and texture. During CMP, pad surface is also planarized. The pad asperities are flattened by the abrasion of slurry particles and wafer surface. The abraded pad material, abrasive particles and re-deposited wafer surface material fills the pad pores, causing glaze. In order to stabilize the pad surface, pad conditioning is done, where

- Polymer is abraded from the surface of the pad
- Inorganic material is removed from the topmost film on the wafer via chemical and/or mechanical processes
- Slurry particle agglomeration to form extended particles

1.2.3. Carrier

The basic function of the wafer carrier is to hold the wafer in place while the wafer is polished. It includes means such as vacuum, to hold the wafer in place while loading and unloading and a retainer ring to keep the wafer from becoming dislodged from the carrier during the polish cycle.

The other functions of the carrier are polished wafers must be flat within a predetermined specification across the wafer, but excluding the so-called edge exclusion region. Where the edge exclusion region is an annular region of the wafer at the wafer edge where the removal rate deviates significantly from that of the bulk of the wafer. Also, the wafer carrier must allow the tool to polish a broad range of films with varying amounts of

film stress. The wafer carrier should also provide means to compensate small amounts of wafer bow, tilt or warp by using carrier film at the back of the wafer.

1.2.4. Platen

The platens on which the wafers are polished have evolved over time. In traditional polishing, a hard platen is used. The reason being that hard platen present as close to absolutely flat surface as possible against with wafer is pressed. Ideally platens rotate perfectly. In practice, however, there is a small amount of run-out or wobble, which limits the ability of the tool to polish films uniformly, especially at high rotation speeds.

1.3. Thesis outline

The thesis presented here revolves around various mechanical aspects of CMP. In order to get high yield output, a uniform surface after polishing is the prime criteria. Many methods and models have been devised in order to achieve this criterion; controlled material removal is one among them. From Preston's equation it is clear that the material removal rate is directly related to the amount of pressure that is experienced by the surface. Hence controlled material removal can be achieved when the pressure applied is controlled.

Fu and Chandra's dishing model explains how the interface pressure between the pad and the wafer, as well as the relative velocity between the pad and wafer is proportional to the Material removal rate across the wafer surface. The first part (chapter 2 and 3) of the thesis explains an effective open loop pressure/velocity control algorithm that has been

devised to obtain uniform wafer surface in die scale using the Fu and Chandra's dishing model.

Though the control over wafer surface uniformity in die scale is achieved in the previous chapter, there is a necessity to know the pressure and loading distribution in the wafer scale, in order to have an effective control of the wafer surface in die scale. Fu and Chandra developed an analytical solution in order to identify the loading distribution based on the desired interface pressure and vice versa. The second part (chapter 4) of the thesis identifies a plate-elastic half space model developed using boundary elements to verify the existing wafer-pad analytical model. It also discusses various ways to implement the analytical model in a realistic environment using finite element analysis with ABAQUS. A design chart is provided to identify the amount of edge effect we will experience based on the loading patterns.

Based on the above 2 models, one in die scale and another in wafer scale, there comes a necessity for us to correlate and program an algorithm involving both wafer and die scale models to make it applicable in a realistic environment. Chapter 5 explains a flow/control chart which identifies ways to relate the models which is followed by conclusion remarks.

CHAPTER 2. Yield improvement via minimization of step height non-uniformity in Chemical Mechanical Planarization (CMP) with pressure as control variable

2.1 Introduction

Achieving local as well as global planarization is one of the prime requirements in micro fabrication methods. Many different methods of dielectric planarization are practiced in order to achieve local and global planarity. Chemical mechanical polishing (CMP) has emerged as the planarization method of choice [Li, 2000] because of its ability to planarize over longer length scales than traditional planarization techniques and is considered to provide far better local and global planarization [Steigerwald, et al 1997, Sivaram et al 1992, Patrick et al 1991]. Besides interlayer dielectric planarization, CMP has also find applications in shallow trench isolation, damascene technologies [e.g., Kaanta 1991, Kranenberg 1998]. Despite the advantages that CMP enjoys, the process still suffers from large global non-uniformities within a die and across a wafer.

2.2 Background

Although CMP can planarize over longer length scales, pattern density variation across a chip leads to large variation in global thickness across the die. CMP therefore removes local steps but generates global steps as illustrated in Figure 2. Due to the initial pattern density difference, the two regions on a chip polish at different rates. At some time

T_1, local planarity is achieved in the low density area of density PD_1. After some time T_2, local planarity is also achieved in the high density region of initial density PD_2. The initial difference in layout pattern density creates a global step height between these two regions due to the difference in removal rates before the local patterns are planarized.[Ouma, 1998] Although the global thickness variation is no longer a serious lithography concern, it still has a serious impact on subsequent process steps such as via etching. Depending on the location of the via, the depth will be different thus making it difficult to determine a suitable etch time. The global thickness variation also impacts circuit performance: long-range clock wires passing through regions of different thicknesses result in different capacitances and may result in clock skew [Stine et al 1997]. The length scale over which complete local planarity is achieved is a function of the elastic properties of the polish pad and other process conditions. This length scale is easily visualized by polishing a step density pattern. As shown in Figure 2.1, away from the density boundary, local planarity is achieved.

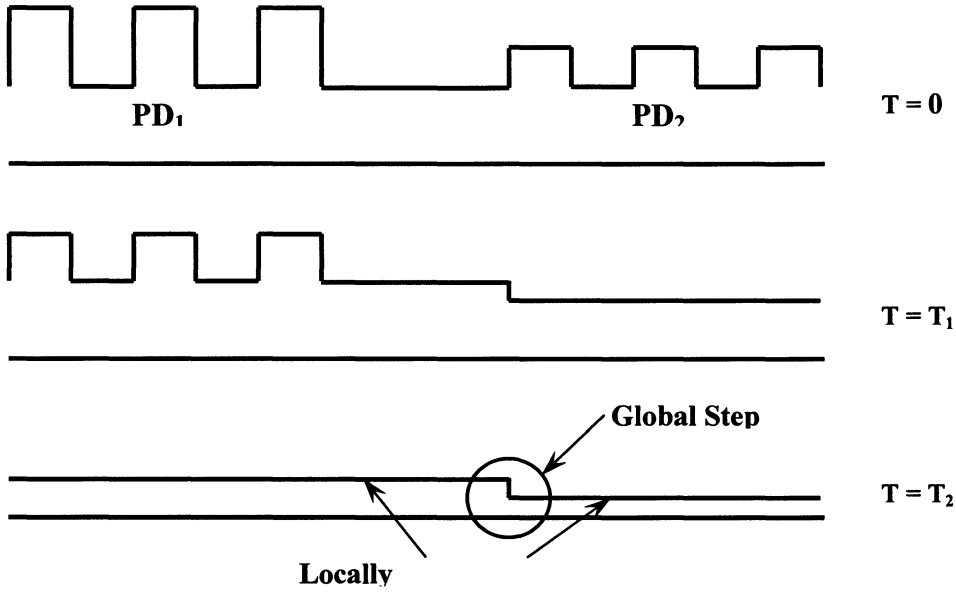

Figure 2.1 Planarization defects due to pattern density variations

Even though many publications have been made on the various modeling techniques in CMP to achieve global planarity, using material removal control techniques, pad property variation etc., not many concentrate on obtaining global planarity over pattern dependant surfaces. Most of them assume a uniform pattern density across the entire polish span. Eamkajornsiri et al [2001] concludes that yield improvement in CMP can be improved considerably by varying the interface pressure, wafer curvature and polishing time, in wafer scale, it does not takes into account the variation in pattern density across the die. Tugbawa et al [2001] proposes a contact mechanics based density step height model of pattern dependencies for predicting thickness evolution. Ouma et al [2002], provides a model using a 2 step FFT of the incoming wafer surface and an elliptic weighting function corresponding to pad deformation profile to obtain estimates of effective pattern densities across the entire wafer.

Based on the effective pattern density in a region, and utilizing the step height reduction model developed by Fu et al [2003], this chapter provides a control based open loop algorithm to obtain uniformity over the pattern dependant non uniform wafer surfaces in a die scale. The model assumes the die in the wafer surface to have 'n' number of zones of different heights and different pattern densities. In order to minimize both local and global step height variations, the applied pressure is varied both spatially and temporally. A 2D simulation process is devised using visual basic to track the amount of removal, and current step heights for every time step.

The Fu et al paper [2003] has the following assumptions: 1. Pad is assumed to deform like an elastic foundation 2. Force redistribution due to pad bending is proportional to dishing

height 3. The material removal rate for metal interconnects and dielectric material follows Preston's equation [Preston, 1927] with different Preston's constants. 4. Wafer and pad are in contact at any point of the interface.

2.3 Notations used and model details

Y_{upper}	current height of the upper surface
Y_{lower}	current height of the lower surface
$D(t)$	step height
P	Interface pressure
V	relative velocity
K	Preston's constant
k	Stiffness
a	Linewidth
b	Pitch
c	$b-a$
α	Bending factor
a/b	Pattern density

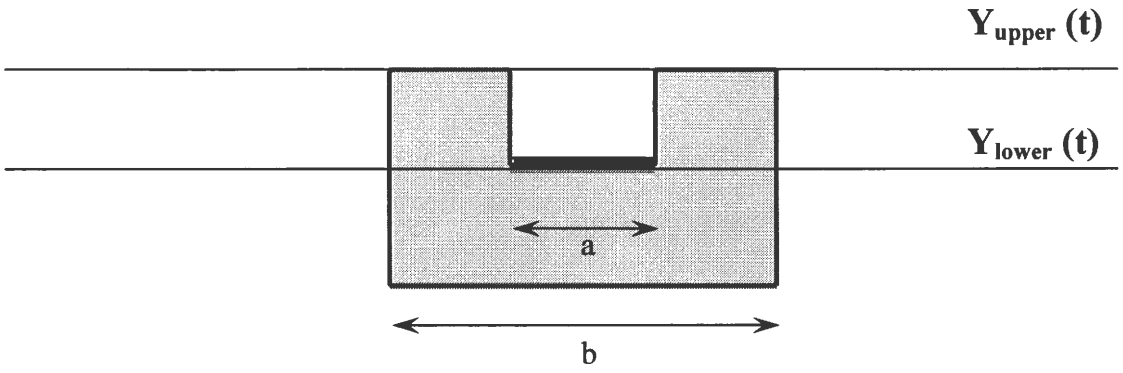

Figure 2.2 Schematic representation of a pattern

The model provides and expression for the step height as a function of time, assuming the selectivity to be 1 and that there exists an upper and lower surface. The expression is as follows

$$D(t)=\left[Y_{upper}(0)-Y_{lower}(0)\right]exp\left\{-K\left[1+\frac{\alpha}{k}\left(\frac{1}{a}+\frac{1}{c}\right)Vkt\right]\right\} \quad (1)$$

The final heights of the upper surfaces and lower surfaces for any time t is expressed as follows

$$Y_{Lower}(t)=\frac{\left(\frac{c}{b}+\frac{\alpha}{ka}\right)Y_{upper}(0)+\left(\frac{a}{b}+\frac{\alpha}{kc}\right)Y_{lower}(0)}{1+\frac{\alpha}{k}\left(\frac{1}{a}+\frac{1}{c}\right)}-KPVt$$

$$+\frac{\frac{c}{b}+\frac{\alpha}{ka}}{1+\frac{\alpha}{k}\left(\frac{1}{a}+\frac{1}{c}\right)}\left[Y_{lower}(0)-Y_{upper}(0)\right]\exp\left\{-K\left[1+\frac{\alpha}{k}\left(\frac{1}{a}+\frac{1}{c}\right)\right]Vkt\right\} \quad (2)$$

$$Y_{upper}(t)=\frac{\left(\frac{c}{b}+\frac{\alpha}{ka}\right)Y_{upper}(0)+\left(\frac{a}{b}+\frac{\alpha}{kc}\right)Y_{lower}(0)}{1+\frac{\alpha}{k}\left(\frac{1}{a}+\frac{1}{c}\right)}-KPVt$$

$$+\frac{\frac{a}{b}+\frac{\alpha}{kc}}{1+\frac{\alpha}{k}\left(\frac{1}{a}+\frac{1}{c}\right)}\left[Y_{upper}(0)-Y_{lower}(0)\right]\exp\left\{-K\left[1+\frac{\alpha}{k}\left(\frac{1}{a}+\frac{1}{c}\right)\right]Vkt\right\} \quad (3)$$

The removal rate equations being

$$\frac{dY_{upper}}{dt}=KVk\left[\left(-\frac{a}{b}-\frac{\alpha}{kc}\right)\left(Y_{upper}-Y_{lower}\right)-\frac{P}{k}\right] \quad (4)$$

$$\frac{dY_{lower}}{dt}=KVk\left[\left(\frac{c}{b}+\frac{\alpha}{ka}\right)\left(Y_{upper}-Y_{lower}\right)-\frac{P}{k}\right] \quad (5)$$

The equations 2 and 3 are terminal equations, meaning the values are the final heights after polishing for a given period of time. The equations 4 and 5 are intermediate equations, meaning the removal rate changes for every time step "dt" and so is the step height.

2.4 Model description

2.4.1 Spatial pressure control – algorithm (Appendix - Flow chart –I)

In this pressure control, the exact pressure to be applied is calculated using the following algorithm for each of 'n' number of zones, and it is then applied simultaneously on all the zones for the entire period of the calculated time. The algorithm is also described in the form of block diagram after a few pages.

The algorithm is as follows

Step 1. *Calculate Total Material*

- Calculate **the total material (*Mat_total*)** to be removed in all zones together. This step and step 4.2 are used together to find when the polishing process will finish. Where $Y_{desired}$ is the final target height and Y_{upper} is the initial upper surface height.

$$Mat\_Total = \sum_{i=1}^{n} \left(Y_{upper}(i) - Y_{desired} \right)$$

Step 2. *Calculate Time Needed*

- Calculate the **polishing time needed** for each zone (T_{zone}) to reach the target or desired surface with the maximum interface pressure (The maximum pressure that the user can apply based on the machine specification) using equation 3 (***f(t)***) by following Newton-Raphson method.

$$t_{i+1} = t_i - f(t)/f'(t) \qquad \text{until } t_{i+1} - t_i < 1e\text{-}8$$

Step 3. *Calculate Applied Pressure*

- Compare the polishing time for all 'n' zones and find the **maximum polishing time needed** (T_{max}) to have all applied interface pressure values of all zones to be less than or equal to maximum interface pressure that we set.

$T_{max} = Max(T_{zone})$, For zone = 1 to n

- With T as the T_{max}, Calculate the **applied interface pressure** for each zone by using equation 3.

Step 4. *Calculate Step Height* and *Check*

With the calculated pressure allow polishing for the stipulated time T_{max} on all 'n' zones.

4.1 *Calculate Step Height*

- Calculate the **new upper and lower surface** of each zone using the rate equations 4 (Y_{upRate}) and 5 (Y_{loRate}) respectively each for upper and lower surfaces.

$$Y_{upper}(i)^{new} = Y_{upper}(i)^{old} - Y_{upRate}(i).\Delta t \quad \text{, For i = 1 to n (zones)}$$

$$Y_{lower}(i)^{new} = Y_{lower}(i)^{old} - Y_{loRate}(i).\Delta t \quad \text{, For i = 1 to n (zones)}$$

Where Δt = 0.1 sec

4.2 *Check*

- Compare the total material left with the previous step till it reaches the least total material left. If it is not, go back to step 4 and continue polishing and calculate the new upper and lower surface again.

Step 5. *Calculate Error* and *Verify*

5.1 *Calculate Error*

- Calculate **error of upper surface and step height** of each zone

$$Error_{upper} = (Y_{upper}(final)_i - Y_{desired}) / (Y_{upper}(0)_i - Y_{desired}) \times 100$$

$$Error_{step\ height} = (Y_{upper}(final)_i - Y_{lower}(final)_i)/(Y_{upper}(0)_i - Y_{lower}(0)_i) \times 100$$

5.2 *Verification*

- Compare the results (final step height from the algorithm) with the final step height calculated from equation 1.

Step 6. *Keep Track*

- Record the initial variables (a, b, Y_{upper}, Y_{lower}), applied interface pressure, total time, and the final variables (Y_{upper}, Y_{lower}).

2.4.2 Spatial and temporal pressure control – algorithm (Appendix - Flow chart – II)

In the previous algorithm, the pressure is varied spatially across the die. From the results, we came to an understanding that, this variation of pressure would only help us achieve a uniform upper surface. This means, we cannot control the step height to achieve planarity. It is found that, at very low pressures, the removal rate of the lower surface is negligible. This criteria, is used as the basis for controlling step height. An algorithm is devised in such a way that, minimum pressures are applied in a proportional way across the die, over the 'n' zones, such that both global and local step heights are minimized, which in turn results in maximum uniformity. The algorithm is explained in the following pages. The assumption made is that the relation between step height and time is considered linear.

Step 1. *Calculate Minimum Step height*

- From the machine specifications, the minimum pressure capability is calculated. And with that pressure as the applied pressure, the smallest step height achievable

(such that only the upper surface is polished) for each zone (SH_i^{min}) is calculated. Equation 5 is used in calculation.

$$\frac{dY_{lower}}{dt}(P_{min}) = 0 \qquad => \qquad SH_1^{min}, SH_2^{min}, SH_3^{min} \ldots$$

where P_{min} is the minimum pressure capability for a specific CMP machine

Step 2. *Calculate Max pressure*

- With the respective step heights of each zone, the maximum pressure that can be applied is calculated for each zone (P_i^{max}) such that only the upper surface is polished and the lower surface is left untouched.

$$\frac{dY_{lower}}{dt}(SH_i) = 0 \qquad => \qquad P_1^{max}, P_2^{max}, P_3^{max} \ldots$$

where SH_i is the present step height of i-th zone

Step 3. *Calculate the interface pressure for each zone (P_i)*

- Calculate material removal rate on the upper surface of each zone ($\overline{\dot{Yup}_i}$) with P_i^{max} and Calculate material need to be removed of each zone (Mat_i) by setting

$$Mat_i = SH_i - \max(SH_i^{min})$$

- Calculate the ratio (R_i) by setting

$$R_i = \frac{Mat_i}{\overline{\dot{Yup}_i}}$$

- Assuming relation between step height and time to be linear, calculate the material removal rate on the upper surface

$$Yup_i^{'} = \frac{Mat_i}{\max(R_i)}$$

- Calculate interface pressure (P_i) and material removal rate on the lower surface ($Ylo_i^{'}$)

Step 4. *Polish*

- Now using removal rate equations 4 and 5, the polishing is carried out on the wafer surface

Step 5. *Check*

- Repeat step 2 to 4 until the following condition is satisfied. The condition helps, finding out whether the surface has reached the least step height $SH_1^{\min}$

$$\exists\left(Mat_i < \max\left(SH_i^{\min}\right)\right)$$

Step 6. *Spatial pressure control*

- After reaching the stipulated step height, now the spatial pressure control algorithm is applied to attain the target surface.

By using the spatial and temporal pressure control, the step height is first reduced. Then to attain the target surface, the spatial pressure algorithm is applied over this newly evolved surface. It should be noted that, in the step 4 of the algorithm, the removal rate equations follow a polishing process such that the time step is 1 sec. So for every second, the steps 2 to 4 will be repeated, which is not practically applicable. The following algorithm provides a solution to this issue.

2.4.3 Look-ahead scheduled pressure control – algorithm (Appendix - Flow chart –III)

The possibility of changing the applied pressure for every one second is indeed

impractical. The look ahead pressure control algorithm is programmed such that, the time step is user controlled. Here, the step height to be formed when applied a specific set of pressure values across 'n' zones is viewed ahead of the process and the pressure is modified again based on the desired step height. The time for look ahead is equal to the time step selected.

Step 1. *Calculate Minimum step height*

- From the machine specifications, the minimum pressure capability is calculated. And with that pressure as the applied pressure, the smallest step height achievable (such that only the upper surface is polished) for each zone ($SH_i^{\min}$) is calculated.

$$\frac{dY_{lower}}{dt}(P_{\min}) = 0 \qquad \Rightarrow \qquad SH_1^{\min}, SH_2^{\min}, SH_3^{\min} \ldots$$

where $P_{\min}$ is the minimum pressure capability for a specific CMP machine

Step 2. *Calculate Max Pressure*

- With the respective step heights of each zone, the maximum pressure that can be applied is calculated for each zone ($P_i^{\max}$) such that only the upper surface is polished and the lower surface is left untouched.

$$\frac{dY_{lower}}{dt}(SH_i) = 0 \qquad \Rightarrow \qquad P_1^{\max}, P_2^{\max}, P_3^{\max} \ldots$$

where SH_i is the present step height of i-th zone

Step 3. *Procedure to calculate the interface pressure for each zone (P_i)*

- The material to be removed (in terms of length) from each zone (Mat_i) is calculated using the equation given below. The reason that the biggest step height is taken into consideration is that, its assumed that while polishing we always try to follow the un said rule that, its better to remove less than the actual, rather than removing more.

$$Mat_i = SH_i - \max(SH_i^{\min})$$

- With $P_{\min}$ and $P_i^{\max}$ as inputs for each zone, the minimum possible step height left is identified in each zone ($MSH_i^{\min}$) after a specific period of time using look-ahead procedure

$$Look-ahead(t,P) \quad => \quad MSH_1^{\min}, MSH_2^{\min}, MSH_3^{\min} \ldots$$

- The step height that is to be removed (RSH_i) or polished from each zone is calculated after the specific time

$$RSH_i = SH_i - MSH_i^{\min}$$

- The ratio is calculated as follows

$$R_i = \frac{Mat_i}{RSH_i}$$

- Calculate the material to be removed from each zone, based on zonal ratio, that should occur by setting

$$LSH_i = Mat_i / \max(R_i)$$

- Find the interface pressure of each zone using look-ahead procedure for MSH_i (the step height to be left after the prescribed time step)

$$MSH_i = SH_i - LSH_i$$

$$Look-ahead(t, MSH_i) \quad => \quad P_1, P_2, P_3 \ldots$$

Step 4. *Polish*

- Now using removal rate equations 4 and 5, the polishing is carried out on the wafer surface

Step 5. *Check*

- Repeat step 2 to 4 until the following condition is satisfied. The condition helps, finding out whether the surface has reached the least step height SH_1^{min}

$$\exists\left(Mat_i < \max\left(SH_i^{min}\right)\right)$$

Step 6. *Spatial pressure control*

- After reaching the stipulated step height, now the spatial pressure control algorithm is applied to attain the target surface.

Procedure Look-ahead (t, P)

- Calculate the step height after specific time for two interface pressures (P_1, P_2).
- Calculate another step height after specific time for interface pressure $(P_1+P_2)/2$.
- Compare the step height from step 2 to step 1 and substitute the pressure from step 2 to one of the pressures of step 1 to get new (P_1, P_2).
- Do until $P_2 - P_1 < 0.1xP_{min}$ for minimum possible step height left MSH_i^{min}

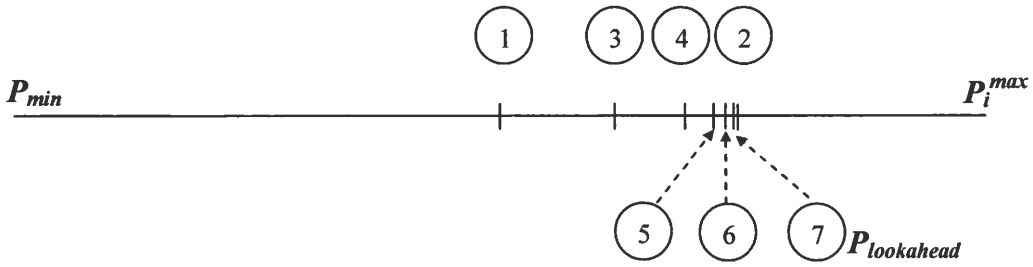

Figure 2.3 Pressure selection loop

The above schematic diagram shows the way in which the next pressure value is selected. With P_{min} and P_i^{max} as inputs, the minimum step heights are calculated. The next pressure is selected.

Procedure Lookahead (t, MSH_i)

- Calculate the step height after specific time for two interface pressures (P_1, P_2).
- Calculate another step height after specific time for interface pressure $(P_1+P_2)/2$.
- Compare the step height from step 2 to step 1 and substitute the pressure from step 2 to one of the pressures of step 1 to get new (P_1, P_2).
- Do until $P_2 - P_1 < 0.1xP_{min}$ we reach the step height left to be equal to MSH_i

2.5 Results

Table 1 show the examples which are taken into consideration for checking the algorithm. It is assumed that the die has 3 different pattern densities, and hence divided into 3 zones. The table has the upper and lower surface heights for each zones.

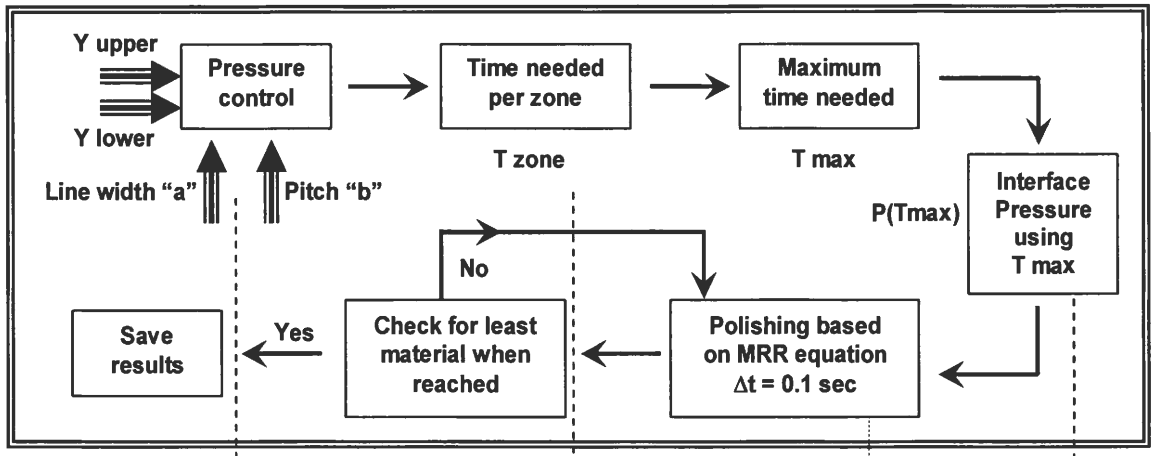

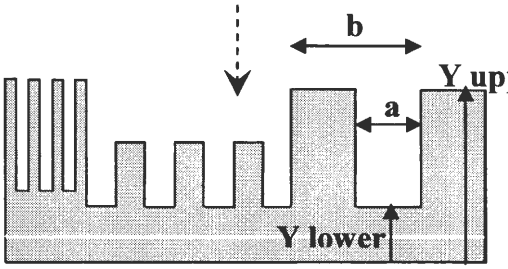

$$Y_{upper}(t) = \frac{\left(\frac{c}{b}+\frac{\alpha}{ka}\right)Y_{upper}(0)+\left(\frac{a}{b}+\frac{\alpha}{kc}\right)Y_{lower}(0)}{1+\frac{\alpha}{k}\left(\frac{1}{a}+\frac{1}{c}\right)} - KPVt$$

$$+\frac{\frac{a}{b}+\frac{\alpha}{ka}}{1+\frac{\alpha}{k}\left(\frac{1}{a}+\frac{1}{c}\right)}\left[Y_{upper}(0)-Y_{lower}(0)\right]\exp\left\{-K\left[1+\frac{\alpha}{k}\left(\frac{1}{a}+\frac{1}{c}\right)\right]Vkt\right\} \quad (3)$$

$$\frac{dY_{upper}}{dt} = KVk\left[\left(-\frac{a}{b}-\frac{\alpha}{kc}\right)\left(Y_{upper}-Y_{lower}\right)-\frac{P}{k}\right] \quad (4)$$

$$\frac{dY_{lower}}{dt} = KVk\left[\left(-\frac{c}{b}+\frac{\alpha}{ka}\right)\left(Y_{upper}-Y_{lower}\right)-\frac{P}{k}\right] \quad (5)$$

"Spatial Pressure Control" - The figure gives a detailed block/flow diagram of the algorithm, along with the respective equations which is used in that instant

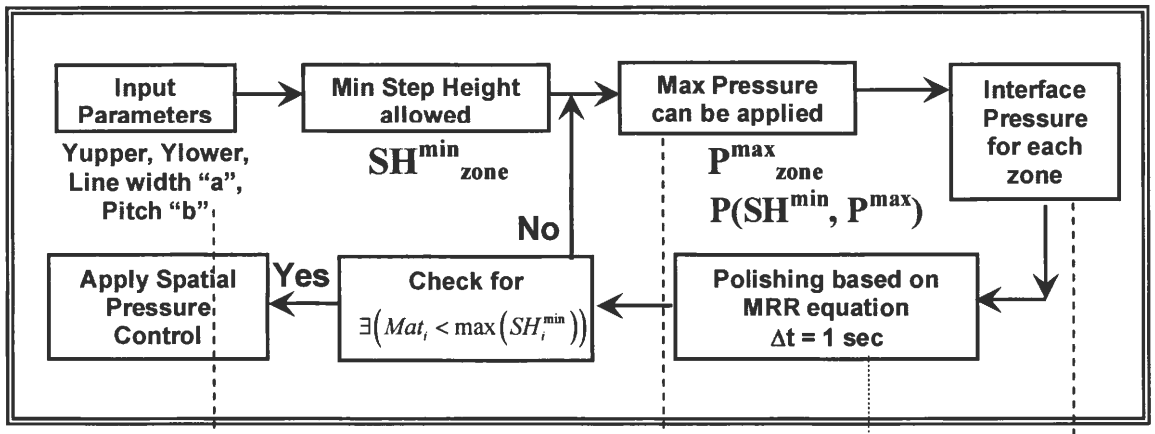

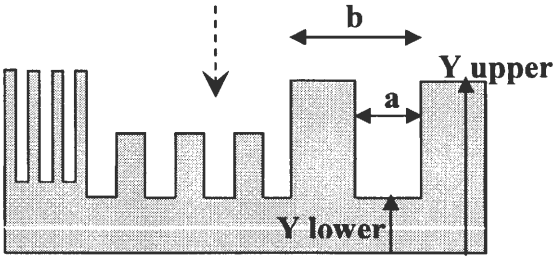

$$Y_{upper}(t) = \frac{\left(\frac{c}{b}+\frac{\alpha}{ka}\right)Y_{upper}(0)+\left(\frac{a}{b}+\frac{\alpha}{kc}\right)Y_{lower}(0)}{1+\frac{\alpha}{k}\left(\frac{1}{a}+\frac{1}{c}\right)} - KPVt$$

$$+\frac{\frac{a}{b}+\frac{\alpha}{ka}}{1+\frac{\alpha}{k}\left(\frac{1}{a}+\frac{1}{c}\right)}\left[Y_{upper}(0)-Y_{lower}(0)\right]\exp\left\{-K\left[1+\frac{\alpha}{k}\left(\frac{1}{a}+\frac{1}{c}\right)\right]Vkt\right\} \quad (3)$$

$$\frac{dY_{upper}}{dt} = KVk\left[\left(-\frac{a}{b}-\frac{\alpha}{kc}\right)\left(Y_{upper}-Y_{lower}\right)-\frac{P}{k}\right] \quad (4)$$

$$\frac{dY_{lower}}{dt} = KVk\left[\left(-\frac{c}{b}+\frac{\alpha}{ka}\right)\left(Y_{upper}-Y_{lower}\right)-\frac{P}{k}\right] \quad (5)$$

"Spatial and Temporal Pressure Control" - The figure gives a detailed block/flow diagram of the algorithm, along with the respective equations which

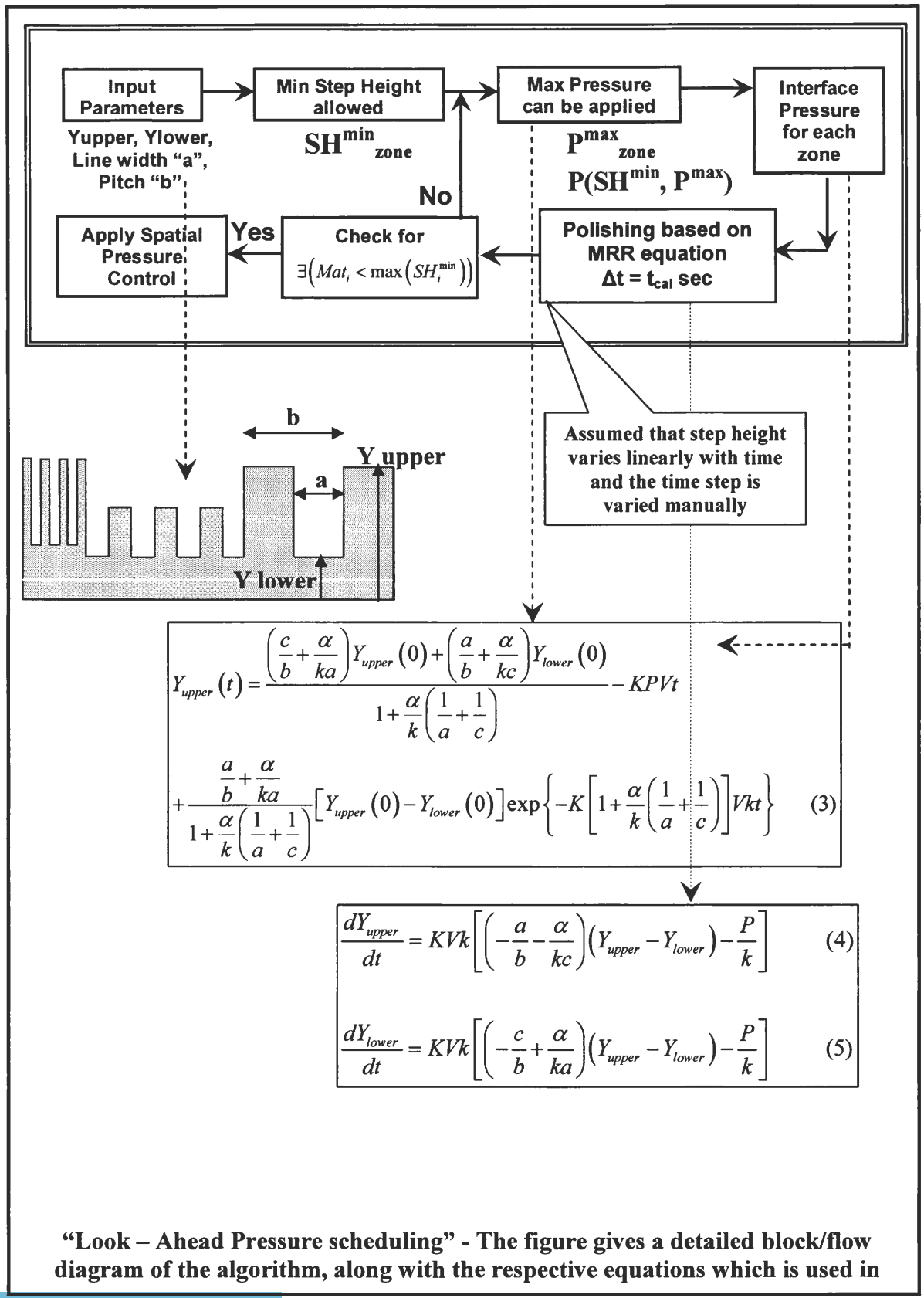

"Look – Ahead Pressure scheduling" - The figure gives a detailed block/flow diagram of the algorithm, along with the respective equations which is used in

In the first and third example, the heights and pattern densities are reversed. Example 2 and 4 are random variations and they lie along the value range of 1 and 3. The constants are [Stavreva et al 1997]

K	Preston's constant	$=1.566 * 10^{-13}\ m^2/N$
k	Stiffness	$=8.027 * 10^{10}\ N/m^3$
α	Bending factor	$=2.16 * 10^{6}\ N/m$
V	Velocity	$=0.5\ m/s$

Zone	Example 1			Example 2			Example 3			Example 4		
	Initial Y_{upper} (nm)	Initial Y_{lower} (nm)	a/b	Initial Y_{upper} (nm)	Initial Y_{lower} (nm)	a/b	Initial Y_{upper} (nm)	Initial Y_{lower} (nm)	a/b	Initial Y_{upper} (nm)	Initial Y_{lower} (nm)	a/b
1	1350	1000	0.3	1250	1000	0.3	1250	1100	0.3	1350	1000	0.3
2	1300	1050	0.5	1300	1050	0.5	1300	1050	0.5	1400	1250	0.5
3	1250	1100	0.6	1350	1100	0.6	1350	1000	0.6	1300	1150	0.6

Example sets

Example 1	No Control			Spatial Pressure Control			Spatial and Temporal Pressure Control			Look-Ahead Pressure Scheduling		
Zone	Final Y_{upper} (nm)	Final Y_{lower} (nm)	Final SH (nm)	Final Y_{upper} (nm)	Final Y_{lower} (nm)	Final SH (nm)	Final Y_{upper} (nm)	Final Y_{lower} (nm)	Final SH (nm)	Final Y_{upper} (nm)	Final Y_{lower} (nm)	Final SH (nm)
1	737.9	735.8	2.0	676.2	674.3	1.9	699.5	697.9	1.5	699.5	698.0	1.5
2	699.5	697.5	2.0	699.8	697.7	2.1	699.5	697.4	2.1	699.5	697.5	2.1
3	685.7	684.7	1.0	701.5	700.5	1.0	699.5	698.0	1.4	699.3	697.9	1.4
Time (s)	144.1 with 6.1 psi			143.8 with 7 psi			145.8			145.0		
%Error	8.1	-	-	3.9	-	-	0.2	-	-	0.3	-	-
Stdev	-	-	0.6	-	-	0.5	-	-	0.3	-	-	0.3

Results for example 1

Example 2	**No Control**			**Spatial Pressure Control**			**Spatial and Temporal Pressure Control**			**Look-Ahead Pressure Scheduling**		
Zone	Final Y_{upper} (nm)	Final Y_{lower} (nm)	Final SH (nm)	Final Y_{upper} (nm)	Final Y_{lower} (nm)	Final SH (nm)	Final Y_{upper} (nm)	Final Y_{lower} (nm)	Final SH (nm)	Final Y_{upper} (nm)	Final Y_{lower} (nm)	Final SH (nm)
1	687.9	687.0	0.8	688.6	687.8	0.8	699.7	698.7	1.1	699.8	698.8	0.9
2	699.5	698.0	1.5	699.5	698.0	1.5	699.6	698.1	1.6	699.5	698.1	1.4
3	726.8	725.5	1.2	702.1	700.9	1.2	699.5	698.0	1.4	699.5	698.2	1.3
Time (s)	153.8 with 5.7 psi			153.8 with 6 psi			152.1			155.0		
%Error	7.2	-	-	2.5	-	-	0.22	-	-	0.22	-	-
Stdev	-	-	0.3	-	-	0.3	-	-	0.3	-	-	0.2
Example 3	**No Control**			**Spatial Pressure Control**			**Spatial and Temporal Pressure Control**			**Look-Ahead Pressure Scheduling**		
Zone	Final Y_{upper} (nm)	Final Y_{lower} (nm)	Final SH (nm)	Final Y_{upper} (nm)	Final Y_{lower} (nm)	Final SH (nm)	Final Y_{upper} (nm)	Final Y_{lower} (nm)	Final SH (nm)	Final Y_{upper} (nm)	Final Y_{lower} (nm)	Final SH (nm)
1	730.4	730.0	0.4	701.6	701.3	0.4	699.4	698.4	1.0	699.5	698.5	0.9
2	699.5	698.0	1.5	699.6	698.1	1.4	699.3	697.6	1.7	699.6	698.0	1.6
3	660.4	658.6	1.8	692.3	690.6	1.7	699.6	697.9	1.7	699.7	698.2	1.6
Time (s)	153.8 with 5.7 psi			155.1 with 6 psi			154.5			156.0		
%Error	12.8	-	-	1.8	-	-	0.3	-	-	0.2	-	-
Stdev	-	-	0.7	-	-	0.7	-	-	0.4	-	-	0.4
Example 4	**No Control**			**Spatial Pressure Control**			**Spatial and Temporal Pressure Control**			**Look-Ahead Pressure Scheduling**		
Zone	Final Y_{upper} (nm)	Final Y_{lower} (nm)	Final SH (nm)	Final Y_{upper} (nm)	Final Y_{lower} (nm)	Final SH (nm)	Final Y_{upper} (nm)	Final Y_{lower} (nm)	Final SH (nm)	Final Y_{upper} (nm)	Final Y_{lower} (nm)	Final SH (nm)
1	696.1	695.3	0.8	664.8	664.1	0.7	699.7	699.2	0.5	700.1	699.6	0.5
2	814.8	814.3	0.5	699.8	699.4	0.4	699.6	698.9	0.7	699.7	699.1	0.6
3	699.8	699.4	0.4	699.7	699.3	0.4	699.4	698.9	0.5	699.6	699.1	0.5
Time (s)	171.8 with 5.5 psi			172.8 with 6.7 psi			171.8			173.0		
%Error	18.3	-	-	5.5	-	-	0.2	-	-	0.1	-	-
Stdev	-	-	0.2	-	-	0.2	-	-	0.1	-	-	0.1

Results for example 2,3 and 4

In the above tables, No control represents, applying just a uniform pressure across the die. The pressure is to be applied is calculated such that, the time taken by the no control algorithm equals the time taken by the other control algorithms. The error for the upper surface uniformity is calculated using the following equation.

$$\%Error = \sum_{i=1}^{n} sum\left(\left|\text{target surface} - \left(Y_{upper}\right)_i\right| / \left(Y_{upper}\right)_i^{init} - \text{target surface}\right) * 100$$

Stdev represents standard deviation between the step height values.

Our objective is to polish the initial variable pattern density surface such that, the final surface is uniform and has the minimum possible uniform step height all across the die. Hence the error for the step height is calculated in terms of standard deviation. The results for all the 4 sets of examples, clearly shows that, there is a significant improvement in the uniformity of the upper surface when the pressure across the die is controlled spatially. But this spatial pressure control, removes the upper as well as lower surfaces at varying rates. This results in higher deviation in step heights across the die. The results for spatial and temporal control as well as look-ahead scheduling show considerable improvement for both upper surface as well as step height deviation. It is realized that the combined spatial and temporal pressure control scheme is very difficult to realize in practice. To obviate this difficulty a predictive control strategy, called the "Look-Ahead Pressure Scheduling" is introduced. The results show that both of these schemes are equally effective. The results for Example 1 are shown next. Similar results are obtained for all four examples.

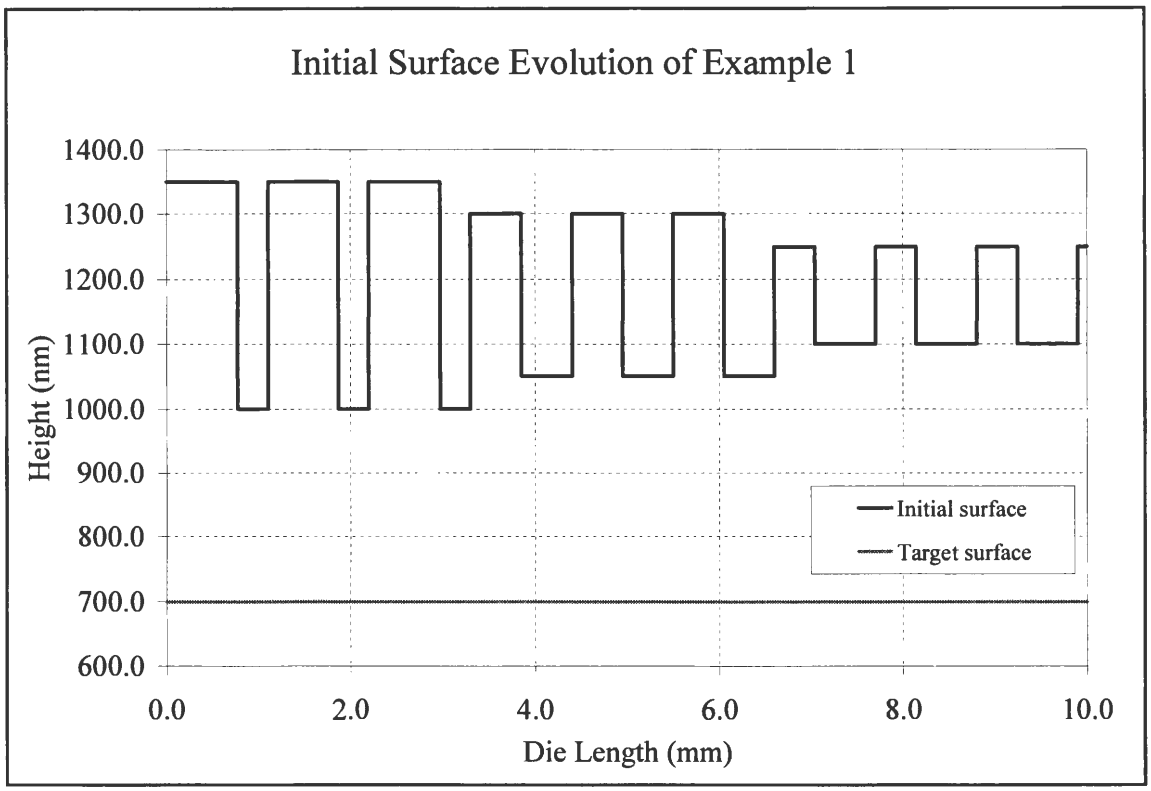

Figure 2.4 Initial or starting surface

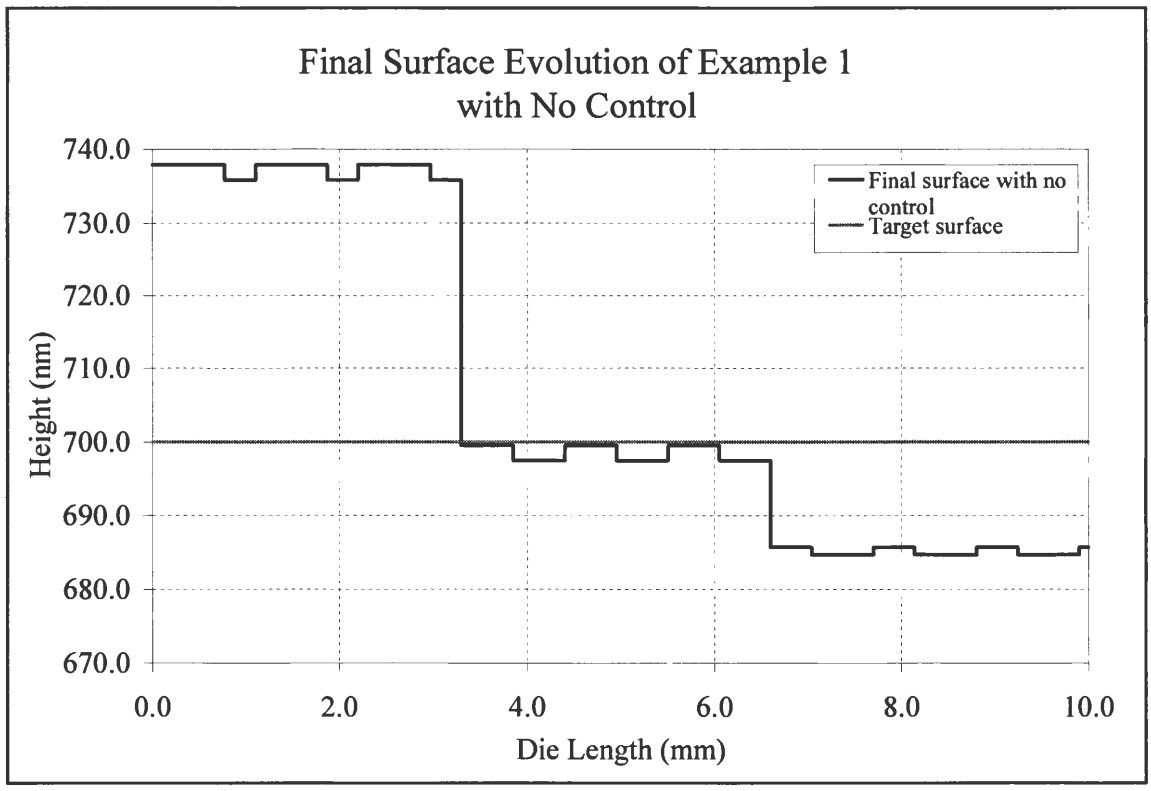

Figure 2.5 Final surface for "No Control "

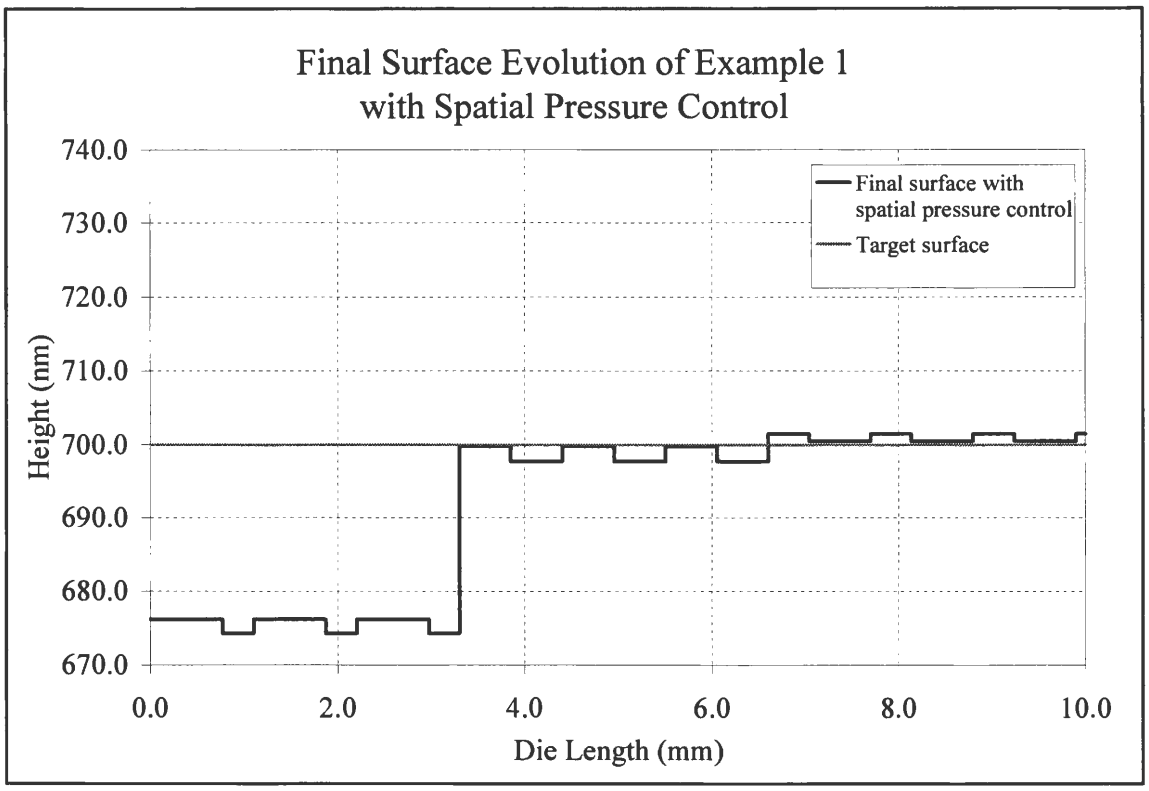

Figure 2.6 Final surface for "Spatial Pressure control"

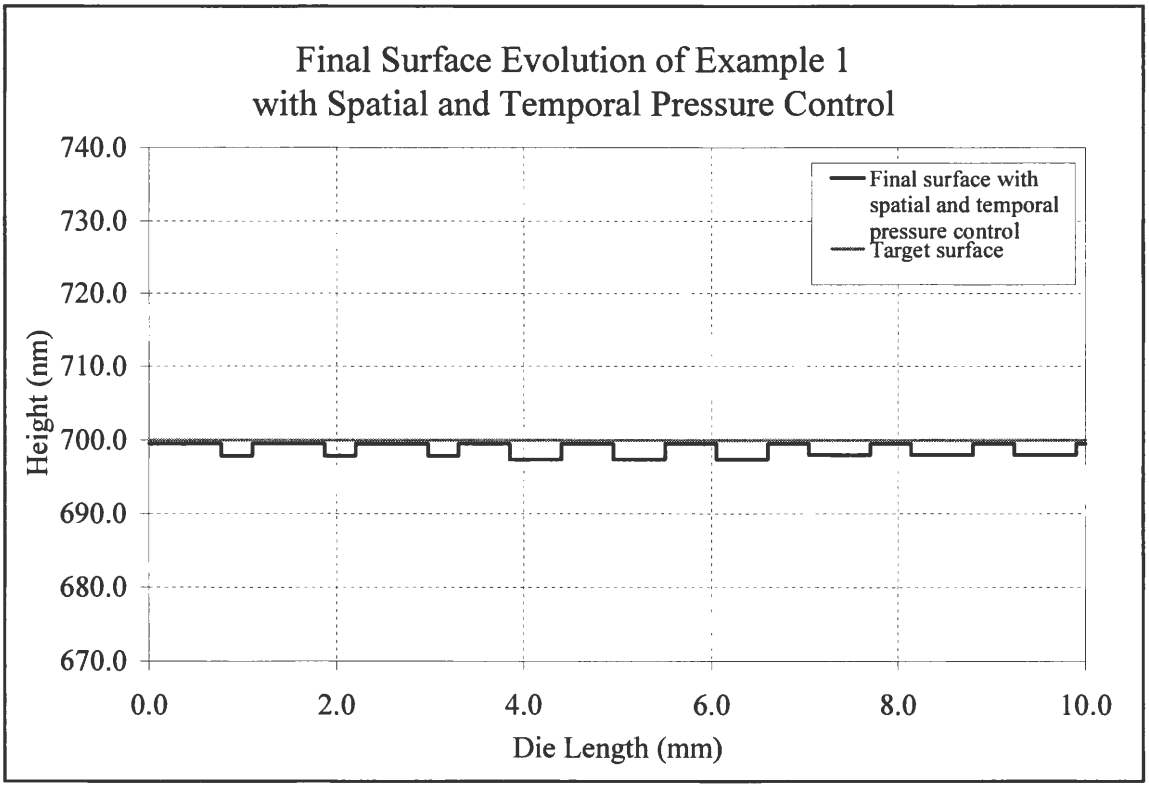

Figure 2.7 Final surface for "Spatial and Temporal pressure control

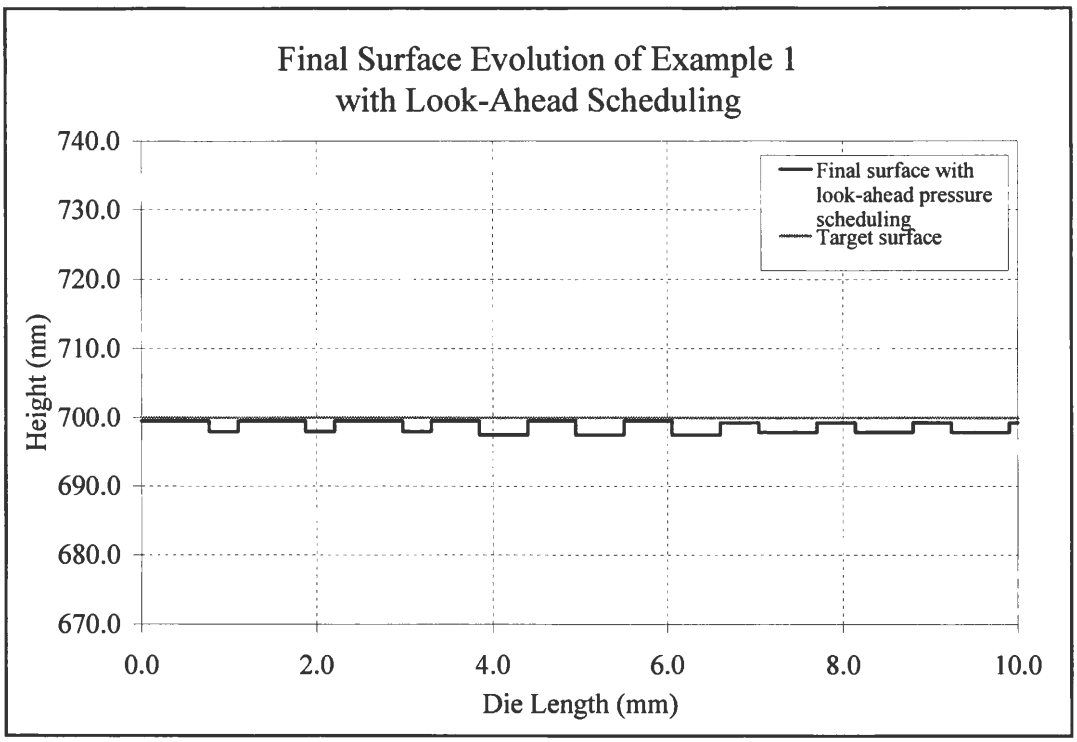

Figure 2.8 Final surface for "Look-ahead Scheduled Pressure control"

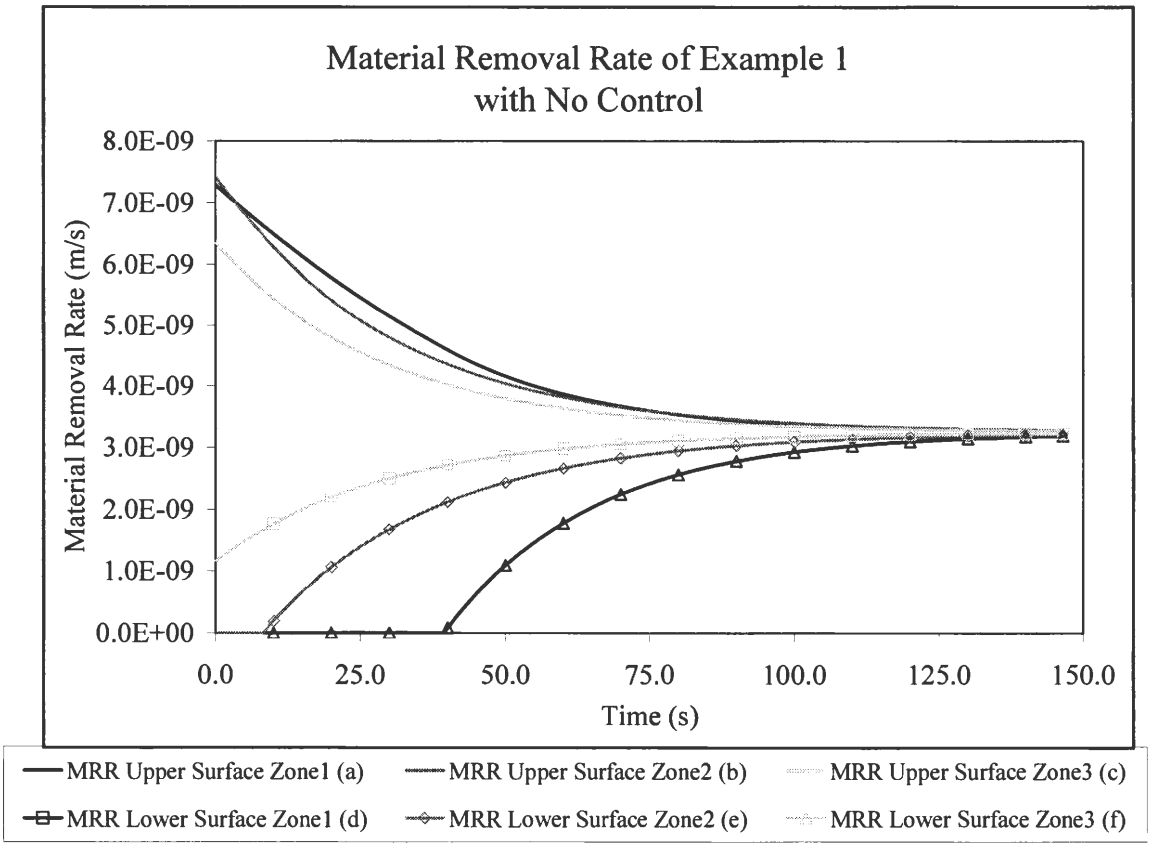

Figure 2.9 MRR vs. Time for "No control"

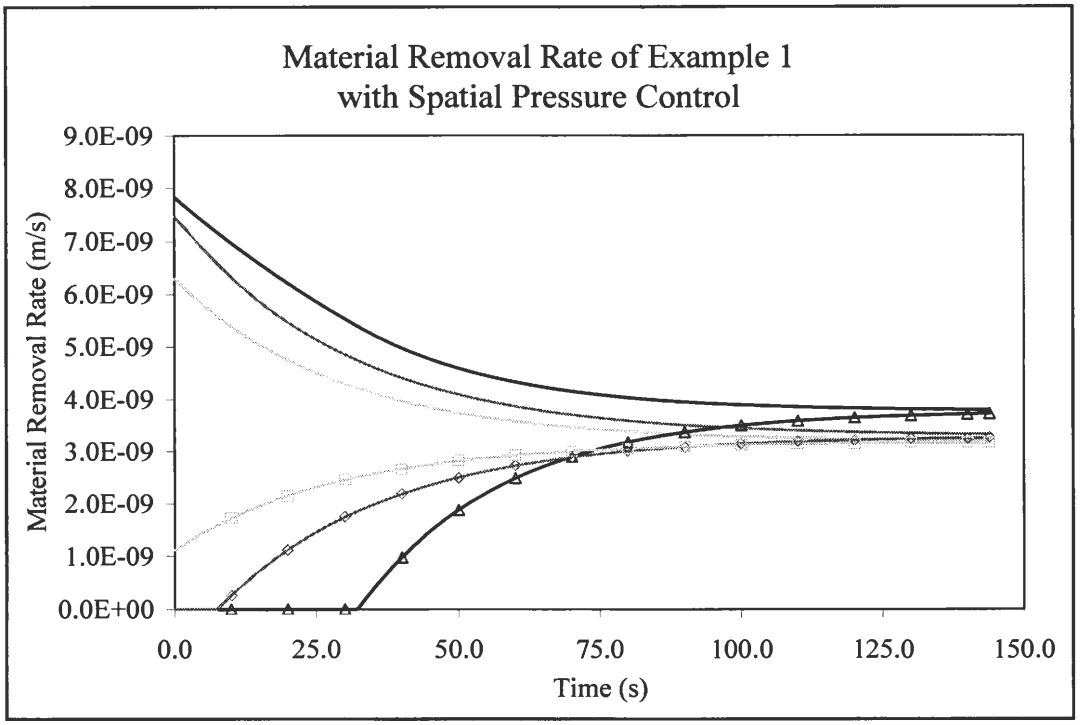

Figure 2.10 MRR vs. Time for "Spatial Pressure control

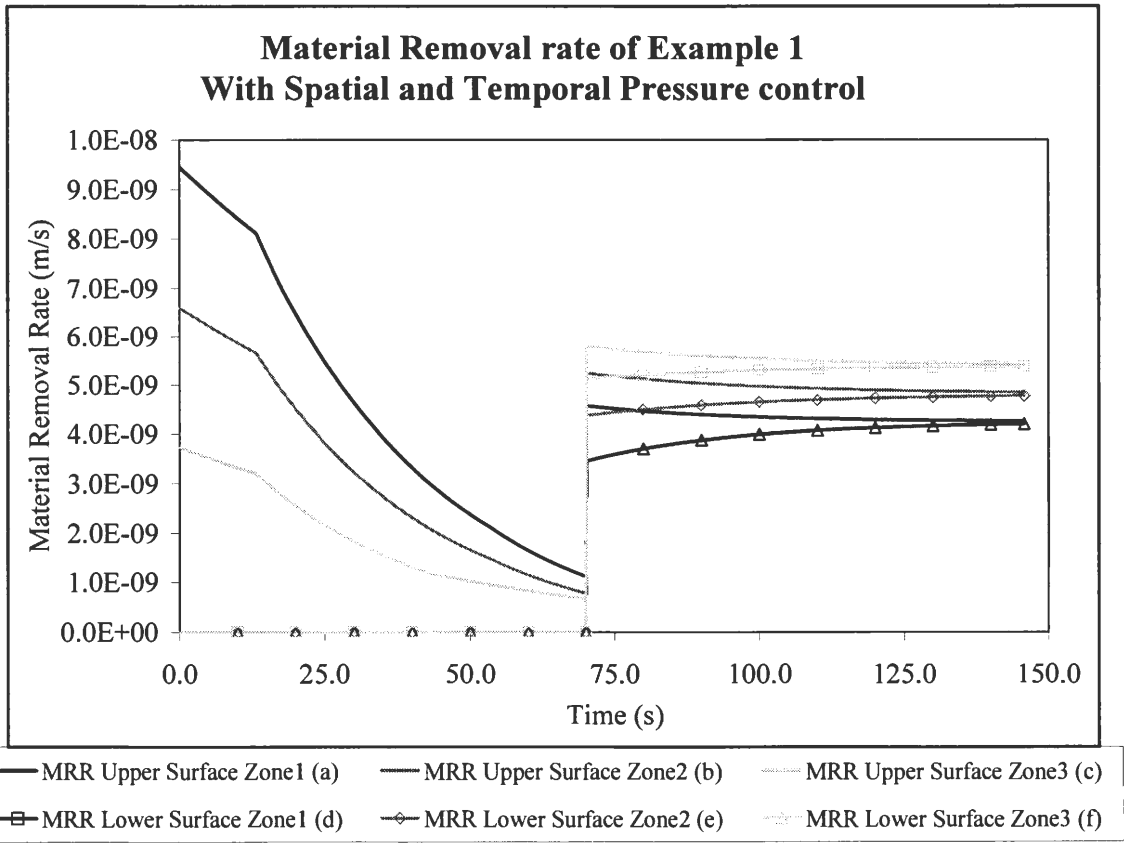

Figure 2.11 MRR vs. Time for "Spatial and Temporal"

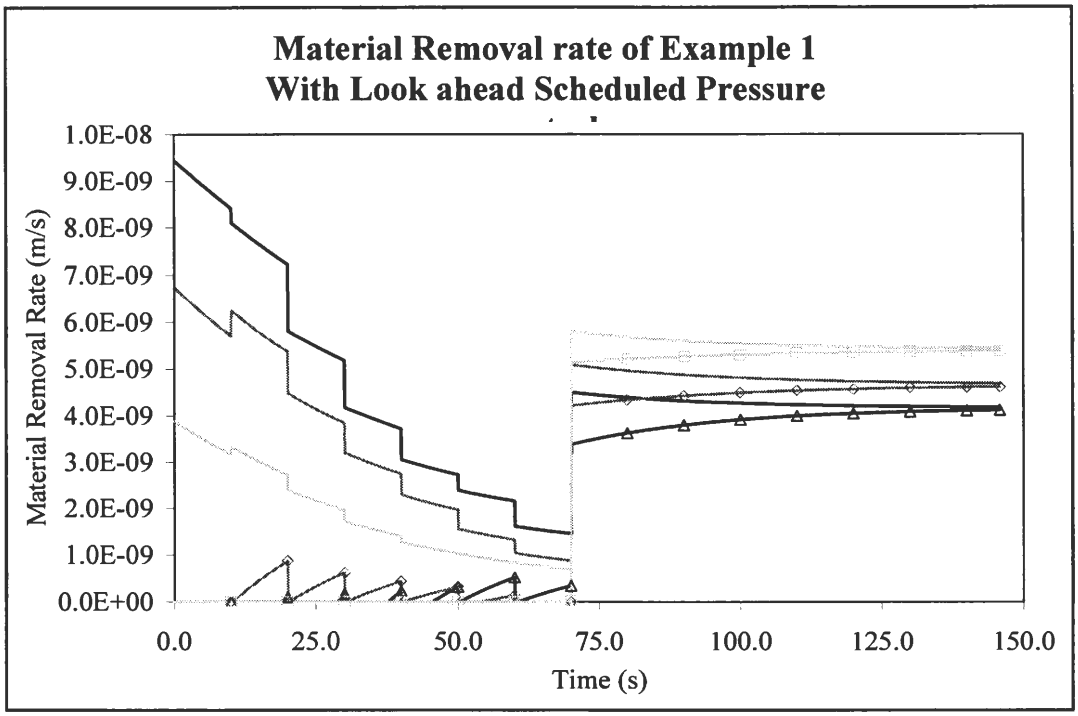

Figure 2.12 MRR vs. Time for Look Ahead control"

The series of graphs in the previous pages clearly show the distinctness between the various control algorithms. Figures 2.5, 2.6, 2.7 and 2.8 shows how the uniformity of the final upper surface as well as step heights is improved from one algorithm to another. Figures 2.10 and 2.11 show the material removal rate variation across the entire polishing time for spatial and temporal pressure controls. For the first 75 seconds, the MRR for lower surface is negligible. It is because of this reason that the step height is controlled and brought to the minimum value. For this example, the uniformity of the step height is achieved by proper variation of pressure value across the die within the first 75 seconds. In the look-ahead control, there is a small variation in the MRR for lower surface in the first 75 seconds. But that is the lowest possible MRR that can be achieved on the lower surface using this algorithm. The variation or the sudden change in the MRR after the first 75 seconds in Figure 2.10 and 2.11 is due to the change of algorithm to spatial control.

2.6 Error analysis

The models and the results clearly states how pressure and/or velocity can be used as control variables to govern the uniformity of the final surface evolution. It should be noted that at in reality for every polishing time step, a measurement feed back is necessary to identify the current surface measurements (Upper surface and Step Height). The following error analysis provides an idea about the tolerance level of the simulation based on measurement errors during feed back.

The analysis is done in 2 stages on the Look Ahead Pressure Scheduling model. Let us assume that at a particular time step, the actual surface measurement value as "Current value". In the first stage, a measurement error of $\pm$ X value is implanted in the simulation, such that every time the surface measurement is taken, the simulation identifies the new number randomly between the current value + X and current value – X values. The new "to be" applied pressure is calculated using this randomly generated surface measurement and this pressure is applied over the original surface value that is the current value. In this way, the simulation is tested for a real polishing condition with error. The values of X that is taken for the analysis are 2, 4, 6, 8 and 10 nm. In the second stage, instead of obtaining a random value from the tolerance, a definite measurement error is added to the current surface value. The final top surface error and step height error is calculated for this measurement error.

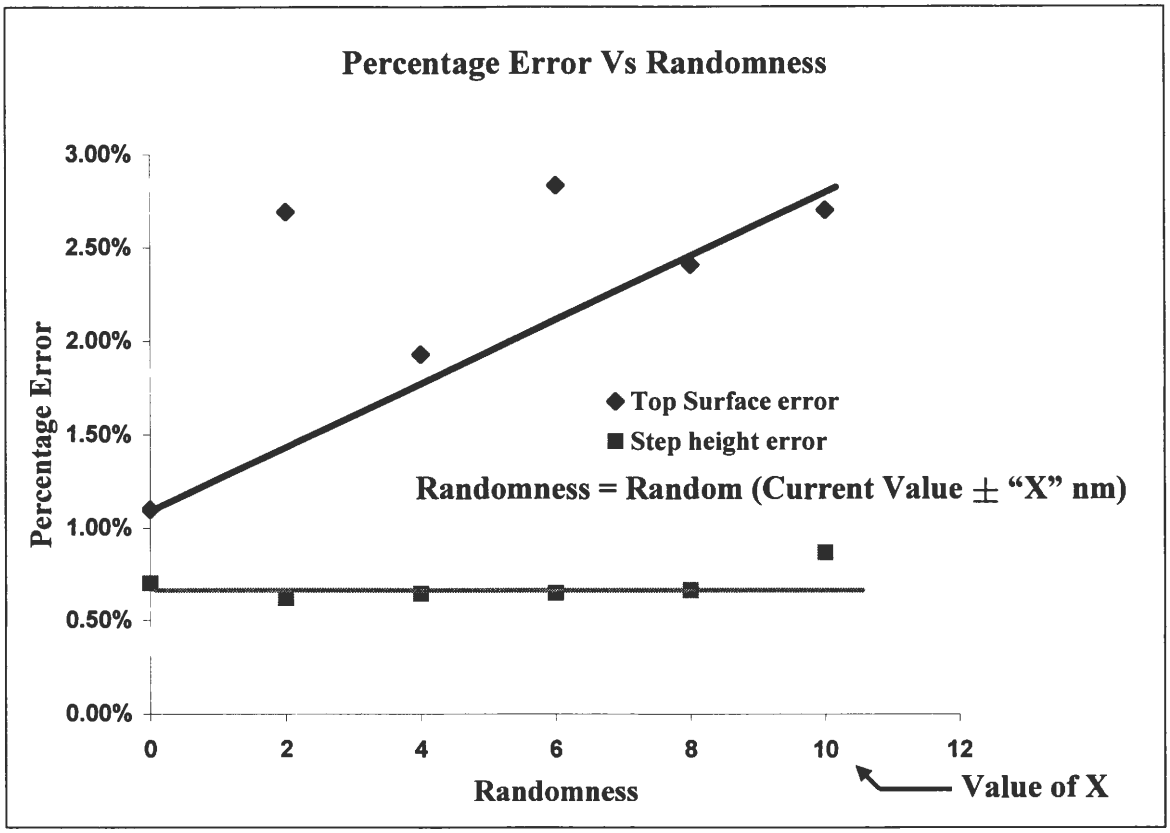

Figure 2.13 Error graph with randomness within Tolerance

The simulation was recoded with the necessary details, and was run for test data with an error of ± 2, 4, 6, 8 and 10. Total of 10 runs was undertaken for each tolerance and the top surface error and step height error were tabulated. The average top surface error and step height error for each tolerance band is calculated. The final error values are shown in Figure 2.13. The graph shows that, there is no significant change in the final error value for the step height, although the top surface error increases as the tolerance band increases. Figure 2.14 shows the error as percentage for a specific measurement error. For example, every time a measurement feedback is provided to the simulation algorithm, an error of 4 nm is added or subtracted through out the simulation process. Hence the error is termed as peak error

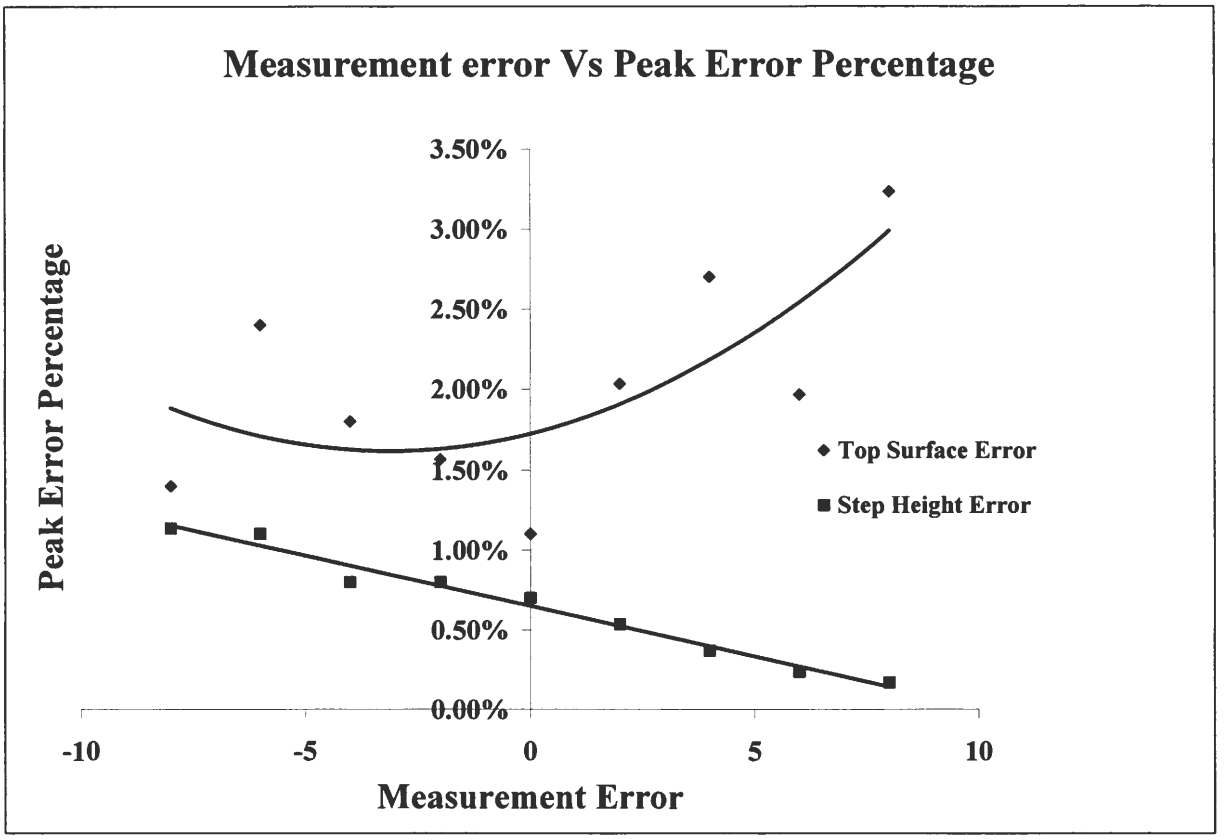

Figure 2.14 Error graph with NO randomness and fixed error

possible with that measurement error. The graph in Figure 2.14 shows that the step height is again within a small tolerance band of 0.3 to 1.2 %. There is no significant change in the final step height values even with a large error, but for the top surface error, the error percentage increases as the error in measurement increases.

CHAPTER 3. Yield Improvement via minimization of step height non-uniformity in Chemical Mechanical Planarization (CMP) with pressure and velocity as control variables

3.1 Background

There is a need to look into the possibility of controlling the global step height formation, in order to obtain uniformity in the final surface evolution. Based on the understanding from the analytical model by Fu et al [2003], it is determined that the surface evolution mainly depends on the amount of pressure and velocity that is applied. Therefore in order to obtain uniform surface evolution on a surface that has variable pattern densities and step heights, the option of varying pressure and velocity across the die is considered. Then the problem is approached in two different ways.

1. Here the pressure alone is varied, but in both spatial as well as temporal, and the results were analyzed. The results showed us significant improvement in the final surface evolution.
2. Based on the relationship between velocity and step height formation, we later decided to vary velocity across the die scale along with pressure.

Hence, based on the effective pattern density in a region, and utilizing the step height reduction model developed by Fu et al [2003], this paper provides a control based open loop algorithm to obtain uniformity over the pattern dependant non uniform wafer surfaces in a die scale using pressure and velocity variations.

The model assumes the die in the wafer surface to have 'n' number of zones of different heights and different pattern densities. In order to minimize both local and global step height variations, the applied pressure and velocity is varied spatially. The variation is done such that, the pressure and velocities across the pattern (spatial) are varied individually and later varied simultaneously. A 2D simulation process is devised using visual basic to track the amount of removal, and current step heights for every time step. The assumptions, notations and the relations used are same as in previous chapter.

3.2. Model description

3.2.1 Velocity control – algorithm (Appendix - Flow chart – II)

In the previous algorithm, the pressure is varied spatially across the die. From the results, we came to an understanding that, this variation of pressure would only help us achieve a uniform upper surface. This means, we cannot control the step height to achieve local planarity. Based on the equations from the Fu et al model it can be easily identified that the step height is proportional to the relative velocity between the wafer surface and the pad. An algorithm is devised in such a way that variable velocities are applied in a proportional way across the die, over the 'n' zones, such that both global and local step heights are minimized.

Step 1. *Calculate Total Material*

- Calculate **the total material** (***Mat _Total***) to be removed in all zones together. This step and step 4.2 are used together to find when the polishing process will finish.

$$Mat\_Total = \sum_{i=1}^{n} \left(Y_{upper}(i) - Y_{desired} \right)$$

Step 2. *Calculate Time Needed*

- The total **polishing time needed** for each zone is calculated with a specified velocity and a desired step height using equation 1.

Step 3. *Calculate Velocity for Each Zone*

- Find the **minimum polishing time needed** among all zones. The reason being, to ensure that the polishing process even though may leave some material behind (which can be removed later) but doesn't remove more than required.

$$TimeNeeded = Min(T_{needed}(step2)) \quad \text{, For i = 1 to n}$$

- Calculate the **velocity** for each zone using the equation with time equal to the ***TimeNeeded*** (calculated from step 3).

Step 4. *Calculate Applied Pressure, Calculate Step Height* and *Check*

- With the given or initial interface pressure the following sub routines 4.1 and 4.2 are run. The error for the iterations are calculated and compared. The procedure is carried out till the pressure corresponding to the smallest error is determined. In the iteration the starting interface pressure is 1 psi with increment interface pressure of 0.1 psi.

4.1 *Calculate Step Height*

- Calculate the **new upper and lower surface** for each zone by varying the variables a, b, Y_{upper}, Y_{lower} and with the **given range of interface pressure**.

$$Y_{upper}(i)^{new} = Y_{upper}(i)^{old} - Y_{UpRate}(i).\Delta t \quad \text{, For i = 1 to n}$$

$$Y_{lower}(i)^{new} = Y_{lower}(i)^{old} - Y_{LoRate}(i).\Delta t \quad \text{, For i = 1 to n}$$

Where Δt = 0.1 sec

4.2 *Check*

- Compare the total material left with the previous step till it reaches the least total material left. If it is not, go back to step 4.1 and calculate the new upper and lower surface again.

Step 5. *Simulation*

- The polishing procedure is simulated to verify the solution, using the best interface pressure.

Step 6. *Calculate Error* and *Verify*

6.1 *Calculate Error*

- The **error for upper surface and step height** for each zone is calculated using the following equations.

$$Error_{upper} = (Y_{upper}(final)_i - Y_{desired}) / (Y_{upper}(0)_i - Y_{desired}) \times 100$$

$$Error_{step\ height} = (Y_{upper}(final)_i - Y_{lower}(final)_i) / (Y_{upper}(0)_i - Y_{lower}(0)_i) \times 100$$

6.2 *Verification*

- Using equation 1 the final step height is calculated and it is then compared with the difference between MRR_{upper} and MRR_{lower}.

By using the spatial velocity control, there is a possibility that better step height can be evolved. Whereas the spatial pressure control helps us attain an uniform upper surface.

Hence based on the 2 individual variable control process, a procedure was devised to calculate a proportional velocity and pressure for each zone in order to attain uniform surface with uniformly proportional step heights after a specific period of time.

3.2.2 Pressure and velocity control – algorithm (Appendix - Flow chart –III)

As explained earlier controlling pressure and velocity separately doesn't result in local and global planarity. Hence there is a need to control both the variables simultaneously. The following algorithm, explains the procedure for combined pressure and velocity control.

Step 1. *Calculate Total Material*

- Calculate **the total material** to be removed in all zones together. This step and step 4.2 are used together to find when the polishing process will finish.

$$Mat\_Total = \sum_{i=1}^{n} \left(Y_{upper}(i) - Y_{desired} \right)$$

Step 2. *Calculate Time Needed*

- The total **polishing time needed** for each zone is calculated with a specified velocity and a desired step height using equation 1.

Step 3. *Calculate Velocity of Each Zone*

- Find the **minimum polishing time needed** among all zones. The reason being, to ensure that the polishing process even though may leave some material behind (which can be removed later) but doesn't

  $TimeNeeded = Min(T_{needed}(step2))$, For i = 1 to n

- Calculate the **velocity** for each zone using the equation with time equal to the ***TimeNeeded*** (calculated from step 3).

Step 4. *Calculate Applied Pressure*

- Using equation 3 the **applied interface pressure** is calculated with **time needed** and **velocity** of each zone values calculated from the previous steps.

Step 5. *Calculate Step Height* and *Calculate Check Done*

5.1 *Calculate StepHeight*

- Calculate the **new upper and lower surface** of each zone via vary variables (a, b, Y_{upper}, Y_{lower}), fixed variables (K, V, α, k), and **applied interface pressure** computed from step 4.

$$Y_{upper}(i)^{new} = Y_{upper}(i)^{old} - Y_{UpRate}(i).\Delta t \qquad \text{, For i = 1 to n}$$

$$Y_{lower}(i)^{new} = Y_{lower}(i)^{old} - Y_{LoRate}(i).\Delta t \qquad \text{, For i = 1 to n}$$

Where Δt = 0.1 sec

5.2 *Check*

- Compare the total material left with the previous step till it reaches the least total material left. If it is not, go back to step 5.1 and keep calculate the new upper and lower surface again.

Step 6. *Calculate Error* and *Verification*

6.1 *Calculate Error*

- The **error for upper surface and step height** for each zone is calculated using the following equations.

$$Error_{upper} = (Y_{upper(final)i} - Y_{desired}) / (Y_{upper(0)i} - Y_{desired}) \times 100$$

$$Error_{step\ height} = (Y_{upper(final)i} - Y_{lower(final)i}) / (Y_{upper(0)i} - Y_{lower(0)i}) \times 100$$

6.2 *Verification*

- Using equation 1 the final step height is calculated and it is then compared with the difference between MRR_{upper} and MRR_{lower}.

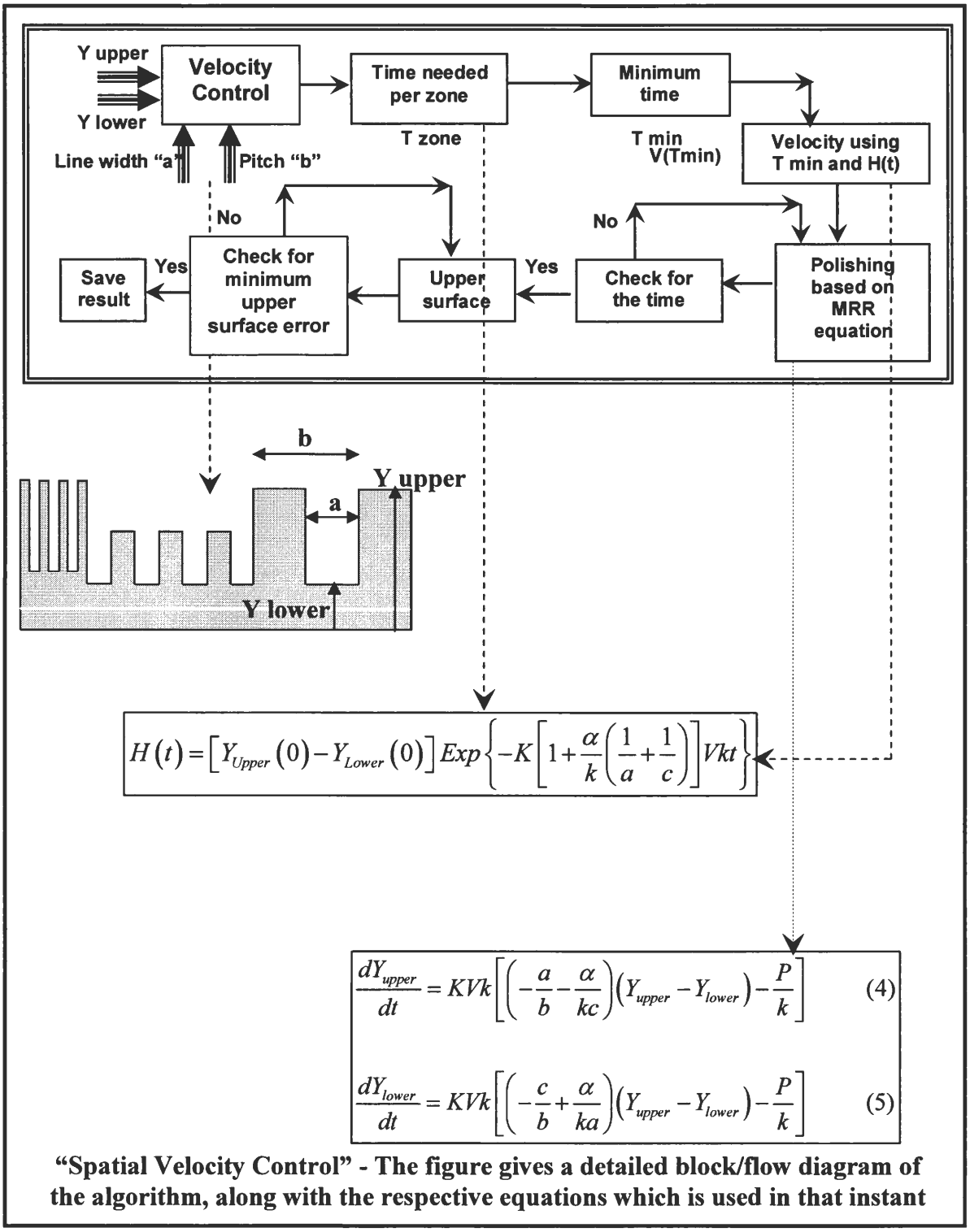

"Spatial Velocity Control" - The figure gives a detailed block/flow diagram of the algorithm, along with the respective equations which is used in that instant

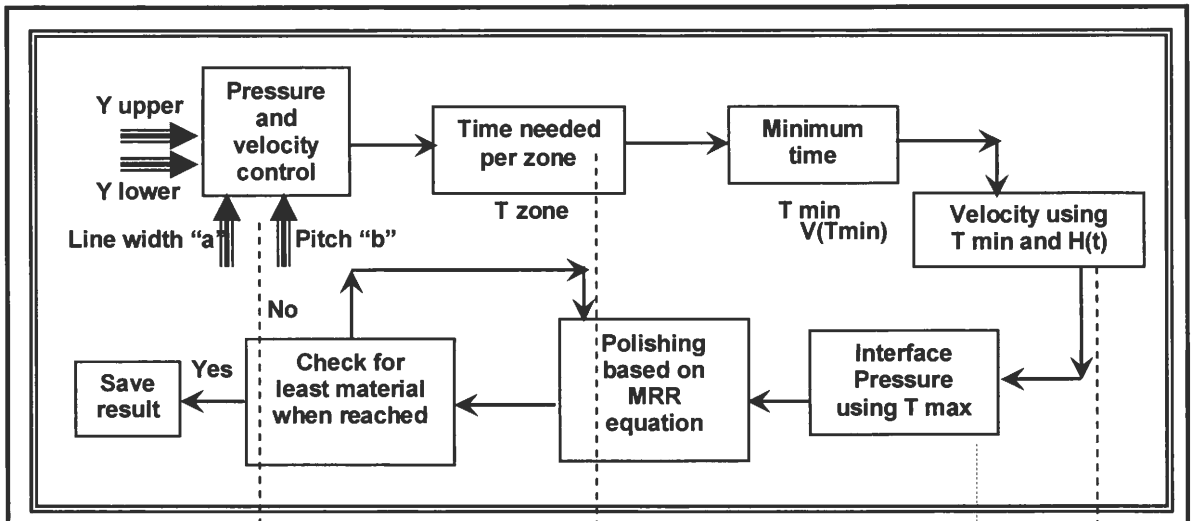

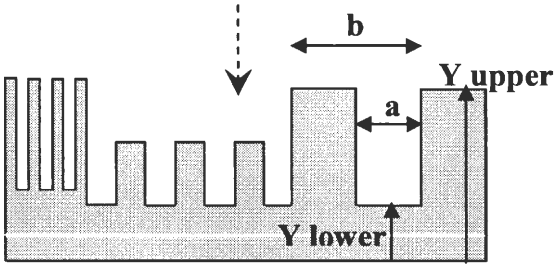

$$H(t) = \left[Y_{Upper}(0) - Y_{Lower}(0)\right] Exp\left\{-K\left[1 + \frac{\alpha}{k}\left(\frac{1}{a} + \frac{1}{c}\right)\right] Vkt\right\}$$

$$\frac{dY_{upper}}{dt} = KVk\left[\left(-\frac{a}{b} - \frac{\alpha}{kc}\right)\left(Y_{upper} - Y_{lower}\right) - \frac{P}{k}\right] \quad (4)$$

$$\frac{dY_{lower}}{dt} = KVk\left[\left(-\frac{c}{b} + \frac{\alpha}{ka}\right)\left(Y_{upper} - Y_{lower}\right) - \frac{P}{k}\right] \quad (5)$$

"Spatial Pressure and Velocity Control" - The figure gives a detailed block/flow diagram of the algorithm, along with the respective equations which is used in

3.3 Results

Table 1 has the examples which are taken into consideration for checking the algorithm. It is assumed that the die has 3 different pattern densities, and hence divided into 3 zones. The table has the upper and lower surface heights for each zones. In the first and third example, the heights and pattern densities are reversed. Example 2 and 4 are random variations and they lie along the value range of 1 and 3.

The constants are [Stavreva et al 1997]

K	Preston's constant	$=1.566 * 10^{-13}\ m^2/N$
k	Stiffness	$=8.027 * 10^{10}\ N/m^3$
α	Bending factor	$=2.16 * 10^{6}\ N/m$
V	Velocity	$=0.5\ m/s$

Zone	Example 1			Example 2			Example 3			Example 4		
	Initial Y_{upper} (nm)	Initial Y_{lower} (nm)	a/b	Initial Y_{upper} (nm)	Initial Y_{lower} (nm)	a/b	Initial Y_{upper} (nm)	Initial Y_{lower} (nm)	a/b	Initial Y_{upper} (nm)	Initial Y_{lower} (nm)	a/b
1	1350	1000	0.3	1250	1000	0.3	1250	1100	0.3	1350	1000	0.3
2	1300	1050	0.5	1300	1050	0.5	1300	1050	0.5	1400	1250	0.5
3	1250	1100	0.6	1350	1100	0.6	1350	1000	0.6	1300	1150	0.6

Example sets

For Ex1, using stopping criteria of step height = 1.7 nm

For Ex2, using stopping criteria of step height = 1.2 nm

For Ex3, using stopping criteria of step height = 1.2 nm

For Ex4, using stopping criteria of step height = 0.5 nm

Ex. 1	No Control			Spatial Pressure Control			Velocity Control			Spatial Pressure and Velocity Control		
Zone	Final Y_{upper} (nm)	Final Y_{lower} (nm)	Final SH (nm)	Final Y_{upper} (nm)	Final Y_{lower} (nm)	Final SH (nm)	Final Y_{upper} (nm)	Final Y_{lower} (nm)	Final SH (nm)	Final Y_{upper} (nm)	Final Y_{lower} (nm)	Final SH (nm)
1	737.9	735.8	2.1	676.2	674.3	1.9	724.1	721.6	2.4	678.9	676.6	2.3
2	699.5	697.5	2.1	699.8	697.7	2.1	641.8	640.1	1.7	699.7	697.9	1.7
3	685.7	684.7	1.0	701.5	700.5	1.0	698.0	696.3	1.7	701.9	700.1	1.7
Time(s)	144.1 with 6.1 psi			143.8 with 7 psi			129.9			129.9		
%Error	8.1	-	-	3.9	-	-	15.3	-	-	4.2	-	-
Stdev	-	-	0.6	-	-	0.5	-	-	0.4	-	-	0.3

Ex. 2	No Control			Spatial Pressure Control			Velocity Control			Spatial Pressure and Velocity Control		
Zone	Final Y_{upper} (nm)	Final Y_{lower} (nm)	Final SH (nm)	Final Y_{upper} (nm)	Final Y_{lower} (nm)	Final SH (nm)	Final Y_{upper} (nm)	Final Y_{lower} (nm)	Final SH (nm)	Final Y_{upper} (nm)	Final Y_{lower} (nm)	Final SH (nm)
1	687.9	687.0	0.8	688.6	687.8	0.8	714.0	712.6	1.5	692.3	690.8	1.5
2	699.5	698.0	1.5	699.5	698.0	1.5	655.1	653.9	1.2	699.7	698.5	1.3
3	726.8	725.5	1.2	702.1	700.9	1.2	698.9	697.7	1.2	702.7	701.4	1.2
Time(s)	153.8 with 5.7 psi			153.8 with 6 psi			138.6			137.8		
%Error	7.2	-	-	2.5	-	-	10.9	-	-	1.9	-	-
Stdev	-	-	0.3	-	-	0.3	-	-	0.2	-	-	0.1

Ex. 3	No Control			Spatial Pressure Control			Velocity Control			Spatial Pressure and Velocity Control		
Zone	Final Y_{upper} (nm)	Final Y_{lower} (nm)	Final SH (nm)	Final Y_{upper} (nm)	Final Y_{lower} (nm)	Final SH (nm)	Final Y_{upper} (nm)	Final Y_{lower} (nm)	Final SH (nm)	Final Y_{upper} (nm)	Final Y_{lower} (nm)	Final SH (nm)
1	730.4	730.0	0.4	701.6	701.3	0.4	831.6	830.3	1.2	703.1	701.9	1.2
2	699.5	698.0	1.5	699.6	698.1	1.4	697.0	695.7	1.2	699.6	698.4	1.3
3	660.4	658.6	1.8	692.3	690.6	1.7	642.5	642.5	1.2	690.9	689.6	1.3
Time(s)	153.8 with 5.7 psi			155.1 with 6 psi			125.3			124.6		
%Error	12.8	-	-	1.8	-	-	34.9	-	-	2.3	-	-
Stdev	-	-	0.7	-	-	0.7	-	-	0	-	-	0

Results for example 1, 2 and 3

Ex. 4	No Control			Spatial Pressure Control			Velocity Control			Spatial Pressure and Velocity Control		
Zone	Final Y_{upper} (nm)	Final Y_{lower} (nm)	Final SH (nm)	Final Y_{upper} (nm)	Final Y_{lower} (nm)	Final SH (nm)	Final Y_{upper} (nm)	Final Y_{lower} (nm)	Final SH (nm)	Final Y_{upper} (nm)	Final Y_{lower} (nm)	Final SH (nm)
1	696.1	695.3	0.8	664.8	664.1	0.7	684.9	684.1	0.8	665.7	664.9	0.7
2	814.8	814.3	0.5	699.8	699.4	0.5	798.9	798.4	0.5	699.7	699.2	0.5
3	699.8	699.4	0.4	699.7	699.3	0.4	701.2	700.1	0.5	700.0	699.5	0.5
Time (s)	171.8 with 5.5 psi			172.8 with 6.7 psi			165.4			165.5		
%Error	18.3	-	-	5.5	-	-	17.7	-	-	5.3	-	-
Stdev	-	-	0.2	-	-	0.2	-	-	0.2	-	-	0.1

Results for example 4

In the above tables, No control represents, applying just a uniform pressure across the die. The pressure is to be applied is calculated such that, the time taken by the no control algorithm equals the time taken by the spatial pressure control algorithm. The error for the upper surface uniformity is calculated using the following equation.

$$\%Error = \sum_{i=1}^{n} sum\left(\left|\text{target surface} - \left(Y_{upper}\right)_i\right| / \left(\left(Y_{upper}\right)_i^{init} - \text{target surface}\right)\right) * 100$$

Stdev represents standard deviation between the step height values.

Our objective is to polish the initial variable pattern density surface such that, the final surface is uniform and has the minimum possible uniform step height all across the die. Hence the error for the step height is calculated in terms of standard deviation. The results for all the 4 sets of examples, clearly shows that, there is a significant improvement in the uniformity of the upper surface when the pressure across the die is controlled spatially.

But this spatial pressure control, removes the upper as well as lower surfaces at varying rates. This results in higher deviation in step heights across the die. The results for

velocity control show considerable step height deviation. Based on the results, we then decided to combine both the algorithms, such that through out the entire process both pressure and velocity is controlled spatially. The results show that this method produces results which have significant improvement in both upper surface as well as step heights. The results for Example 1 are shown next. Similar results are obtained for all four examples. It can be noted that, the combined pressure and velocity control provides results very similar to the temporal pressure controls in the previous chapter.

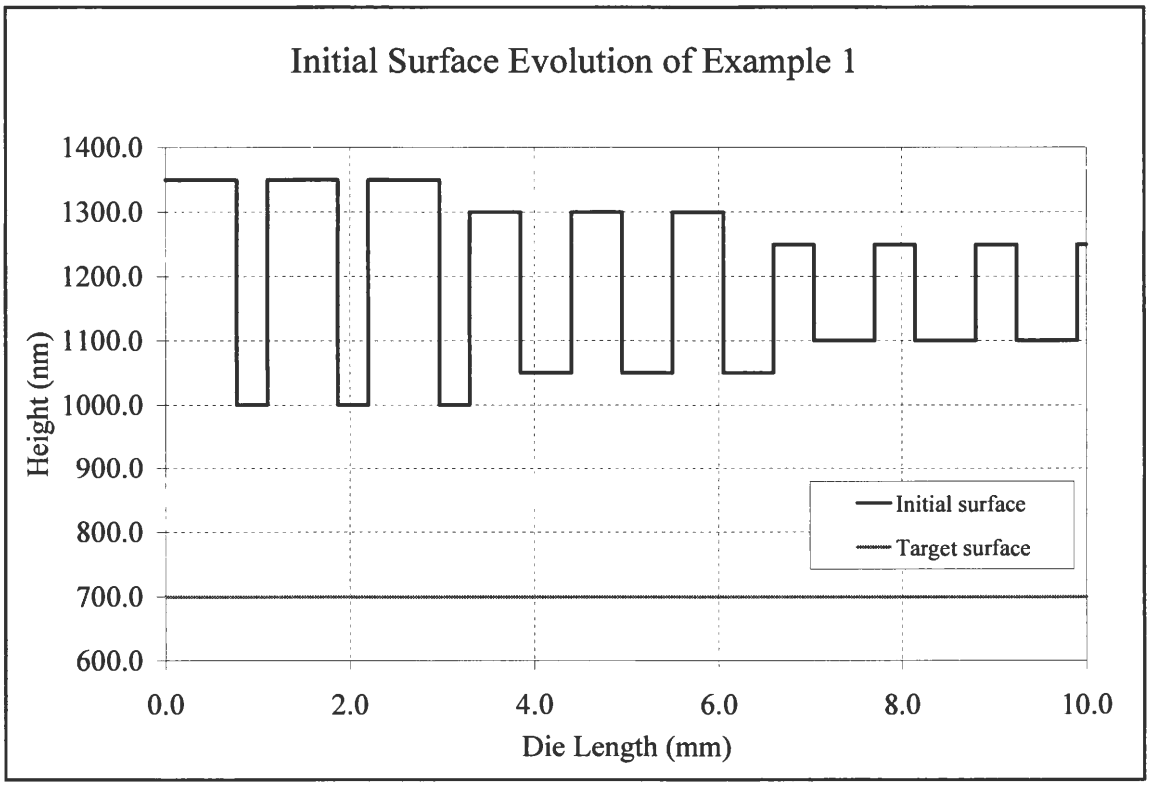

Figure 3.1 Initial or starting surface

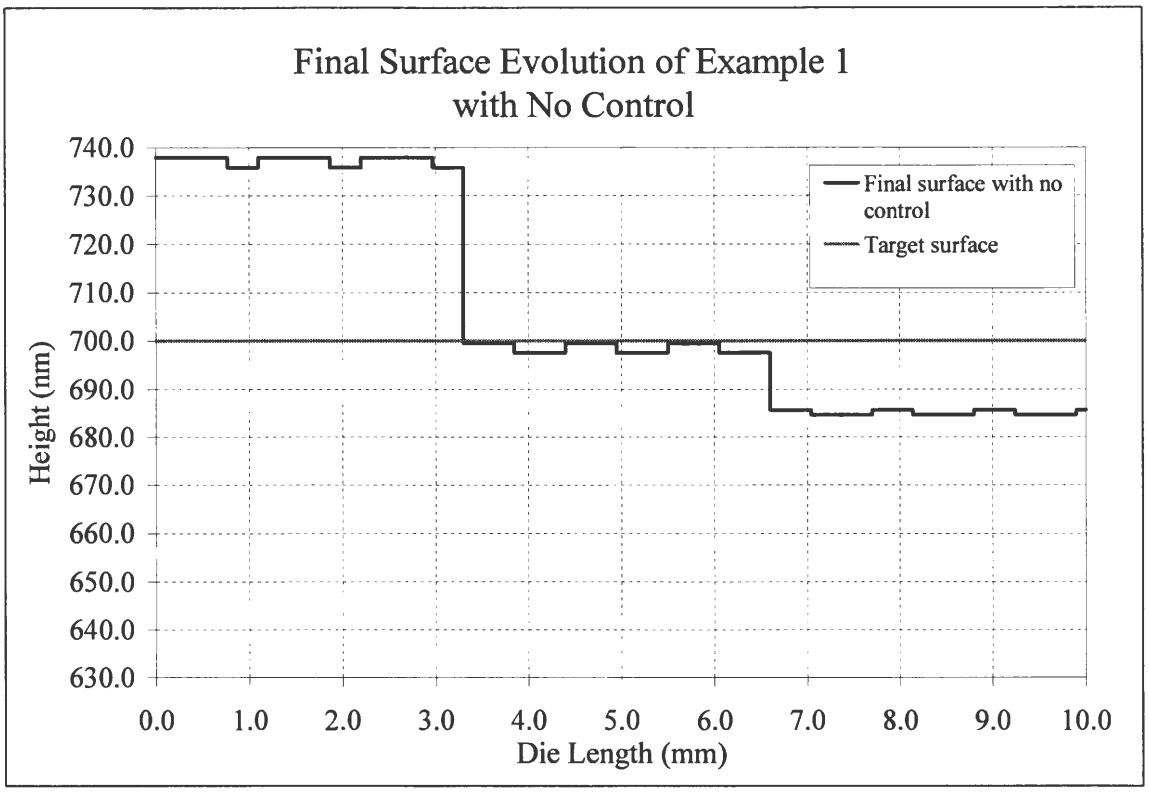

Figure 3.2 Final surface for "No control"

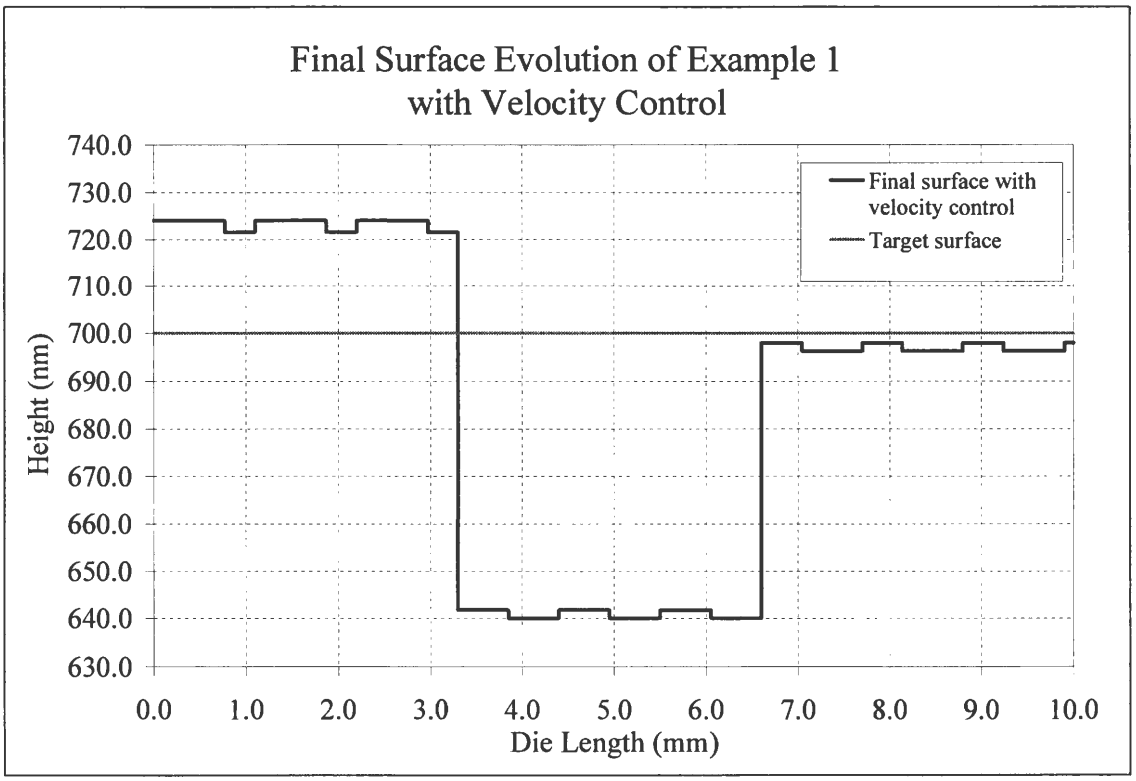

Figure 3.3 Final surface for "Spatial velocity control"

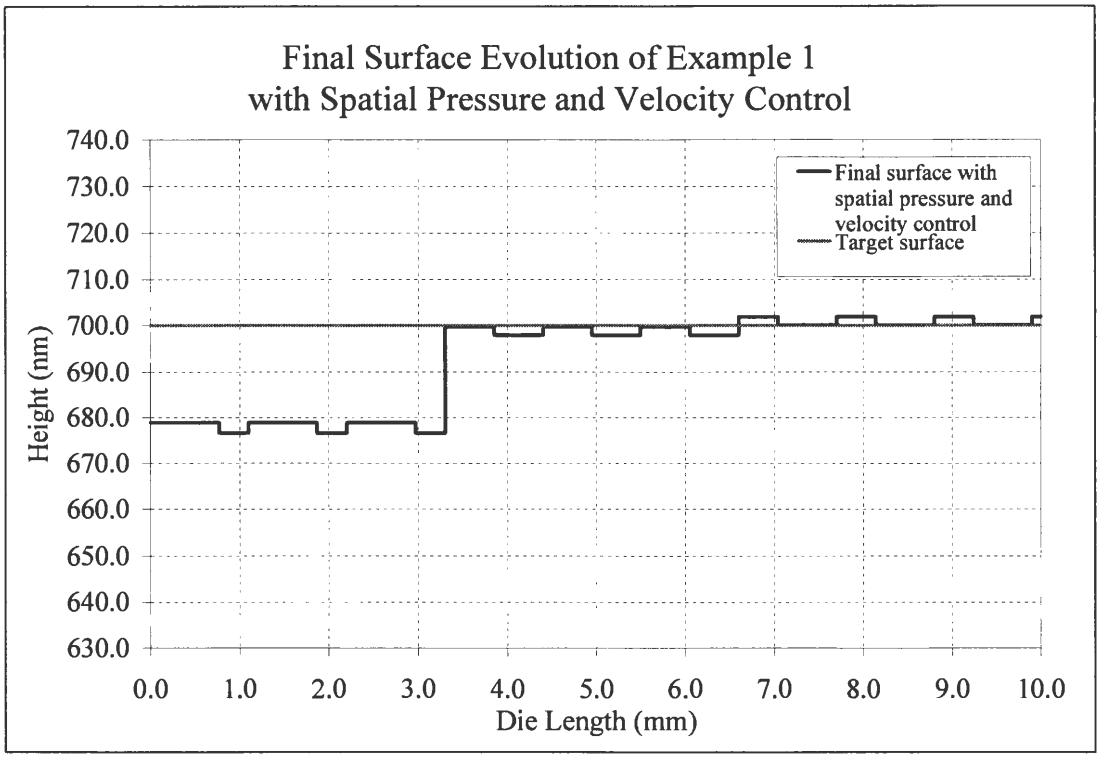

Figure 3.4 Final surface for "Spatial Pressure and Velocity control"

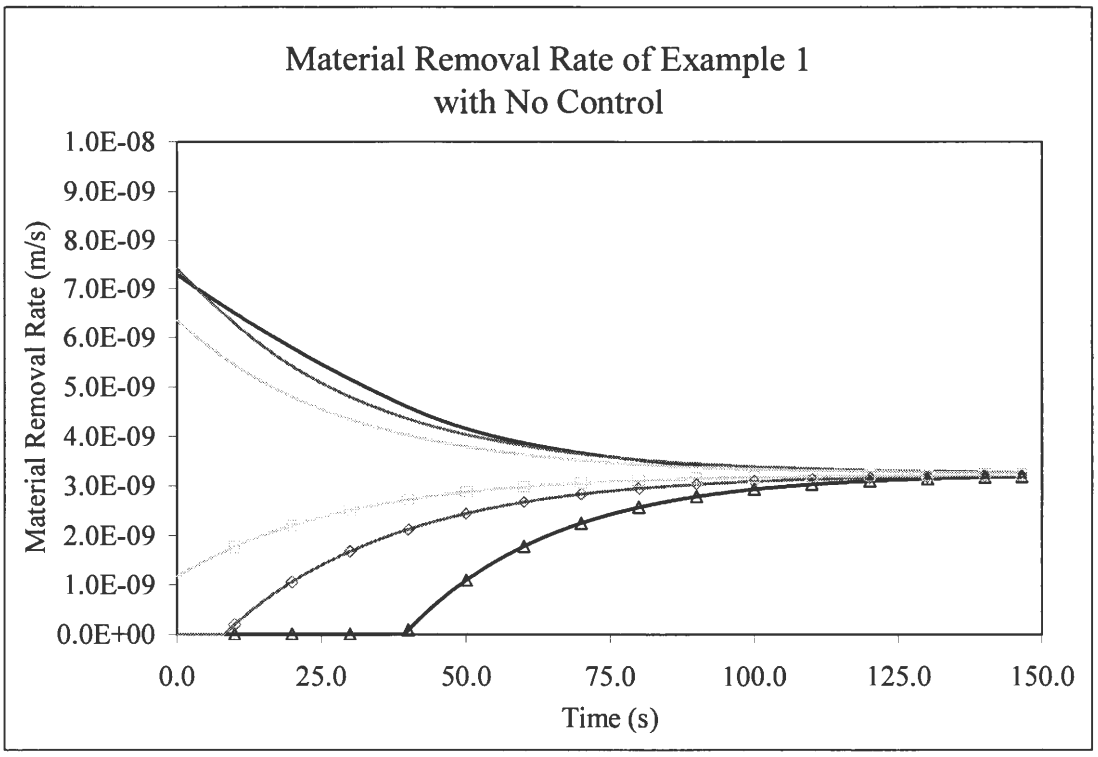

Figure 3.5 MRR vs. Time for "No control"

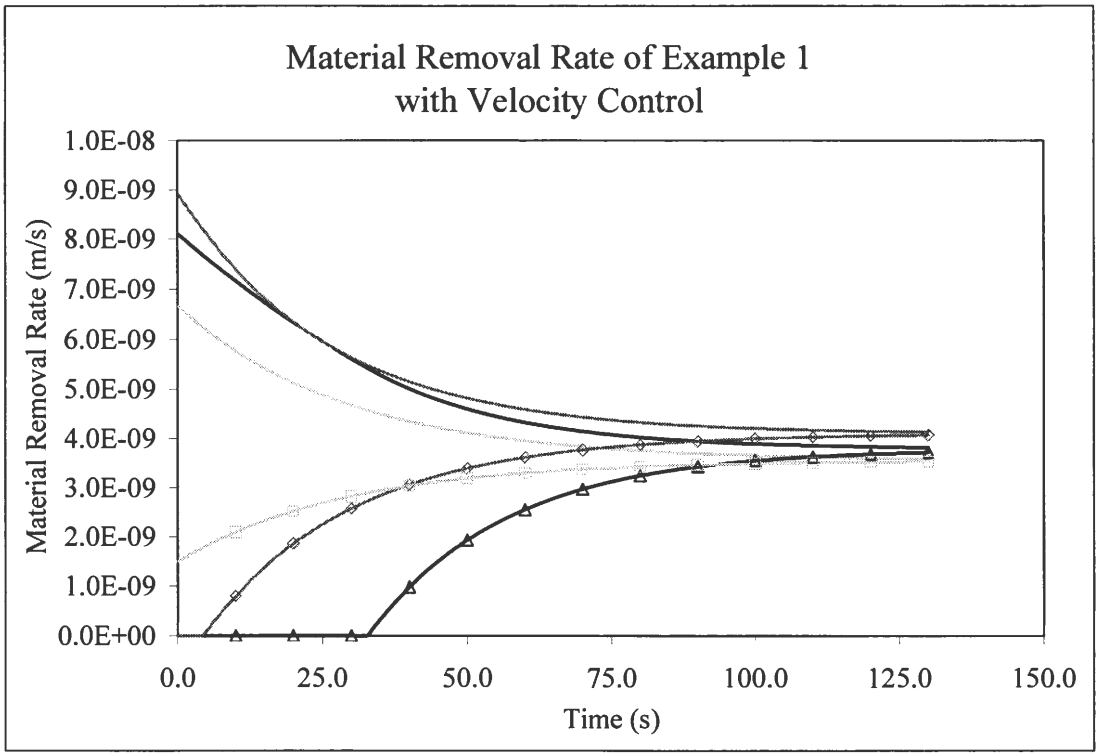

Figure 3.6 MRR vs. Time for "Spatial Velocity control"

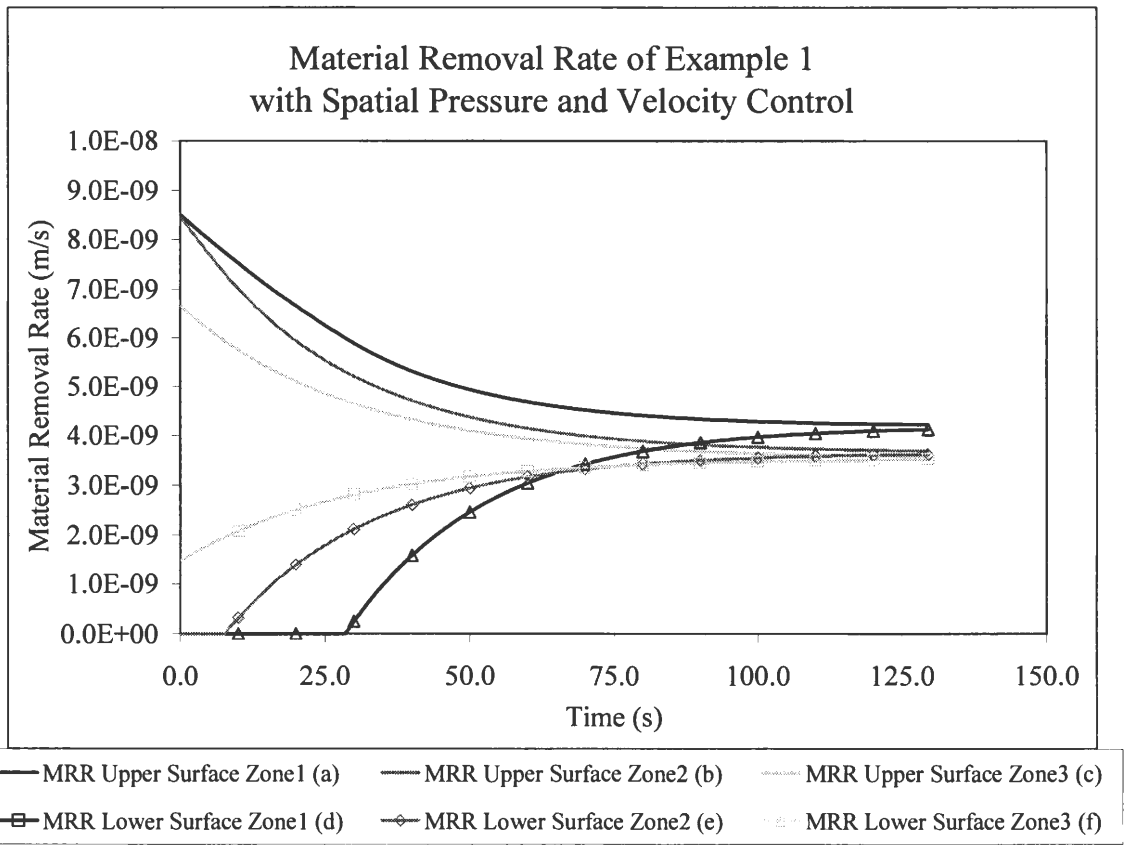

Figure 3.7 Final surface for "Spatial Pressure and Velocity control"

The series of graphs in the previous pages clearly show the distinctness between the various control algorithms. Figures 2.5 and 2.6 show how the uniformity of the final upper surface is improved when pressure is varied spatially across the die. From Figure 3.3 it can be understood that, the step heights can be controlled using spatial variation of velocity. The improvement in the uniformity of the upper surface as well as in the uniformity of the step heights can be seen in figure 3.4, where both pressure and velocity are varied spatially across the die. Figure 3.6, 3.7 and 3.8 explains the material removal rate variation in upper and lower surface for various controls.

CHAPTER 4a. Wafer scale variation of interface pressure for yield improvement in CMP

4a.1 Background

4a.1.1 Wafer –pad interface pressure model

Controlled material removal has always been the prime criteria in the process of chemical mechanical polishing in the manufacture of micro-electro mechanical systems. Material removal in CMP is widely based on the Preston's equation (Preston 1927) $dH/dt = CPV$ where dH/dt is the material removal rate, P is the pressure, V is the relative velocity between the pad and the wafer surface and C is the Preston's constant. The applied uniform pressure P over the wafer carrier head is not the same as the interface pressure experienced between the pad and the wafer surface.

Many researchers have focused on the modeling of the interface pressure distribution between wafer and the pad. Runnels and Renteln [Runnels and Renteln 1993] have used continuum mechanics to investigate wafer edge effect and wafer curvature effect. They attribute the increase in material removal at the wafer edge to the increased contact pressure. Their finite element based elasticity solutions, however have always shown larger pressure at the wafer center, dropping to zero at the wafer edge. They hypothesized the cause to be a partial contact between the pad and the wafer. Baker [Baker 1996] had developed a model for interface pressure based on plate theory, and has shown that the predicted pressure variation in the edge region matches well with the non-uniform material removal. Wang et al [Wang 1997] and Srinivasa Murthy et al [Srinivasa Murthy 1997] have investigated the effects of

various process parameters on the degree of wafer scale non-uniformity. They find that von mises stress correlates with the polishing non-uniformity, and uniformity improves with decreasing pad compressibility. Sasaki et al [Sasaki et al 1998] have conducted a detailed FEM analysis of the pressure distribution under a wafer, and investigated the influences of the back film, wafer chamber and retainer ring on the pressure distribution. Byrne et al [Byrne et al 1999] have considered the effects of pad wear. Utilizing finite element analysis, they predict that the material removal in wafer center region will be reduced over time due to pad wear. Tseng et al [Tseng et al 1999] relate the film stress to wafer curvature and give a theoretical model on how this curvature influences the removal rate and the wafer scale non-uniformity. Fu and Chandra [Fu and Chandra 2001, 2002] derive an analytical solution for the interface pressure distribution based on an elastic / visco-elastic half-space assumption for the pad. They show how to obtain a nearly uniform pressure distribution through tight control of the load and wafer curvature, and how visco-elastic pad deformation lead to decreasing material removal rate.

There is little work done on the relationship between the wafer surface pressure distribution and wafer backside loading, although this relationship is important for the wafer carrier design. And moreover, the interface pressure even though is directly dependent on the carrier loading; it is not necessary that they are one and the same. This was explained and proved by Fu and Chandra in the study on relationship between wafer-pad and carrier loading. The wafer and pad interface can be effectively treated as plate-half space interaction. Syngellagis and Bai [Syngellagis and Bai 1993] use boundary element formulations for a

numerical implementation of plate-half space interaction to identify various parameters like stress, pressure distribution, deformation profile etc.

The first part of this chapter explains Fu and Chandra's analytical model, that determines the interface pressure distribution between the wafer pad interface in terms of the loading distribution over the wafer and vice versa. The model is developed based on contact mechanics and plate theory. The second part of chapter explains the verification of the model results, with the results obtained from application of Boundary element method over plate-half space interaction. The final part of the chapter discusses ways to use the results of the analytical model to increase the polishing yield. A loading design chart is provided based on the analytical model at the end of this chapter, which provides an approximate idea about the percentage of wafer that could have high uniformity. The chart is devised based on finite element analysis using ABAQUS.

4a.2 Model description

The wafer pad interface pressure model was developed based on the contact mechanics and plate theory. As explained in the introduction, we need to control the interface pressure in order to control the material removal on the wafer surface, and for this we need to understand the relationship between the interface pressure and the carrier loading. The assumptions made are a) pad deforms like an elastic half space b) wafer is a circular plate and is flat under no loading c) wafer and pad are in complete contact d) the case is axi-symmetric. The paper devised a model to identify the relationship between the interface pressure distribution and wafer carrier loading. The paper gave two different methods/model,

one to obtain the loading for the given interface pressure and the second to obtain the interface pressure from the wafer back side loading. The latter one is discussed here.

4a.3 Notations used

a – radius of the wafer

ν_{pad} - Poisson's ration for pad

ν_{wafer} - Poisson's ration for wafer

p – interface or wafer surface pressure

q – carrier loading

$D_{wafer} = \frac{E_{wafer} t_{wafer}^3}{12\left(1-\nu_{wafer}^2\right)}$ -Flexural rigidity of the wafer

t_{wafer} - Thickness of the wafer

E_{wafer} - Young's modulus of the wafer

E_{pad} - Young's modulus of the pad

4a.4 Interface pressure for a specified carrier loading

The following page explains in detail to calculate the interface pressure from carrier loading. The loading distribution is assumed to be $q(r) = \sum_{m=0}^{\infty} c_{2i} r^{2i}$, where the constants are

known. We assume the pad deformation as an even polynomial $w(r) = u_z(r) = \sum_{i=0}^{n} a_{2i} r^{2i}$ and

the corresponding wafer surface pressure $p(r) = \sum_{i=0}^{n} b_{2i}(a_{2i}) r^{2i}$.

From the plate theory $\frac{D_{wafer}}{r}\frac{d}{dr}\left[r\frac{d}{dr}\left\{ \frac{1}{r}\frac{d}{dr}\left(r\frac{dw}{dr} \right) \right\} \right] = q(r) - p(r)$,

we have $D_{wafer}\sum_{i=2}^{\infty}(2i-2)^2(2i)^2 a_{2i} r^{2i-4} = \sum_{i=0}^{\infty} c_{2i} r^{2i} - p(r)$.

The above equation can be simplified in a polynomial form as follows,

$$\left(\sum_{i=0}^{\infty} e_{2i} r^{2i} \right)\left(\sum_{i=0}^{\infty} d_{2i} r^{2i} \right) = \sum_{i=0}^{\infty} b_{2i} r^{2i} \ ,$$

where $e_{2i} = e_{2i}(a_{2i})$ and $b_{2i} = b_{2i}(a_{2i})$.

This equation will give a recurrence relationship for a_{2i}, (i = 0,1,2....). After, all the a_{2i}'s are solved, the corresponding interface pressure can be obtained. This method is valid for infinite series, but for finite series an approximate solution is devised as follows,

The error function is calculated to be

$$err(r) = q(r) - p(r) - D_{wafer}\sum_{i=2}^{n}(2i-2)^2(2i)^2 a_{2i} r^{2i-4}$$

From plate theory, if it is accurate solution, $err(r) = 0$; to have approximate solution, we use the following function,

$U(a_0, a_2, \ldots, a_{2n}) = \int_0^a [err(r)]^2 \omega(r) dr$, where weight function $\omega(r) = \sqrt{1 - (\frac{r}{a})^2}$.

$$\frac{\partial U}{\partial a_{2i}} = 0, (i = 0,1,2,\ldots,n).$$

The above equation will give a matrix, which can be solved for a_i, (i = 0,1,2...2m).

4a.5 Solution

Based on the model developed by Fu and Chandra as explained in the previous pages, a solution is derived for both load and interface pressure equations. Let us assume the displacement of the pad under pressure p is a 4th order polynomial $U_z(r) = a_0 + a_2 r^2 + a_4 r^4$.

Using the equations to calculate the shape profile, the constants a_0, a_2, a_4 are determined and plugged in back in the above equation.

$$U(a_0,a_2,a_4) = \int_0^a \left\{ \left[\begin{array}{l} q - 64 D_{wafer} a_4 - \dfrac{E_{pad}}{\pi\left(1-v_{pad}^2\right)} \dfrac{1}{\sqrt{1-\left(\dfrac{r}{a}\right)^2}} \\ \left(\dfrac{a_0}{a} - 2a_2 a - \dfrac{8}{9} a_4 a^3\right) + \left(4a_2 a - \dfrac{32}{9} a_4 a^3\right)\left(\dfrac{r}{a}\right)^2 \\ + \dfrac{64}{9} a_4 a^3 \left(\dfrac{r}{a}\right)^4 \end{array} \right] \right\}^2 \sqrt{1-\left(\frac{r}{a}\right)^2}\, dr$$

$$\frac{\partial U}{\partial a_0} = 0 \text{ gives } \frac{\pi}{2}\left(\frac{a_0}{a}\right) + 64\pi \frac{1-v_{pad}^2}{E_{pad}} \frac{D_{wafer}}{a^3} a_4 a^3 = \pi q \frac{1-v_{pad}^2}{E_{pad}}$$

$$\frac{\partial U}{\partial a_2} = 0 \text{ gives } \frac{\pi}{2}(a_2 a) + \left(\frac{4\pi}{9} - \frac{64}{3}\pi \frac{1-v_{pad}^2}{E_{pad}} \frac{D_{wafer}}{a^3}\right) a_4 a^3 = -\frac{\pi q}{3} \frac{1-v_{pad}^2}{E_{pad}}$$

$$\frac{\partial U}{\partial a_4}=0 \text{ gives } \left(72\pi\frac{1-v_{pad}^2}{E_{pad}}\frac{D_{wafer}}{a^3}\right)\left(\frac{a_0}{a}\right)+\left(\pi-48\pi\frac{1-v_{pad}^2}{E_{pad}}\frac{D_{wafer}}{a^3}\right)(a_2 a)$$

$$+\left(\frac{10\pi}{9}-\frac{1408}{15}\pi\left(\frac{1-v_{pad}^2}{E_{pad}}\frac{D_{wafer}}{a^3}\right)+1152\pi^3\left(\frac{1-v_{pad}^2}{E_{pad}}\frac{D_{wafer}}{a^3}\right)^2\right)a_4 a^3$$

$$=\left(18\pi\left(\frac{1-v_{pad}^2}{E_{pad}}\right)^2\frac{D}{a^3}-\frac{11}{15}\pi\frac{1-v_{pad}^2}{E_{pad}}\right)q$$

In matrix form, we have

$$\begin{pmatrix} \frac{\pi}{2} & 0 & 64\pi\frac{1-v_{pad}^2}{E_{pad}}\frac{D_{wafer}}{a^3} \\ 0 & \frac{\pi}{2} & \left(\frac{4\pi}{9}-\frac{64}{3}\pi\frac{1-v_{pad}^2}{E_{pad}}\frac{D_{wafer}}{a^3}\right) \\ \left(72\pi\frac{1-v_{pad}^2}{E_{pad}}\frac{D_{wafer}}{a^3}\right) & \left(\pi-48\pi\frac{1-v_{pad}^2}{E_{pad}}\frac{D_{wafer}}{a^3}\right) & \left(\frac{10\pi}{9}-\frac{1408}{15}\pi\left(\frac{1-v_{pad}^2}{E_{pad}}\frac{D_{wafer}}{a^3}\right)+1152\pi^3\left(\frac{1-v_{pad}^2}{E_{pad}}\frac{D_{wafer}}{a^3}\right)^2\right) \end{pmatrix}\begin{pmatrix} \frac{a_0}{a} \\ a_2 a \\ a_4 a^3 \end{pmatrix}=$$

$$\begin{pmatrix} \pi q\frac{1-v_{pad}^2}{E_{pad}} \\ -\frac{\pi q}{3}\frac{1-v_{pad}^2}{E_{pad}} \\ \left(18\pi\left(\frac{1-v_{pad}^2}{E_{pad}}\right)^2\frac{D}{a^3}-\frac{11}{15}\pi\frac{1-v_{pad}^2}{E_{pad}}\right)q \end{pmatrix}$$

The above matrix equation is solved for a_0, a_2, a_4 and the constants are as follows,

$$a_0=\frac{\left[2aq\left(-1+v_{pad}^2\right)\left(-5a^6E_{pad}^2+1824a^3D_{wafer}E_{pad}\left(-1+v_{pad}^2\right)+92160D_{wafer}^2\left(-1+v_{pad}^2\right)^2\right)\right]}{E_{pad}\left[5a^6E_{pad}^2-1728a^3D_{wafer}E_{pad}\left(-1+v_{pad}^2\right)+8640D_{wafer}^2\left(-40+3\pi^2\right)\left(-1+v_{pad}^2\right)^2\right]}$$

$$a_2 = \frac{\left[-2q\left(-1+v_{pad}^2\right)\left(\begin{array}{l}-a^6E_{pad}^2+4a^3D_{wafer}E_{pad}\left(-272+45\pi^2\right)\left(-1+v_{pad}^2\right)\\+17820\left(-8+\pi^2\right)D_{wafer}^2\left(-1+v_{pad}^2\right)^2\end{array}\right)\right]}{aE_{pad}\left[5a^6E_{pad}^2-1728a^3D_{wafer}E_{pad}\left(-1+v_{pad}^2\right)+8640D_{wafer}^2\left(-40+3\pi^2\right)\left(-1+v_{pad}^2\right)^2\right]}$$

$$a_4 = \frac{\left[3q\left(-1+v_{pad}^2\right)\left(a^3E_{pad}+30\left(-88+9\pi^2\right)D_{wafer}\left(-1+v_{pad}^2\right)\right)\right]}{2\left[5a^6E_{pad}^2-1728a^3D_{wafer}E_{pad}\left(-1+v_{pad}^2\right)+8640D_{wafer}^2\left(-40+3\pi^2\right)\left(-1+v_{pad}^2\right)^2\right]}$$

Having the above constants in $U_z(r)=a_0+a_2r^2+a_4r^4$ shape profile, we can now derive the interface pressure equation. For a fourth order shape profile, the pressure equation is calculated as follows.

The displacement of the pad is written as $w(r)=U_z(r)=\sum_{i=0}^{n}a_{2i}r^{2i}$. For this displacement, the interface pressure is

$$p(r)=-\frac{1}{2\sqrt{\pi}}\frac{E}{1-v^2}\sum_{0}^{\infty}a_{2i}\left(1+2i\right)\frac{\Gamma\left(1+i\right)}{\Gamma\left(\frac{3}{2}+i\right)}\Phi\left(r,2i\right)$$

$$\text{where } \Phi\left(r,2i\right)=\left(1+2i\right)r^{2i-1}\left[\sum_{m=0}^{i}\frac{\Gamma\left(1+i\right)}{\Gamma\left(i+1-m\right)\Gamma\left(1+m\right)}\frac{\left(\frac{\sqrt{a^2-r}}{r}\right)^{2m+1}}{2m+1}\right]-\frac{a^{1+2i}}{r^2}\frac{1}{\sqrt{1-\left(\frac{r}{a}\right)^2}}$$

For a 4th order even polynomial this equation is simplified to,

$$p(r) = -\frac{1}{2\sqrt{\pi}} \frac{E_{pad}}{1-v_{pad}^2} \left[\frac{2}{\sqrt{\pi}} \left(\frac{a_0}{\sqrt{a^2-r^2}} + \frac{2a_2\left(2r^2-a^2\right)}{\sqrt{a^2-r^2}} + \frac{8a_4\left(-a^4-4a^2r^2+8r^4\right)}{9\sqrt{a^2-r^2}} \right) \right]$$

And having a_0, a_2, a_4, the pressure equation can be calculated in terms of r and a. For a uniform carrier backside loading, with a shape profile $U_z(r) = a_0 + a_2 r^2 + a_4 r^4$ the simulation results are as follows.

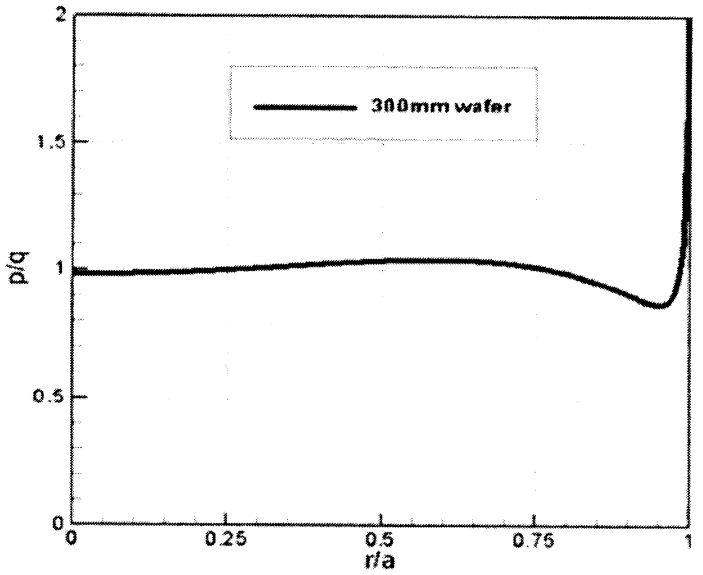

Figure 4.1 Interface pressure distribution for uniform loading

4a.6 The application of BEM technique on plate - half space interaction

The plate-half space interaction problem is very frequently encountered in engineering practice. Syngellakis and Bai [Syngellakis and Bai 1993] discuss a numerical formulation using a boundary element technique to arrive at the solutions for stress, pressure distribution and deformation profile. A uniformly loaded circular plate with a free edge and

in perfectly smooth contact with the half space boundary was initially analyzed. The convergence of the results was tested through boundary and domain element meshes of increasing density. Hemsley [Hemsley 1987] denotes a parameter relative stiffness K_r, where the relativity is between the plate and elastic foundation. A uniformly loaded circular plate with a free edge and in perfectly smooth contact with the half space boundary was initially analyzed. The interface reaction has been computed for various values of the following parameter,

$$K = \frac{E_p\left(1-v_s^2\right)}{E_s\left(1-v_p^2\right)}\left(\frac{h}{a}\right)^3$$

Where

K - Relative stiffness of half space with respect to plate

E_s - Young's modulus of elastic half space.

E_p - Young's modulus of plate.

v_s and v_p - Poisson's ratio for half space and plate respectively.

h - Thickness of the plate

a - radius of the plate

The above parameter is varied from 0.01 to 1. In our calculations we have varied the young's modulus of half space and kept other values constant. The BEM results in Syngellakis and Bai is compared with the results obtained from Wafer-pad interface pressure model.

4a.7 Results

The wafer-pad interface pressure model's predictions are compared with the results obtained from plate-elastic half space reaction using boundary element methods [Syngellagis and Bai 1993]. The simulation parameters are taken from the paper and are as follows, h = 0.1 m, a = 1m, $E_s = E_{pad} = 21\text{MPa}$, $v_s = v_{pad} = 0.2$ and $v_p = v_{wafer} = 0.2$.

The following graph shows the comparison graphs for contact pressure distribution between wafer-pad interaction, and plate-elastic half space interaction (BEM). The distribution is calculated for varying values of relative stiffness K. the relative stiffness is varied by varying the young's modulus of half space.

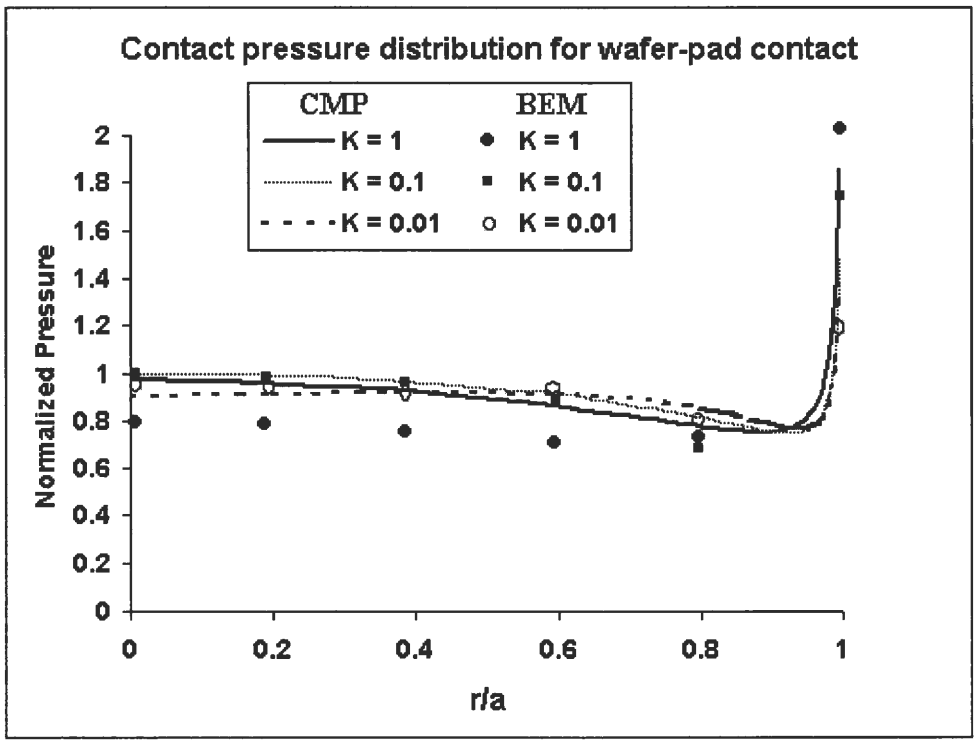

Figure 4.2 Contact pressure distribution comparison between CMP and BEM (Syngellakis and Bai 1993) results for plate –half space

4a.8 Carrier loading distribution for a specified interface pressure

A good head design will have the ability to tune the interface pressure according to the film thickness variation, so that thicker portions of the film experiences higher pressure or high removal rate. In this way, global planarization capability of the CMP processes can be improved. If the desired pad-wafer interface pressure distribution is $p(r)$, the corresponding displacement of the pad under this pressure is [Gladwell 1980]

$$u_z(r)=\frac{4\left(1-v_{pad}^2\right)}{\pi E_{pad}}\left[\int_0^r \frac{s}{r}K\left(\frac{s}{r}\right)p(s)\,ds+\int_r^a K\left(\frac{r}{s}\right)p(s)\,ds\right],0\le r\le a$$

$$\text{where } K(k)=\int_0^{\pi/2}\frac{1}{\sqrt{1-k^2\sin^2\theta}}d\theta$$

Assuming that the wafer and pad are in complete contact, we have wafer shape $w(r)$ to be the same as pad shape $u_z(r)$. From plate theory, the wafer backside loading is

$$q(r)=p(r)+\frac{D_{wafer}}{r}\frac{d}{dr}\left[r\frac{d}{dr}\left\{\frac{1}{r}\frac{d}{dr}\left(r\frac{dw}{dr}\right)\right\}\right]$$

$$\text{where } D_{wafer}=\frac{E_{wafer}t_{wafer}^3}{12\left(1-v_{wafer}^2\right)}$$

Let us consider a special case where we have uniform interface pressure (p is constant), then the desired loading distribution is derived to be

$$q\left(\frac{r}{a}\right)=p\left[1+\frac{1}{3\pi}\frac{1-v_{pad}^2}{1-v_{wafer}^2}\frac{E_{wafer}}{E_{pad}}\left(\frac{h}{a}\right)^2\left(-\frac{7+\left(\frac{r}{a}\right)^2}{\left(1-\left(\frac{r}{a}\right)^2\right)^3}E\left(\frac{r}{a}\right)+\frac{4}{\left(1-\left(\frac{r}{a}\right)^2\right)^2}K\left(\frac{r}{a}\right)\right)\right]$$

The simulation result is shown in the fig. The simulation parameters are Radius a = 100mm, thickness t_{Wafer} = 0.75 mm, E_{pad} = 20 MPa and 200 MPa, E_{Wafer} = 70 GPa v_{pad} = 0.2 and v_{wafer} = 0.3 . From the results it is clear that to obtain uniform wafer-pad interface pressure, the center part of the wafer should be loaded in compression and the edge part of the wafer should be loaded in tension.

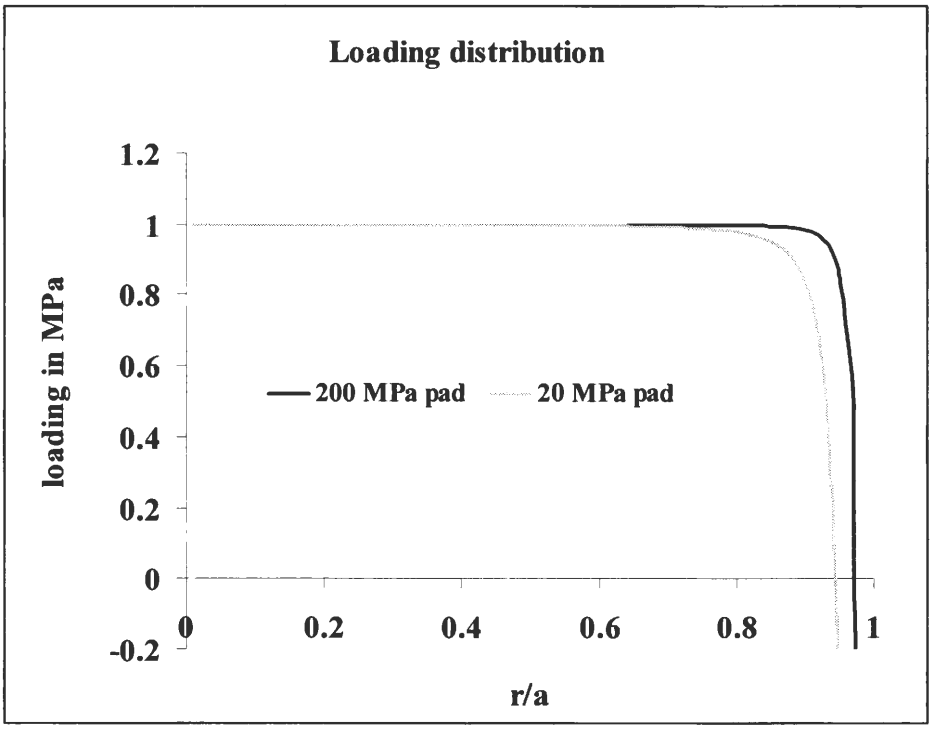

Figure 4.3 Loading distribution across the wafer to obtain uniform interface pressure

As we see in the above distribution, as the pad becomes stiffer, a more uniform load is preferred in order to obtain uniform interface pressure. However, further investigation shows that the loading distribution equation requires infinite down force because of the strong singularity at the wafer edge, which is impossible to achieve. The reason may be that the wafer will not conform to the pad in this situation and one of the assumptions is broken down.

Chapter 4b. FEM Analysis for wafer scale application of non uniform loading

4b.1 Background

Various research works presented earlier, were assuming that the carrier loading distribution and the wafer-pad interface pressure distribution are one and the same. The model results, which are compared here, prove that even though there is a relationship between the contact pressure and loading they are not necessarily one and the same. The model results are compared with plate-elastic foundation results obtained from boundary element methods and are found to be comparable and satisfied. The model shows that under uniform loading on the wafer backside, there still will be edge effect due to the pressure variation at wafer-pad interface. In the figure, the result graph is the loading distribution that should be applied across the wafer in order to obtain a uniform interface pressure between the pad and the wafer interface. So there is a necessity that such loading distribution should be practically implemented to obtain uniform interface pressure. The following FEM analysis results explain a devised strategy which could provide better yield in CMP.

4b.2 FEM analysis for differential or non uniform loading across the wafer

Based on the loading pattern for uniform interface pressure, the following discussion analyses the effects of non uniform loading over the wafer. Using ABAQUS, a pad wafer contact interference model is generated. Both the pad and the wafer is assumed to be elastic with their properties as follows, E_{pad} = 20 MPa, 200 MPa, E_{Wafer} = 70 GPa,

$v_{pad} = 0.2$ and $v_{wafer} = 0.3$. The dimensions are, $r_{pad} = 400$ mm, $r_{wafer} = 100$ mm $t_{pad} = 2$ mm and $t_{wafer} = 0.75$mm.

Contact interference is created between the axi-symmetric pad and the wafer. The parts of meshed with the help of quadratic elements and the simulation results are tabulated. In the following FEM analysis, the loading distribution shown in the fig. earlier is applied over the wafer surface. The region where the strong tension force required in the edge of the wafer is not applied. Those regions are left with no loading. In order to apply non uniform loading over the wafer, the wafer is segmented into as many as 13 divisions.

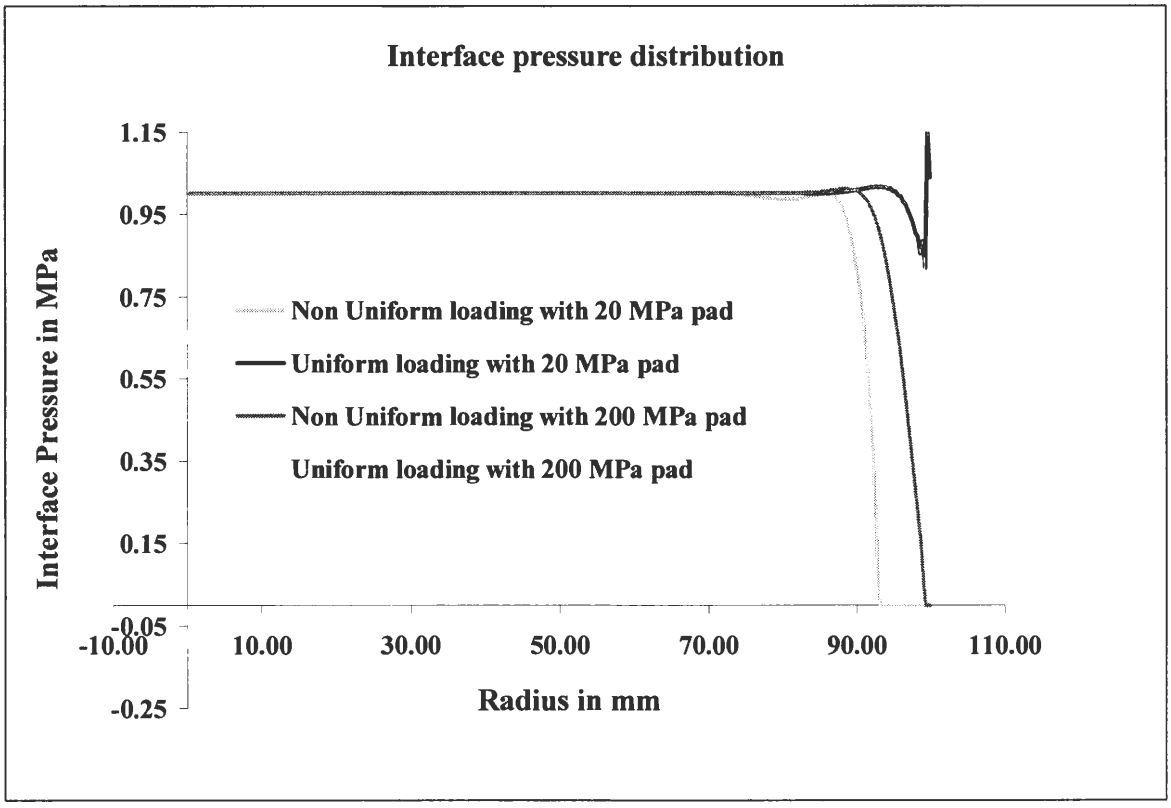

Figure 4.4 Interface pressure distribution across the
for non uniform loading

The figure 4.4 shows the interface pressure distribution for this loading distribution. From the above interface pressure values, it is clear that, the loading results from the analytical solution, helps removing the edge effect, although, the improvement in terms of wafer yield has not improved. The reason can be attributed to the absence of the strong tension that is required at the edge of the wafer.

Even though, the pressure values that were calculated from the loading distribution doesn't help obtaining a uniform pressure across the wafer, the concept of non uniform loading across the wafer was accepted and the analysis was further continued. Based on the analytical results it is found that a strong tension is required at the edge of the wafer. Hence a FEM analysis is carried out to identify the amount of effect a tension at the edge of the wafer, would change the interface pressure distribution between the wafer and pad surface. A loading design chart is created based on this analysis. With a constant pad modulus, the edge length and the tension applied on the wafer edge is varied with a uniform load applied in the remaining segment. The results are listed in the loading chart (figure 4.5 and 4.6).

20 MPa Pad	**10% Load Tension**	**5%**	**1%**	**0.1%**	**0.01%**
80-20	42	48	46	48	48
90-10	52	52	54	54	54
95-5	56	56	58	58	58
98-2	58	58	61	62	62
99-1	72	72	73	73	73

Figure 4.5 Loading design chart

200 MPa Pad	10% Load Tension	5%	1%	0.1%	0.01%
80-20	55	59	68	68	68
90-10	70	75	77	77	77
95-5	81	82	82	82	82
98-2	84	84	84	84	84
99-1	85	85	86	86	86

Figure 4.6 Loading design chart

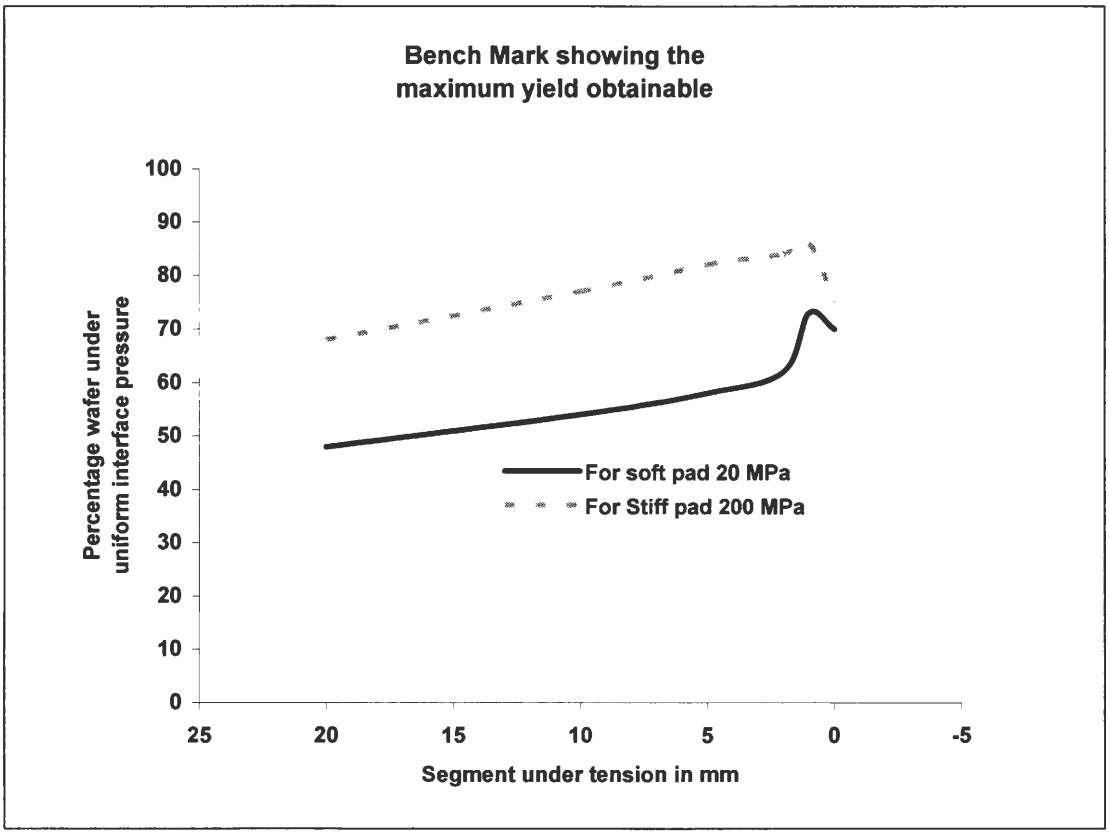

Figure 4.7. Yield Variation for Non Uniform Loading with Tension at the edge

In the above chart, Figure 4.5 assumes the pad to be soft and the second chart Figure 4.6 assumes the pad to be stiffer. The left most column shows how the wafer is split into 2 parts. For example, if the chart reads 80-20, the wafer is applied a uniform compressive load

for the first 80% and uniform tension for the remaining 20%. The column variation reads the amount by which the tension load varies with respect to the compressive load. The data in the remaining boxes shows the percentage of wafer length that experiences a uniform interface pressure.

From the chart, it can be deciphered that, about 86% of the wafer can experience a uniform interface pressure with a slightly stiff pad, with a small tension at the edge. From Figure 4.7, it can be deciphered that, the yield decreases if the tension is reduced to zero or in other words the final segment length is pushed to zero. When a uniform loading is applied with the same loading conditions, the percentage of wafer that experiences interface pressure uniformity is around 75-77%. Hence a significant improvement in uniformity is obtained here. In turn applying a tension and that too for such a small percentage of the wafer may not be possible but a possibility of applying vacuum/suction at the end can't be completely ruled out. Apart from the non uniform loading methods, the two models provide a relationship between wafer-pad contact pressure and loading distribution. So knowing any of them would help us identify the other distribution. This when put together will help us creating a simplified CMP system where knowing the pressure or load can help us find the other value which in turn would help us control the system. The kinematics aspect of CMP from different polishers will influence the model prediction. This relationship is critical in order to get better surface results and to there by improve the yield. Hence further investigations under more realistic CMP configurations are necessary.

CHAPTER 5. Discussion and conclusion

5.1 Control mechanism for Chemical Mechanical Polishing

As explained in Chapter 1, there is a need for developing a complete control mechanism that governs and controls polishing at wafer and die scale level simultaneously. Chapter 2 provides five open loop algorithms to control polishing at die scale as well as analytical models that provides interface pressure versus loading relations at wafer scale. In a realistic environment, controlling the die scale polishing provided there is a global control at the wafer scale ensures uniform polishing. This in turn results in significant yield improvement. This chapter integrates the die scale and the wafer scale model provided in the previous two chapters and provides an integrated algorithm for systemic control of Chemical Mechanical Polishing.

5.2 Control mechanism at die Scale and wafer Scale

In Chapter 2 and 3, 5 die scale models were explained, which controls the Material removal rate having pressure and/or velocity as parametric constraints. Using the Dishing model by Fu and Chandra, the critical interface pressure to be applied for a specific pattern density at a given time is calculated and is applied. In realistic environment, this type of pressure variation can be done using a Zonal Process Controller (ZPC). The ZPC is a pixel based control to vary pressure at die scale levels. The pixel can be of varied square sizes. Chart in Figure 5.1 explains the algorithm, where for a single ZPC area, interface pressure is calculated for the varying pattern density zones (assuming 3 zones) and the corresponding loading is calculated and sent to the ZPC controller. This procedure doesn't require a feed

back process, the reason being, the interface pressure is calculated for every time period based on the current surface evolution. The loading will be calculated for every interface pressure from the analytical relations. As the loading value for each zone will be in the form of distribution, the average/nominal value will be taken into consideration for polishing. For spatial and temporal control, the time step is 1 second. In reality the pressure cannot be varied for every 1 second making this method is practically impossible. This method is overcome in Look-Ahead pressure control, where we increase the time step to 5 seconds.

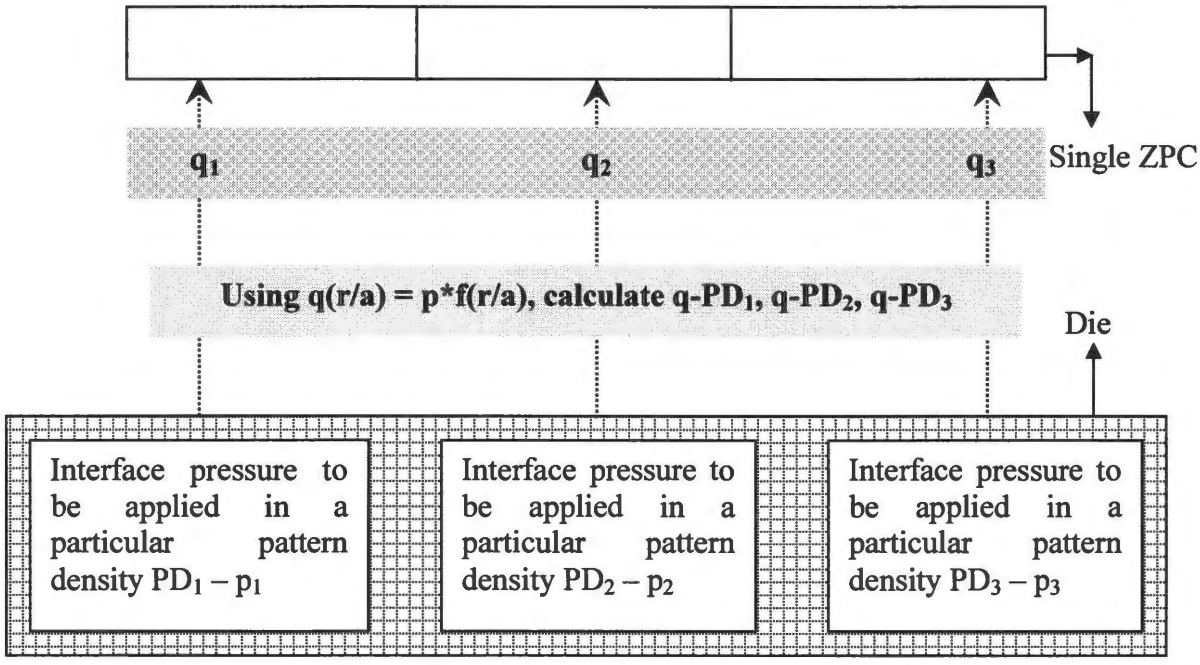

Figure 5.1 Flow Diagram for Control Mechanism at Die Scale

In the earlier mechanism at die scale level, the Zonal Process Controller controls the interface pressure at die scale level. But if the same has to be achieved at the wafer scale level, the pressure has to be controlled through out the entire wafer scale at the same time. In this model, assuming there are 'N' number of dies across the wafer, there is a need to apply

varying interface pressure based on the varying pattern density and step height spatially. This process in turn requires control that can apply varying load across the wafer. A simple ring load control accomplishes this requirement. In this control, the whole carrier is split into concentric rings and different loading is applied on different rings and there by a varying loading pattern is created. Assuming that the whole wafer surface is split into 5 concentric rings, a flow diagram (figure 5.2) is created which will explain the feedback control algorithm for wafer scale control mechanism. The analytical model for converting loading distribution to pressure distribution is explained in chapter 4, where the loading distribution polynomial is a 4^{th} order polynomial. So, this limits our variable pressure points (rings) to 5. The die scale pressure variation model will provide the interface pressure values periodically. The entire pressure values, across the wafer will be computed at a constant time which will then be converted into a polynomial distribution. Currently the model which converts this pressure polynomial to loading polynomial is not completed (refer Appendix I). A best fit polynomial of order 4 is identified from this loading polynomial and the corresponding interface pressure distribution is computed from the analytical model that converts $q(r) \longrightarrow p(r)$. Here a feed back mechanism is incorporated in order to attain a more precise polishing process. This loading is now applied over the carrier and after the specific time step, the step height and surface evolution is computed and the die scale model is again applied to identify new interface pressure values across the wafer.

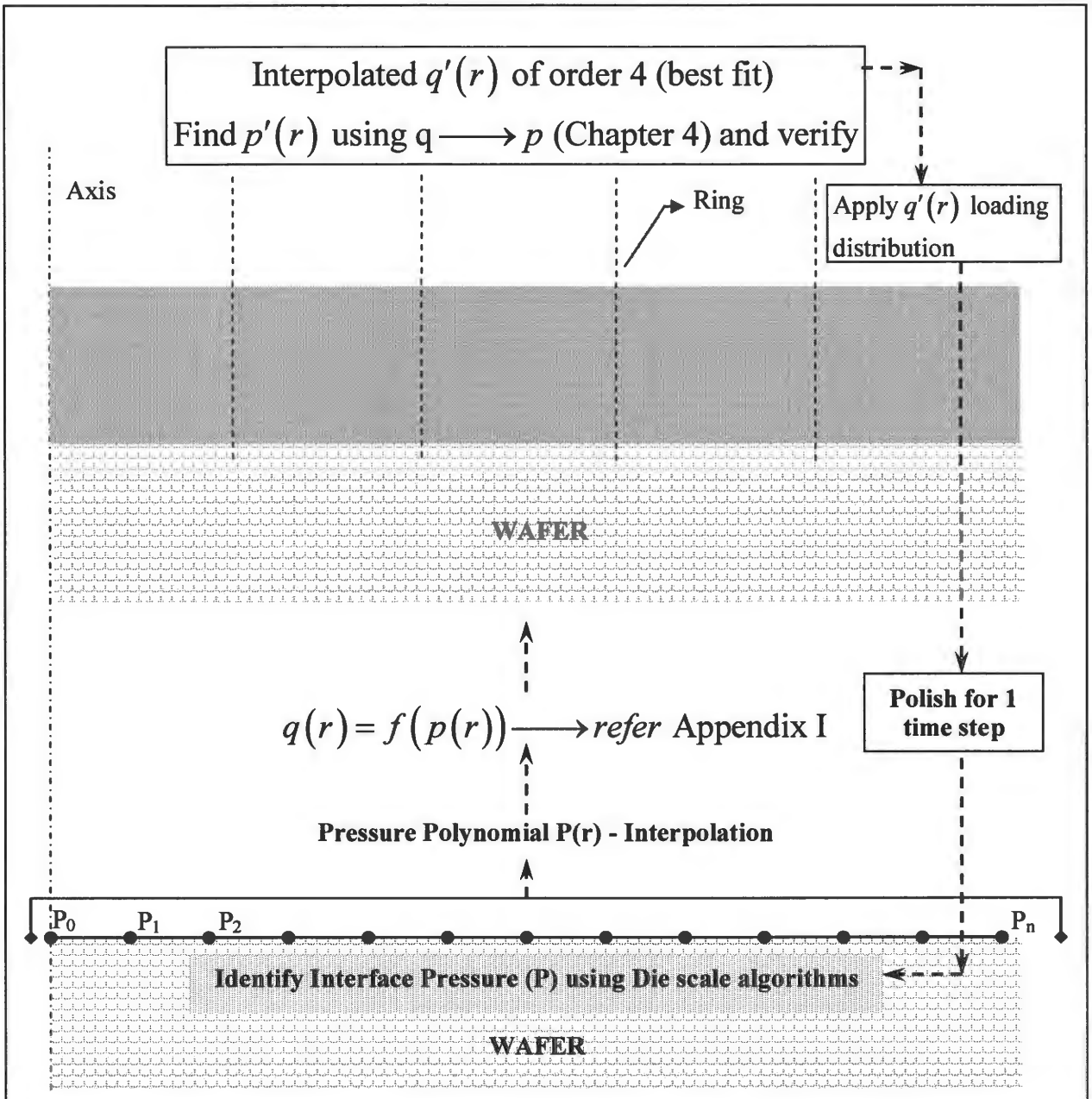

$$p(r) = -\frac{1}{2\sqrt{\pi}} \frac{E_{pad}}{1-\nu_{pad}^2} \left[\frac{2}{\sqrt{\pi}} \left(\frac{a_0}{\sqrt{a^2-r^2}} + \frac{2a_2\left(2r^2-a^2\right)}{\sqrt{a^2-r^2}} + \frac{8a_4\left(-a^4-4a^2r^2+8r^4\right)}{9\sqrt{a^2-r^2}} \right) \right]$$

This is the end equation for converting a 4th order loading polynomial to a pressure distribution (polynomial)

Figure 5.2 The flow diagram explains the control mechanism at wafer scale level

5.3 Conclusion

Material removal rate is one of the prime parameter in Chemical Mechanical Polishing which has significant influence over the polishing rate. Fu and Chandra et al described this impact of material removal rate in detail and its eventual relation to the formation of dishing and erosion in metal and dielectric surfaces respectively. The model explains the influence of interface pressure, velocity, pattern density on material removal rate. Based on the MRR equations, the dishing heights of the surfaces formed due to over polishing were modeled.

Based on this relation, it is clear that step height can be controlled as a function of pressure and/or velocity in a varying pattern density scale. With this concept, five die scale control algorithms were developed, viz., Spatial pressure control, Spatial and Temporal pressure control, look ahead pressure scheduling, Spatial velocity control, and Combined velocity and pressure control. The main objective of the models are to improve the polishing mechanism to obtain better upper surface finish and more uniform step heights on wafer surfaces having variable pattern densities in die scale. The control mechanism was developed based on the fact that modifying pressure across the die over different pattern densities would in turn improve the final surface uniformity. The results show that these control strategies could significantly enhance both the upper surface uniformity and step height in a CMP process. In collaboration with Strasbaugh Inc., work is currently in progress to experimentally verify the simulation results, and implement these control algorithms in a realistic CMP process.

The analytical model based on plate theory which provides a relationship that determines the interface pressure between pad and the wafer surface from uniform nominal pressure (carrier loading) was analyzed and verified. The results are verified based on the plate-elastic foundation results obtained from Boundary element analysis (*). Also, the relationship that converts uniform interface pressure back to loading distribution is studied and based on that a FEM analysis is performed. The concept of non uniform loading and its effect on interface pressure distribution between the pad and wafer is studied using ABAQUS. It is found that a non uniform load calculated based on the analytical model along with a very small tension at the edge of the wafer results in reducing the edge effect, which in turn would result in higher uniformity at wafer scale.

Based on the both wafer and die scale model an integrated control chart is provided which would guide us in developing a complete CMP control system which would achieve significant improvement in uniformity both at die and wafer scale.

Future work

The die scale models were simulated and the results prove that significant improvement in uniformity is obtainable. It is necessary that, the results are verified in a realistic environment using die scale control procedures like Zonal Process Controller (ZPC), which would assist the development of a full fledged CMP control system in the future.

Even though the complete control chart for integrating the wafer and die scale models are provided in chapter five, a control system is not yet in place due to the absence of a analytical model and relationship for converting a pressure polynomial distribution to a loading distribution. This model development is still under research. APPENDIX I explain the first step taken in regard to this development.

APPENDIX I - Wafer –pad interface pressure distribution model

I. Wafer –pad interface pressure model

Many researchers have focused on the modeling of the interface pressure distribution between wafer and the pad. Runnels and Renteln (1993) have used continuum mechanics to investigate wafer edge effect and wafer curvature effect. They attribute the increase in material removal at the wafer edge to the increased contact pressure. Their finite element based elasticity solutions, however have always shown larger pressure at the wafer center, dropping to zero at the wafer edge. They hypothesized the cause to be a partial contact between the pad and the wafer. Baker (1996) had developed a model for interface pressure based on plate theory, and has shown that the predicted pressure variation in the edge region matches well with the non-uniform material removal. Wang et al (1997) and Srinivasa Murthy et al (1997) have investigated the effects of various process parameters on the degree of wafer scale non-uniformity. They find that von mises stress correlates with the polishing non-uniformity, and uniformity improves with decreasing pad compressibility. Sasaki et al (1998) have conducted a detailed FEM analysis of the pressure distribution under a wafer, and investigated the influences of the back film, wafer chamber and retainer ring on the pressure distribution. Byrne et al (1999) have considered the effects of pad wear. Utilizing finite element analysis, they predict that the material removal in wafer center region will be reduced over time due to pad wear. Tseng et al (1999) relate the film stress to wafer curvature and give a theoretical model on how this curvature influences the removal rate and the wafer scale non-uniformity.

Fu and Chandra (2001, 2002) derive an analytical solution for the interface pressure distribution based on an elastic / visco-elastic half-space assumption for the pad. They show how to obtain a nearly uniform pressure distribution through tight control of the load and wafer curvature, and how visco-elastic pad deformation lead to decreasing material removal rate.

The interface pressure even though is directly dependent on the carrier loading; it is not necessary that they are one and the same. This was explained and proved by Fu and Chandra in the study on relationship between wafer-pad and carrier loading. Fu and Chandra (2002) have used contact mechanics and plate theory to model the wafer pad interface pressure in terms of carrier loading and vice versa. But the model can be applied only in theoretical applications as such for finding the distribution between uniform loading and interface pressure only when the input distribution is uniform. In practical applications where both the loading and interface pressure need not be uniform, this model cannot be applied.

Hence, the model needs to be modified in such a way that, for a given distribution of interface pressure or loading say in the form of any series, the model should calculate the loading or interface pressure distribution in the form of series respectively. In the present work, the wafer-pad interface pressure distribution is assumed to be an even polynomial and the corresponding distribution for carrier loading is modeled.

The model is based on the contact mechanics and plate theory. The assumptions made are a) pad deforms like an elastic half space b) wafer is a circular plate and is flat under no

loading c) wafer and pad are in complete contact d) the case is axi-symmetric. The paper devised a model to identify the relationship between the polynomial interface pressure distribution and wafer carrier loading.

II. Notations used

a – radius of the wafer

ν_{pad} - Poisson's ration for pad

ν_{wafer} - Poisson's ration for wafer

p – interface or wafer surface pressure

q – carrier loading

u_z - Displacement profile of pad under the pressure p

w - Displacement of the wafer

$K(k) = \int_0^{\pi/2} \frac{1}{\sqrt{1-k^2 \sin^2\theta}} d\theta$ - Complete elliptic integral of the first kind

$\mathrm{E}(k) = \int_0^{\pi/2} \sqrt{1-k^2 \sin^2\theta}\, d\theta$ - Complete elliptic integral of the second kind

$D_{wafer} = \frac{E_{wafer} t_{wafer}^3}{12\left(1-\nu_{wafer}^2\right)}$ -Flexural rigidity of the wafer

t_{wafer} - Thickness of the wafer

E_{wafer} - Young's modulus of the wafer

E_{pad} - Young's modulus of the pad

III. Model description

The displacement of the pad under the interface pressure p is

$$u_z(r)=\frac{4\left(1-v_{pad}^2\right)}{\pi E_{pad}}\left[\int_0^r \frac{s}{r}K\left(\frac{s}{r}\right)p(s)ds+\int_r^a K\left(\frac{r}{s}\right)p(s)ds\right],0\le r\le a$$

Because wafer surface and pad surface have to conform to each other, we have $w=u_z$.

From plate theory, we have $\frac{1}{r}\frac{d}{dr}\left[r\frac{d}{dr}\left\{\frac{1}{r}\frac{d}{dr}\left(r\frac{dw}{dr}\right)\right\}\right]=\frac{q-p}{D_{wafer}}$.

Thus, the loading condition is $q(r)=p(r)+\frac{D_{wafer}}{r}\frac{d}{dr}\left[r\frac{d}{dr}\left\{\frac{1}{r}\frac{d}{dr}\left(r\frac{dw}{dr}\right)\right\}\right]$.

In the pad displacement equation, the interface pressure p has to be now substituted with some form of distribution series. Lets assume p(s) to be an even polynomial of 8th order

$$p(s)=a_0+a_2s^2+a_4s^4+a_6s^6+a_8s^8$$

Now the equation becomes

$$u_z(r)=\frac{4\left(1-v_{pad}^2\right)}{\pi E_{pad}}\left[\begin{array}{l}\left(\int_0^r \frac{s}{r}K\left(\frac{s}{r}\right)\left(a_0+a_2s^2+a_4s^4+a_6s^6+a_8s^8\right)ds\right)\\+\left(\int_r^a K\left(\frac{r}{s}\right)\left(a_0+a_2s^2+a_4s^4+a_6s^6+a_8s^8\right)ds\right)\end{array}\right],0\le r\le a$$

The integral terms are derived separately for each power.

The following pages show the derivation for the first term in the above equation, that is

$$\left(\int_0^r \frac{s}{r}K\left(\frac{s}{r}\right)\left(a_0+a_2s^2+a_4s^4+a_6s^6+a_8s^8\right)ds\right)$$

The above term is separated further into smaller terms and the integration is shown in the following pages. For the first term a_0

$$\int_0^r \frac{s}{r} K\left(\frac{s}{r}\right) p(s)ds = \int_0^r \frac{s}{r} K\left(\frac{s}{r}\right) a_0 = \int_0^r \int_0^{\pi/2} \frac{s}{r\sqrt{1-\left(\frac{s}{r}\right)^2 \sin^2\theta}} d\theta ds$$

assume $\frac{s}{r}\sin\theta = \sin t$, $ds = \frac{r\cos t}{\sin\theta} dt$, hence

$$= \int_0^{\pi/2} \int_0^{\theta} \frac{\frac{\sin t}{\sin\theta} \frac{r\cos t}{\sin\theta}}{\sqrt{1-\sin^2 t}} dt d\theta$$

$$= r\int_0^{\pi/2} \left(\frac{1}{\sin\theta}\right)^2 (1-\cos\theta) d\theta = r\int_0^{\pi/2} \left(\frac{2\sin\frac{\theta}{2}}{2\sin\frac{\theta}{2}\cos\frac{\theta}{2}}\right)^2 d\theta$$

$$= r\int_0^{\pi/2} \left(\sec\frac{\theta}{2}\right)^2 d\frac{\theta}{2} = r$$

For the second term $a_2 s^2$

$$\int_0^r \frac{s}{r} K\left(\frac{s}{r}\right) p(s)ds = \int_0^r \frac{s}{r} K\left(\frac{s}{r}\right) a_2 s^2 = \int_0^r \int_0^{\pi/2} \frac{s.s^2}{r\sqrt{1-\left(\frac{s}{r}\right)^2 sin^2\theta}} d\theta ds$$

assume $\frac{s}{r}\sin\theta = \sin t$, ds = $\frac{r\cos t}{\sin\theta} dt$,hence

$$= \int_0^{\pi/2} \int_0^{\theta} \frac{\frac{\sin t}{\sin\theta} \cdot \left(\frac{r\sin t}{\sin\theta}\right)^2 \frac{r\cos t}{\sin\theta}}{\sqrt{1-sin^2 t}} dt d\theta$$

$$= r^3 \int_0^{\pi/2} \int_0^{\theta} \frac{\left(\frac{\sin t}{\sin\theta}\right)^3 \frac{\cos t}{\sin\theta}}{\cos t} dt d\theta = r^3 \int_0^{\pi/2} \int_0^{\theta} \frac{\sin^3 t}{\sin^4\theta} dt d\theta = r^3 \int_0^{\pi/2} \int_t^{\pi/2} \frac{\sin^3 t}{\sin^4\theta} d\theta dt$$

$$r^3 \int_0^{\pi/2} \sin^3 t \int_t^{\pi/2} \text{cosec}^4\theta d\theta dt = r^3 \int_0^{\pi/2} \sin^3 t \left[\frac{\cos t}{3\sin^3 t} + \frac{2\cos t}{3\sin t}\right]$$

$$= r^3 \int_0^{\pi/2} \frac{1}{3}\cos t + r^3 \int_0^{\pi/2} \frac{2}{3}\sin^2 t \cos t = \frac{r^3}{3} + \frac{2}{9}r^3 = \frac{5}{9}r^3$$

For the third term $a_4 s^4$

$$\int_0^r \frac{s}{r} K\left(\frac{s}{r}\right) p(s)ds = \int_0^r \frac{s}{r} K\left(\frac{s}{r}\right) a_4 s^4 = \int_0^r \int_0^{\pi/2} \frac{s.s^4}{r\sqrt{1-\left(\frac{s}{r}\right)^2 sin^2\theta}} d\theta ds$$

assume $\frac{s}{r}\sin\theta = \sin t$, $ds = \frac{r\cos t}{\sin\theta} dt$,hence

$$= \int_0^{\pi/2} \int_0^{\theta} \frac{\frac{\sin t}{\sin\theta} \cdot \left(\frac{r\sin t}{\sin\theta}\right)^4 \frac{r\cos t}{\sin\theta}}{\sqrt{1-sin^2 t}} dt d\theta$$

$$= r^5 \int_0^{\pi/2} \int_0^{\theta} \frac{\left(\frac{\sin t}{\sin\theta}\right)^5 \frac{\cos t}{\sin\theta}}{\cos t} dt d\theta = r^5 \int_0^{\pi/2} \int_0^{\theta} \frac{\sin^5 t}{\sin^6\theta} dt d\theta = r^5 \int_0^{\pi/2} \int_t^{\pi/2} \frac{\sin^5 t}{\sin^6\theta} d\theta dt$$

$$r^5 \int_0^{\pi/2} \sin^5 t \int_t^{\pi/2} \mathrm{cosec}^6\theta d\theta dt = r^5 \int_0^{\pi/2} \sin^5 t \left[\frac{\cos t}{5\sin^5 t} + \frac{4\cos t}{15\sin^3 t} + \frac{8\cos t}{15\sin t}\right]$$

$$= r^5 \int_0^{\pi/2} \frac{1}{5}\cos t dt + r^5 \int_0^{\pi/2} \frac{4}{15}\sin^2 t\cos t dt + r^5 \int_0^{\pi/2} \frac{8}{15}\sin^4 t\cos t dt$$

$$= \frac{r^5}{5} + \frac{4}{15}r^5\frac{1}{3} + \frac{8}{15}r^5\frac{1}{5} = \frac{89}{225}r^5$$

For the fourth term $a_6 s^6$

$$\int_0^r \frac{s}{r} K\left(\frac{s}{r}\right) p(s)ds = \int_0^r \frac{s}{r} K\left(\frac{s}{r}\right) a_6 s^6 = \int_0^r \int_0^{\pi/2} \frac{s.s^6}{r\sqrt{1-\left(\frac{s}{r}\right)^2 Sin^2\theta}} d\theta ds$$

assume $\frac{s}{r}\sin\theta = \sin t$, $ds = \frac{r\cos t}{\sin\theta} dt$,hence

$$= \int_0^{\pi/2} \int_0^{\theta} \frac{\frac{\sin t}{\sin\theta} \cdot \left(\frac{r\sin t}{\sin\theta}\right)^6 \frac{r\cos t}{\sin\theta}}{\sqrt{1-Sin^2 t}} dt d\theta$$

$$= r^7 \int_0^{\pi/2} \int_0^{\theta} \frac{\left(\frac{\sin t}{\sin\theta}\right)^7 \frac{\cos t}{\sin\theta}}{\cos t} dt d\theta = r^7 \int_0^{\pi/2} \int_0^{\theta} \frac{\sin^7 t}{\sin^8\theta} dt d\theta = r^7 \int_0^{\pi/2} \int_t^{\pi/2} \frac{\sin^7 t}{\sin^8\theta} d\theta dt$$

$$r^7 \int_0^{\pi/2} \sin^7 t \int_t^{\pi/2} \operatorname{cosec}^8\theta d\theta dt = r^7 \int_0^{\pi/2} \sin^7 t \left[\frac{\cos t}{7\sin^7 t} + \frac{6\cos t}{35\sin^5 t} + \frac{8\cos t}{35\sin^3 t} + \frac{16\cos t}{35\sin t}\right]$$

$$= r^7 \int_0^{\pi/2} \frac{1}{7}\cos t dt + r^7 \int_0^{\pi/2} \frac{6}{35}\sin^2 t \cos t dt + r^7 \int_0^{\pi/2} \frac{8}{35}\sin^4 t \cos t dt + r^7 \int_0^{\pi/2} \frac{16}{35}\sin^6 t \cos t dt$$

$$= r^7\left(\frac{1}{7} + \frac{6}{35}.\frac{1}{3} + \frac{8}{35}.\frac{1}{5} + \frac{16}{35}.\frac{1}{7}\right) = \frac{381}{1225} r^7$$

For the fifth term $a_8 s^8$

$$\int_0^r \frac{s}{r} K\left(\frac{s}{r}\right) p(s) ds = \int_0^r \frac{s}{r} K\left(\frac{s}{r}\right) a_8 s^8 = \int_0^r \int_0^{\pi/2} \frac{s.s^8}{r\sqrt{1-\left(\frac{s}{r}\right)^2 sin^2\theta}} d\theta ds$$

assume $\frac{\mathrm{s}}{\mathrm{r}}\sin\theta = \sin t$, $\mathrm{ds} = \frac{\mathrm{r}\cos t}{\sin\theta} dt$,hence

$$= \int_0^{\pi/2} \int_0^{\theta} \frac{\frac{\sin t}{\sin\theta}.\left(\frac{r\sin t}{\sin\theta}\right)^8 \frac{r\cos t}{\sin\theta}}{\sqrt{1-sin^2 t}} dt d\theta$$

$$= r^9 \int_0^{\pi/2} \int_0^{\theta} \frac{\left(\frac{\sin t}{\sin\theta}\right)^8 \frac{\cos t}{\sin\theta}}{\cos t} dt d\theta = r^9 \int_0^{\pi/2} \int_0^{\theta} \frac{\sin^9 t}{\sin^{10}\theta} dt d\theta = r^9 \int_0^{\pi/2} \int_t^{\pi/2} \frac{\sin^9 t}{\sin^{10}\theta} d\theta dt$$

$$r^9 \int_0^{\pi/2} \sin^8 t \int_t^{\pi/2} \operatorname{cosec}^{10}\theta d\theta dt =$$

$$= r^9 \int_0^{\pi/2} \frac{35}{315}\cos t dt + r^9 \int_0^{\pi/2} \frac{40}{315}\sin^2 t \cos t dt + r^9 \int_0^{\pi/2} \frac{48}{315}\sin^4 t \cos t dt$$

$$+ r^9 \int_0^{\pi/2} \frac{64}{315}\sin^6 t \cos t dt + r^9 \int_0^{\pi/2} \frac{128}{315}\sin^8 t \cos t dt$$

$$= r^9\left(\frac{35}{315} + \frac{40}{315}.\frac{1}{3} + \frac{48}{315}.\frac{1}{5} + \frac{64}{315}.\frac{1}{7} + \frac{128}{315}.\frac{1}{9}\right) = 0.2581 r^9$$

The following equation is the final equation for the left hand side elliptic integral for the term $p(s) = a_0 + a_2 s^2 + a_4 s^4 + a_6 s^6 + a_8 s^8$

$$a_0 r + a_2 \frac{5}{9} r^3 + a_4 \frac{89}{225} r^5 + a_6 \frac{381}{1225} r^7 + a_8 0.2581 r^9$$

The second elliptic integral $\left(\int_r^a K\left(\frac{r}{s}\right)\left(a_0 + a_2 s^2 + a_4 s^4 + a_6 s^6 + a_8 s^8\right) ds \right)$ is solved as follows,

The following is a general expression for any limits

$$\int k^\alpha \, EllipticK[k] dk = J_\alpha$$

where $J_\alpha = \frac{1}{\alpha^2}\left[(\alpha - 1)^2 J_{\alpha-2} + k^{\alpha-1}\left\{ E(k) - \alpha(1-k^2) K(k) \right\} \right]$,

which can be written as

$$J_{\alpha-2} = \frac{1}{(\alpha-1)^2}\left[\alpha^2 J_\alpha - k^{\alpha-1}\left\{ E(k) - \alpha(1-k^2) K(k) \right\} \right]$$

$$\int_r^a K\left(\frac{r}{s}\right) p(s) ds$$

for m=0, the integral value is $aEllipticE[k]$, where $k = \frac{r}{a}$

i.e for α=-2 the answer is the above integral

for m, $\int_r^a K\left(\frac{r}{s}\right) s^m ds$, assume $k = \frac{r}{s}$, $dk = -\frac{r}{s^2} ds = -\frac{k^2}{r}$,

then the intergal trasnforms into $r^{m+1} \int_{r/a}^{1} K(k) k^{-m-2} ds$

The following is the integrated answer for each individual term. The limits are not applied to the solved integral. The final answer for the second term can be obtained by adding all the following terms.

$$J_{-2} = r^{m+1}\left(-\frac{E(k)}{k}\right]_{r/a}^{1} \right)$$

$$J_{-4} = r^{m+1}\left(\frac{1}{9k^3}\left[-E(k)(1+4k^2)-2(1-k^2)K(k)\right]\right]_{r/a}^{1} \right)$$

$$J_{-6} = r^{m+1}\left(\frac{1}{225k^5}\left[-E(k)(9+16k^2+64k^4)+4\left(-9+k^2+8k^4\right)K(k)\right]\right]_{r/a}^{1} \right)$$

$$J_{-8} = r^{m+1}\left(\frac{1}{1225k^7}\left[\begin{matrix}-E(k)(25+36k^2+64k^4+256k^6)\\ +2(-75+3k^2+8k^4+64k^6)K(k)\end{matrix}\right]\right]_{r/a}^{1} \right)$$

$$J_{-10} = r^{m+1}\left(\frac{1}{99225k^9}\left[\begin{matrix}-E(k)(1225+1600k^2+2304k^4+4096k^6+16384k^8)\\ +8(-1225+25k^2+48k^4+128k^6+1024k^8)K(k)\end{matrix}\right]\right]_{r/a}^{1} \right)$$

Applying the limits r/a to 1 and multiplying with the respective r^{m+1} value

Note: each K(k) of term vanishes to 0 for the constant terms when the limit 1 is applied

And again assuming r/a as k, we have

$$J_{-2} = -a_0 r\left[1 - a\frac{E(k)}{r}\right]$$

$$J_{-4} = a_2 r^3\left[-\frac{5}{9} - a^3\left(\frac{-E(k)(1+4k^2)}{9r^3} - \frac{2(1-k^2)K(k)}{9r^3}\right)\right]$$

$$J_{-6} = a_4 r^5\left[-\frac{89}{225} - a^5\left(\frac{-E(k)(9+16k^2+64k^4)+4\left(-9+k^2+8k^4\right)K(k)}{225r^5}\right)\right]$$

$$J_{-8} = a_6 r^7\left[-\frac{381}{1225} - a^7\left(\begin{array}{l}\dfrac{-E(k)(25+36k^2+64k^4+256k^6)}{1225r^7} \\ +\dfrac{2(-75+3k^2+8k^4+64k^6)K(k)}{1225r^7}\end{array}\right)\right]$$

$$J_{-10} = a_8 r^9\left[-\frac{25609}{99225} - a^9\left(\begin{array}{l}\dfrac{-E(k)(1225+1600k^2+2304k^4+4096k^6+16384k^8)}{99225r^9} \\ +\dfrac{8(-1225+25k^2+48k^4+128k^6+1024k^8)K(k)}{99225r^9}\end{array}\right)\right]$$

The sum of the terms forms the final solution for the right hand side integral. And if when added with the first integral, we will see that the total terms of the first integral will be cancelled by the second integral's first terms.

So the final solution for the integration terms will be (where k=r/a)

$$A = a_0 aE(k) + a_2\left[a^3\left(\frac{E(k)(1+4k^2)}{9} + \frac{2(1-k^2)K(k)}{9}\right)\right]$$
$$+a_4 a^5\left(\frac{E(k)(9+16k^2+64k^4) - 4\left(-9+k^2+8k^4\right)K(k)}{225}\right)$$
$$+a_6 a^7\left(\begin{array}{l}\dfrac{E(k)(25+36k^2+64k^4+256k^6)}{1225} \\ -\dfrac{2(-75+3k^2+8k^4+64k^6)K(k)}{1225}\end{array}\right)$$
$$+a_8 a^9\left(\begin{array}{l}\dfrac{E(k)(1225+1600k^2+2304k^4+4096k^6+16384k^8)}{99225} \\ -\dfrac{8(-1225+25k^2+48k^4+128k^6+1024k^8)K(k)}{99225}\end{array}\right)$$

And from plate theory

$$\frac{1}{r}\frac{d}{dr}\left[r\frac{d}{dr}\left\{\frac{1}{r}\frac{d}{dr}\left(r\frac{dw}{dr}\right)\right\}\right] = \frac{q(r)-p(r)}{D_{wafer}}$$

Where $w = \dfrac{4\left(1-v_{pad}^2\right)}{\pi E_{pad}} A$.

The term w is now substituted in the plate theory function and the differentiated as per the procedure. The equation when differentiated 4 times (we will have alternative multiplication and division of k), the following is the answer obtained.

$$A = a_0\left[\frac{-E(k)\left(7+k^2\right)+4\left(1-k^2\right)K(k)}{3\left(1-k^2\right)^3}\right]$$

$$+a_2a^2\left[\frac{-E(k)(81-37k^2+12k^4)+2(19-24k^2+5k^4)K(k)}{\left(1-k^2\right)^3}\right]$$

$$+a_4a^4\left(\frac{-E(k)(-33+153k^2-176k^4+64k^6)}{\frac{-4\left(6-21k^2+23k^4-8k^6\right)K(k)}{\left(1-k^2\right)^3}}\right)$$

$$+a_6a^6\left(\frac{-E(k)(-9-147k^2+612k^4-704k^6+256k^8)}{\frac{-2(3+48k^2-171k^4+184k^6-64k^8)K(k)}{\left(1-k^2\right)^3}}\right)$$

$$+a_8a^8\left(\frac{-E(k)(-129-759k^2-9408k^4+39168k^6-45056k^8+16384k^{10})}{\frac{-4(21+93k^2+1518k^4-5472k^6+5888k^8-2048k^{10})K(k)}{25\left(1-k^2\right)^3}}\right)$$

So the equation is as follows

$$q(k) = p(k)+\frac{1}{3\pi}\frac{1-v_{pad}^2}{1-v_{wafer}^2}\frac{E_{wafer}}{E_{pad}}\left(\frac{t_{wafer}}{a}\right)^3 A$$

The above equation is the final expression for loading distribution in terms of pressure distribution, where we assume the pressure distribution to be a eighth order even polynomial.

APPENDIX II – Flow charts

I. Spatial pressure control – Flowchart

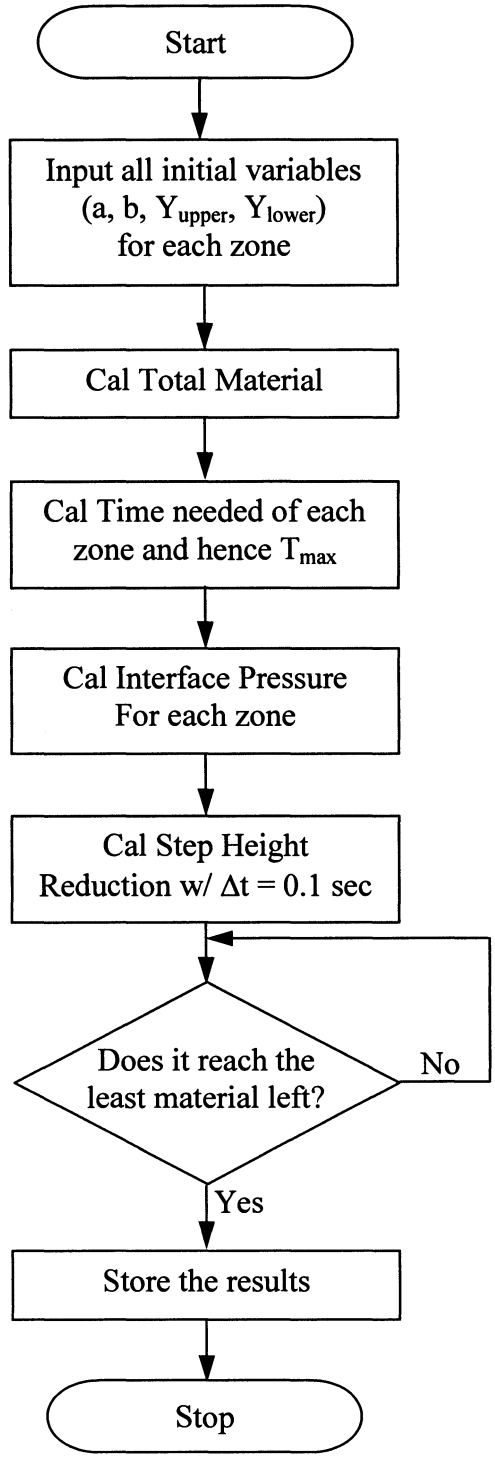

II. Spatial and Temporal pressure control – Flowchart

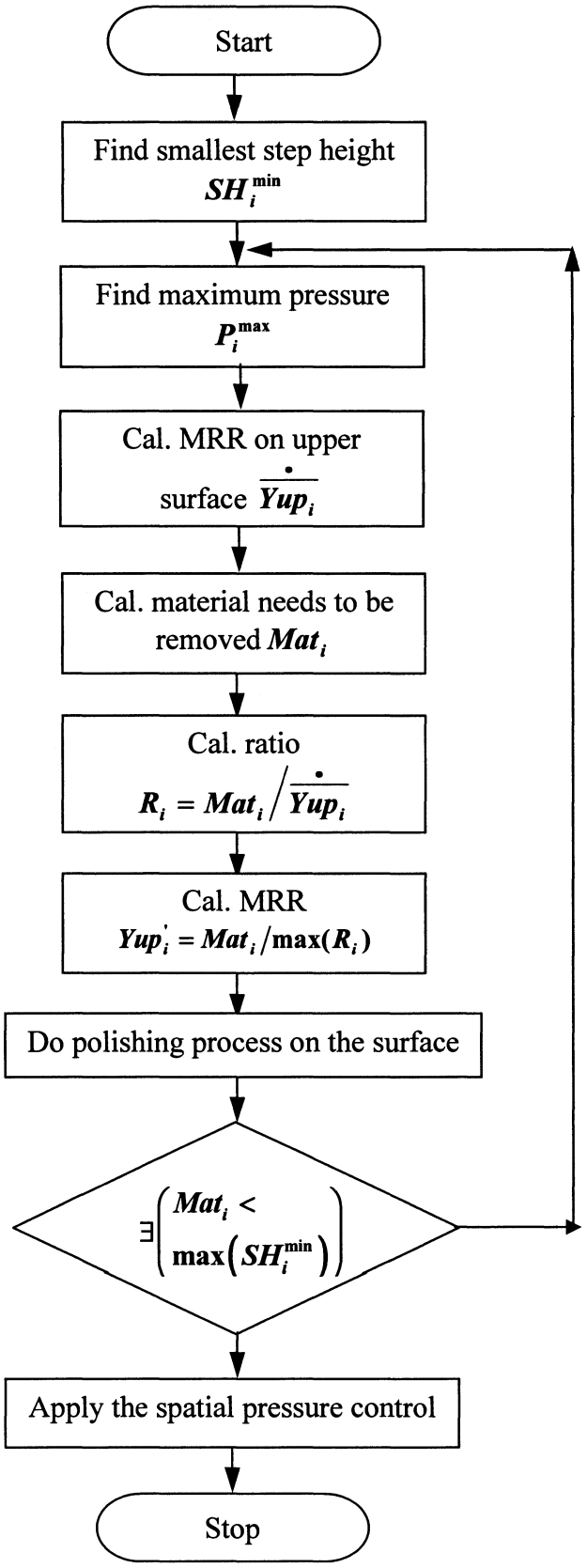

III. Look ahead scheduled pressure control – Flowchart

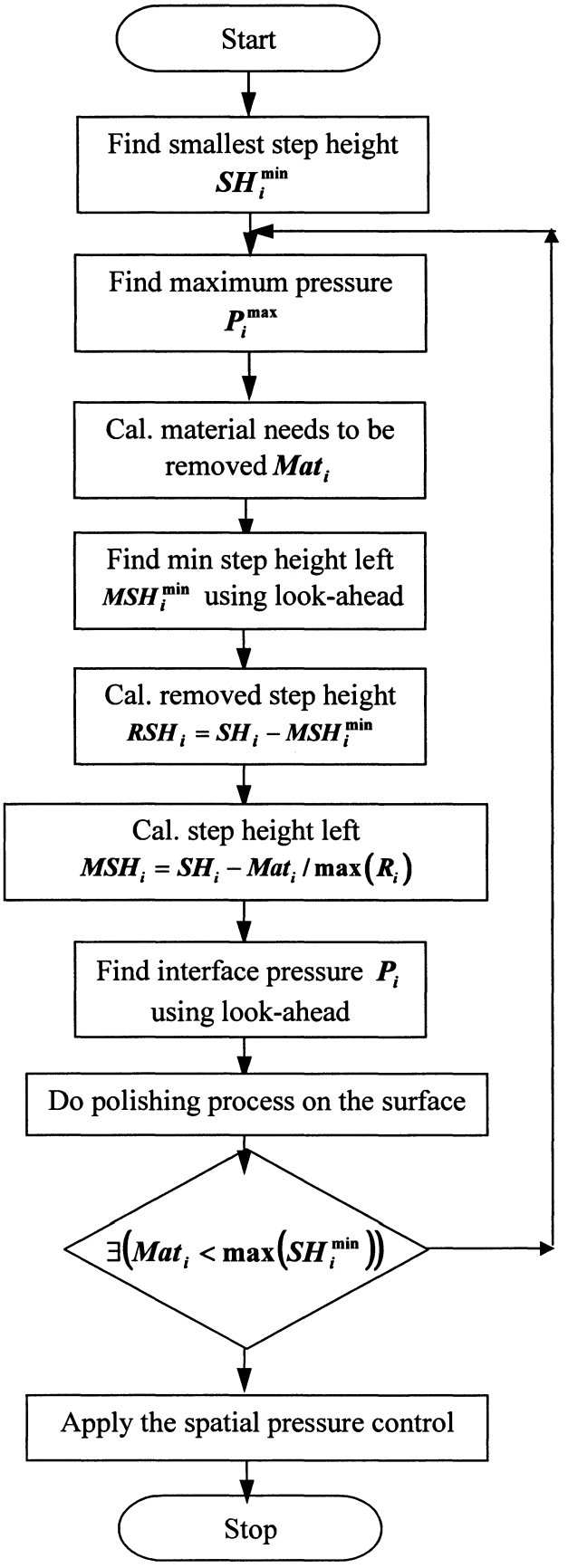

IV. Spatial velocity control – Flowchart

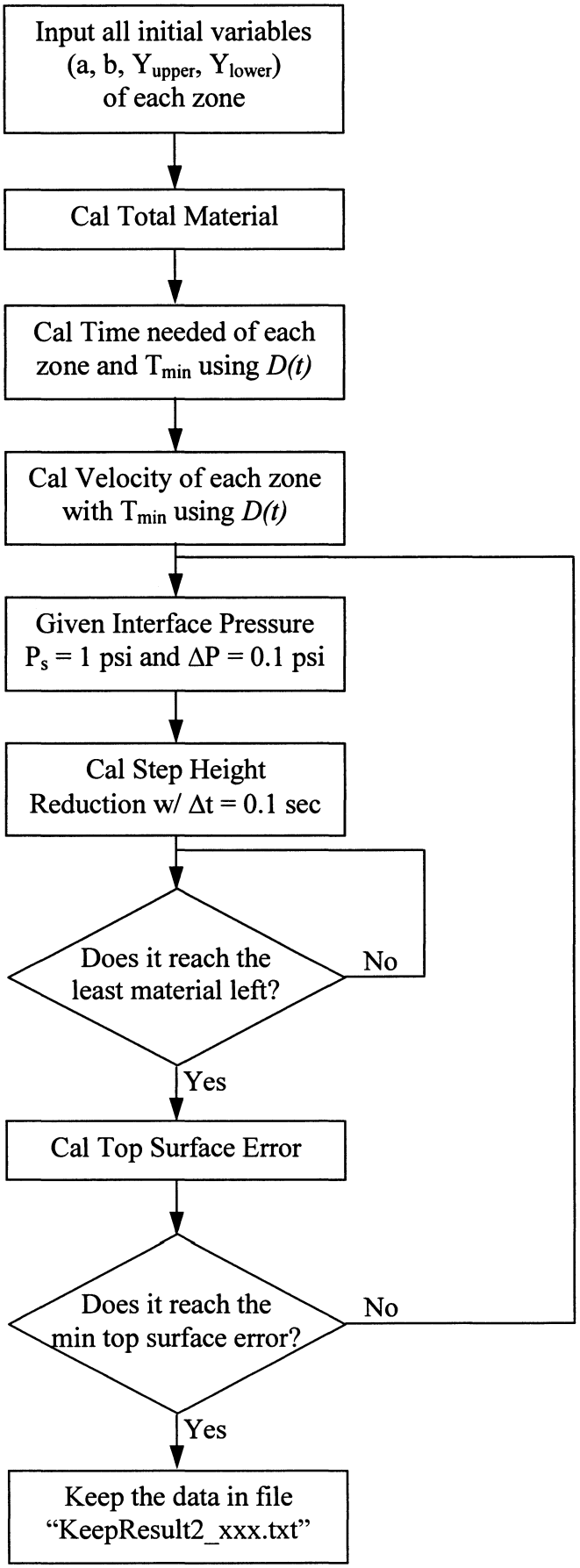

V. Spatial velocity and pressure control – Flowchart

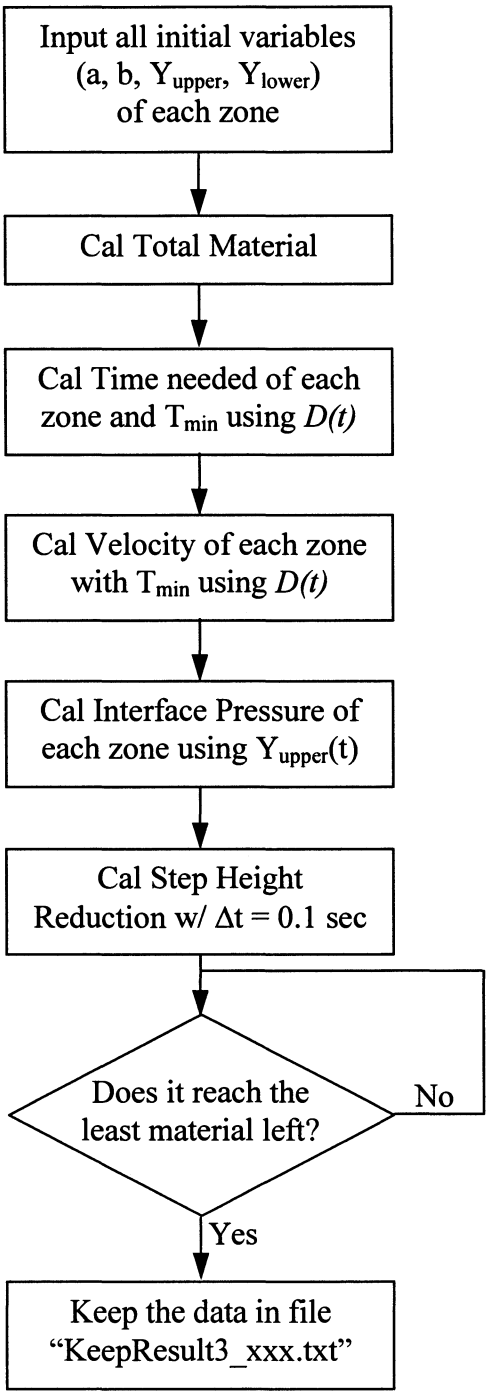

REFERENCES

A.R. Baker, "The origin of the edge effect in CMP", *Proceedings of the First International Symposium on Chemical Mechanical Planarization,* Vol. 96, No. 22, pp. 228-238, 1996.

G. Byrne, B. Mullany, P. Young, "The effect of pad wear on the chemical mechanical polishing of silicon wafers," *Annals of the CIRP*, Vol.48, No.1, pp. 143-146, 1999.

L. M. Cook, "Chemical processes in glass polishing," *J. Non-Crystalline Solids*, vol. 120, pp. 152-171, 1990.

S. Eamkajornsiri, G. Fu, R. Narayanaswami, A. Chandra, "Simulation of wafer scale variations in CMP," *Transactions of NAMRI XXIX, SME*, pp 221-228, 2001.

G. Fu, A. Chandra, "An analytical dishing and step height reduction model for CMP", *IEEE Transactions on Semiconductor Manufacturing*, Vol. 16, pp. 477-485, 2003.

G. Fu, A. Chandra, "Normal indentation of elastic half space with a rigid frictionless axisymmetric punch," *Journal of Applied Mechanics,* ASME, 2001.

A. Hemsley, "Elastic solutions for axisymmetrically loaded circular raft with free or clamped edges founded on winkler springs or a half space, *Proc. Instn. Civil Engrs.,part2* , Vol. 83, pp. 61-90, 1987.

C.W. Kaanta, S.G. Bombardier, W.J. Cote, W.R. Hill, G. Kerzkowski, H.S. Landis, D.J. Poindexter, C.W. Pollard, G.H. Ross, J.G Ryan, S. Wolff, J.R. Cronin, "Dual damascene: a ULSI wiring technology," *Proceedings of VMIC Conf.*, pp 144-152, 1991.

H. Kranenberg, P.H. Woerlee, "Influence of overpolish time on the performance of W damascene technology," *J. Electrochem. Soc.,* Vol. 145, no. 4, pp 1285-1291, 1998.

S.H. Li, R.O. Miller, "Chemical Mechanical Polishing in Silicon Processing," *Semiconductors and Semimetals*, Vol. 63, Academic press, 2000

D.O Ouma, "Modeling of Chemical Mechanical Polishing for Dielectric Planarization," PhD thesis, MIT, 1998.

D. Ouma, D. Boning, J. Chung, W.G. Easter, V. Saxena, S. Misra, A. Crevasse, Characterization and modeling of oxide CMP using planarization length and pattern density concepts," *IEEE Transactions on Semiconductor Manufacturing*, Vol. 15, no.2, 2002

W. J. Patrick, W. L. Guthrie, C. L. Standley, P. M. Schiable, "Application Chemical Mechanical Polishing to the Fabrication of VLSI Circuit Interconnections,"
J. Electrochem. Soc., Vol. 138, No. 6, pp. 1778-1784, June 1991.

F.W. Preston, "The theory and design of plate glass polishing machines," *J. Soc. Glass Technol.*, Vol. 11, pp. 214-256, 1927.

S.R. Runnels, P. Renteln, "Modeling the effect of polish pad deformation on wafer surface stress distributions during CMP," *Dielectric Science and Technology,* pp. 110-121, 1993.

Y. Sasaki, H. Aoyama, I. Inasaki, H. Miyari, H. Shibaya, "Evaluation of effective CMP conditions by estimation of pressure distribution on semiconductor wafer," *Proceedings of Silicon Machining (Spring Topical Meeting)*, Vol.17, pp. 92-95, 1998.

S. Sivaram, H. Bath, R. Leggett, A. Maury, K. Monning, R." Interlevel Dielectrics by Chemical-Mechanical Polishing," *Solid 91*, May 1992.

C. Srinivasa Murthy, D. Wang, S.P. Beaudoin, T. Bibby, K. Holland, T.S. Cale, "Stress distribution in chemical polishing," *Thin Solid Films*, Vol.308-309, pp. 533-537, 1997.

Z. Stavreva, D. Zeidler, M. Plotner, K.Drescher, "Influence of process parameters on Chemical Mechanical Polishing of Copper," *Microelectronic Engineering,* Vol. 37-38, pp. 142-149, 1997.

J.M. Steigerwald, S.P. Murarka, R.J. Gutmann, "Chemical Mechanical Planarization of Microelectronic materials," *John Wiley & Sons Pub.,* New York, 1997.

B. Stine, V. Mehrotra, D. Boning, J. Chung, D. Ciplickas, "A Simulation Methodology for Assessing the Impact of Spatial/Pattern Dependent Interconnect Parameter Variation on Circuit Performance," *IEDM Tech. Digest*, pp. 133-136,1997.

S. Syngellagis, C.-X. Bai, "On the application of boundary element method to plate-half space interaction," *Engineering Analysis with Boundary Elements,* Vol 12, pp. 119-125, 1993.

W.T. Tseng, Y.L. Wang, "Re-examination of pressure and speed dependences of removal rate during chemical mechanical polishing processes," *J. Electrochem. Soc.,* Vol.144, No.2, pp. L15-L17, 1999.

T. Tugbawa, T. Park, B. Lee, D. Boning, P. Lefevre, L. Camilletti, "Modeling of pattern dependencies for multi-level Copper chemical-mechanical polishing processes," *Mat. Research Soc.*, spring meeting, 2001.

D. Wang, J. Lee, K. Holland, T. Bibby, S. Beaudoin, T. Cale, "Von mises stress in chemical mechanical polishing processes," *J. Electrochem. Soc.,* Vol.144, No.3, pp.1121-1127, 1997.